Experimental Study of Universal Three-Body Physics with Ultracold Bosonic Lithium

Noam Gross

Department of Physics

Ph.D. Thesis

Submitted to the senate of Bar-Ilan University

Ramat-Gan, Israel April 2011

This work was carried out under the supervision of

Dr. Lev Khaykovich

Department of Physics

Bar-Ilan University

Acknowledgments

First, I would like to express my deepest gratitude to my advisor Dr. Lev Khaykovich who gave me an opportunity to be involved in this exciting and challenging project of building an atom cooling lab from the ground up and then using it in a leading-edge research. Lev guided me through this journey with a sincere passion for science. His vision and professionalism were inspiring and educative. I thank him for that.

I would also like to extend my warmest thanks to Servaas Kokkelmans of Eindhoven University of Technology for theoretical support and fruitful discussions and to my collaborators here, Zav Shotan and Olga Machtey.

I wish to thank Menahem Schneeberg of the mechanical workshop and Eli Perel and Valery Jourvsky, electronics engineers, for their resourceful thinking and creative designs.

I would like to express my sincere gratitude to Rachel Rotberg and Sara Bialkovitch, secretaries of the department, who have been there for me ever since I arrived at Bar-Ilan University.

I am grateful to Mr. Marcel Adams of Canada and the Israel Academy of Sciences and Humanities who provided me generous financial assistance via the Adams Fellowships Program during the last 3 years.

Finally, I thank my beloved wife Gal whose love and support are constant fuel to the realization of my fullest potential.

Abstract

Universality is a fundamental property of diverse few-body systems such as atomic nuclei, simple molecules or ultracold atoms. It is related to a peculiar quantum mechanical phenomenon which was discovered by Russian theoretician Vitaly Efimov in the early 1970-s. A consequence of his prediction was the existence of an infinite number of bound energy levels for three particles even if a short-range two-body potential is just not deep enough to bind two particles together. This counterintuitive discovery attracted a great deal of interest but lacked an experimental verification for many years. Difficulties in finding a system where the inter-particle potential can be changed easily were answered recently with the experimental demonstration of Feshbach resonances in ultracold atoms.

In the limit of zero collision energy the two-body interactions are determined by a single parameter, the scattering length a, which is defined by the low energy s-wave scattering phase-shift. In the vicinity of a Feshbach resonance this parameter diverges and thus can be readily tuned to large values and different signs by an experimentally easy-to-use change of the external magnetic field. A universal behavior is expected when a becomes the largest length scale in the system. In this case the three-body observables depend only on the scattering length and on a three-body parameter which serves as a boundary condition for the short range physics.

The first experimental evidence for the existence of Efimov quantum states was reported in 2006 in a system of ultracold ^{133}Cs atoms by the Innsbruck group. They investigated three-body recombination induced loss of atoms from a shallow optical trap and showed the enhancement of this loss at certain values of the scattering length. It was

attributed to an indirect manifestation of an Efimov state. This work was performed in the absolute ground state where two-body induced loss is forbidden.

In this Ph.D. thesis I present our study of universal three-body physics in a dilute gas of ultracold bosonic lithium atoms. We measure three-body recombination rates in two different nuclear-spin energy sublevels and across two different Feshbach resonances of the same atomic system. We identify enhancements and suppressions of the recombination rate which we associate with Efimov physics and find that these features are identical within the experimental errors in both states. As the properties of Efimov features are governed by the three-body parameter, our study indicates that the short-range physics is thus nuclear-spin independent. We also confirm the basic result of universal theory that Efimov features are universally related across Feshbach resonances.

Our studies are performed on the absolute ground state and the one but lowest Zeeman sublevel of the lower hyperfine state of bosonic lithium. While in the absolute ground state the two-body induced loss is forbidden, in the one but lowest Zeeman state it is allowed in principle. However, we show that this loss is completely negligible in our case and thus does not influence the study of the higher-order process of the three-body induced loss.

The study of universal three-body physics depends crucially on a precise knowledge of the two-body potential because a has to be carefully mapped on to the experimental variable, the magnetic field, in order to allow direct comparison with universal theory. We characterize Feshbach resonances using a very powerful experimental technique that measures directly the binding energy of weakly bound molecules in the vicinity of the resonances with high precision. Apart from providing a solid ground to our study of Efimov physics, these measurements allowed for the calculation of improved values of the singlet and triplet scattering length that characterize the interatomic potential.

Contents

List of Figures

Introduction

Few-body physics is universal when inter-particle interactions are insensitive to the microscopic details of the short-range interaction potentials and can be characterized by only one or few universal parameters [1]. In the limit of zero collision energy the two-body interactions are determined by a single parameter, the s-wave scattering length a. Universality requires a to greatly exceed the two-body potential range. This can be achieved by a resonant enhancement of a in the vicinity of Feshbach resonances [2], yielding the appearance of peculiar quantum states known as quantum halos whose wavefunction acquires long-range properties and gives rise to loosely bound states of size $\sim a$ [3]. In the case of three interacting bosons, universality means that the three-body observables show log-periodic behavior that depends only on the scattering length a and on a three-body parameter which serves as a boundary condition for the short-range physics. Such a behavior is associated with the so called Efimov physics. The recent years' remarkable progress in the study of Efimov quantum states in ultracold atoms has renewed a great deal of interest in this "old-new" quantum few-body problem. Since the first prediction made by V. Efimov in the early 70's [4, 5, 6], many systems were considered for an experimental study of these quantum states, however all of them were attempted in vain. The first experimental evidence of Efimov physics was reported in 2006 in a system of ultracold ^{133}Cs atoms [7] which was later on enhanced and verified in an additional study of the same system [8]. Since then, signatures of Efimov physics have been observed in other ultracold atomic species [9, 10, 11, 12, 13, 14, 15, 16] which turn out to be the only suitable platform up to now.

In this thesis I present our study of Efimov physics across two Feshbach resonances in two different energy sublevels of the same atomic system where a universal scaling across a region of $|a| \to \pm\infty$ was verified. As both Feshbach resonances occur at high magnetic fields where nuclear and electronic spins are decoupled, the two energy sublevels are associated with different nuclear-spin states. Our main finding is that the Efimov features are identical within the experimental errors in these two states.

The absolute location and lifetime of an Efimov state is defined by the unknown short-range part of the three-body potential. Most generally, the short range potential is given in terms of two-body potential permutations of the two-body subsystems and a true three-body potential which is of importance only when three particles are very close together. It is very difficult to solve the short-range physics exactly, and therefore this region is usually treated in terms of a three-body parameter [17, 18]. Thus, our results should be interpreted as a proof that the three-body parameter (and thus the short range physics) is identical for the two states

To study Efimov physics with ultracold atoms we designed and constructed an all-optical apparatus that cools ^{7}Li to quantum degeneracy. All-optical schemes became a well accepted experimental technique for many other atomic species [19, 20, 21, 22, 23, 24, 25] because of several inherent advantages. Optical traps allow strong confinement resulting in high collision rates and rapid evaporative cooling. Confinement of arbitrary spin states and spin state mixtures is readily obtained. The possibility to tune interactions via Feshbach resonances usually requires optical trapping as they frequently occur in states that cannot be trapped magnetically [26, 27]. Finally, large current coils needed for magnetic-field trapping that restrict optical access are avoided.

The first successful demonstration of an all-optically achieved ^{87}Rb Bose-Einstein condensation (BEC) allowed significant increase in the rate of BEC production and the resulting condensates were F=1 spinors [19]. However, the main driving force behind the search for all-optical techniques was the need to condense specific atoms where the 'conventional' evaporation in the magnetic trap was not possible. Two prominent examples

are spinless, and thus magnetically untrappable, BEC of Yb atoms achieved in a doubled YAG crossed dipole trap [20] and a BEC of ^{133}Cs atoms [21] for which the strongly enhanced two-body losses from the magnetically trappable states prevent the condensate formation in the 'standard' way [28].

Although ^{7}Li atoms can be evaporatively cooled in a magnetic trap [29], the task remains challenging due to several reasons. First, ^{7}Li atoms possess a relatively small scattering length ($a = -27a_0$, where a_0 is the Bohr radius) and a high two-body loss rate [30]. Second, the initial phase space density is unfavorably limited by the absence of a polarization-gradient cooling mechanism. Third, since the scattering length drops as the temperature increases and crosses zero at $T = 8$ mK [31], the use of adiabatic compression to increase the elastic collisional rate is ineffective. Therefore, the strong magnetic confinement needed to keep the evaporation time comparable with heavier alkalies, such as Rb and Na, requires the design of a miniaturized trap. This is done by either a small-volume vacuum chamber and high currents [32] or a vacuum compatible minitrap [33] which both increase the experimental complexity. Finally, even if the strong confinement is achieved the scattering length is still negative which prevents the formation of a stable BEC. Armed with this motivation we developed an experimental system for all-optical ^{7}Li atoms cooling using tunable interatomic interactions.

This Ph.D. thesis is divided into seven chapters. In Chapter 1 I elaborate on the experimental setup we designed and constructed in our lab. In Chapter 2 we investigate two Feshbach resonances on the $|F = 1, m_F = 0\rangle$ state of ^{7}Li that were not observed experimentally before and we demonstrate a spontaneous spin-purification of atoms at high magnetic fields. We describe the route to BEC that was achieved with the help of the Feshbach resonances. A theoretical background to Efimov physics is given in Chapter 3. In Chapters 4 and 5 we study experimentally Efimov physics in two nuclear-spin sublevels of ^{7}Li in the vicinity of Feshbach resonances and find that the Efimov features are universally related across the resonances and identical in both spin states (within the experimental error). As the properties of Efimov features are governed by the three-body parameter,

our study indicates that the short-range physics is thus nuclear-spin independent. In Chapter 6 we provide new and accurate characterizations of the Feshbach resonances on the two states which allow us to determine the values of the singlet and triplet scattering lengths that characterize the molecular potentials of lithium. We reevaluate our previous results in accordance with this study. Though small changes in the positions of the Efimov features can be identified, the main conclusion is not affected. We conclude in Chapter 7.

Chapter 1

Apparatus

1.1 Vacuum system layout

Our vacuum system is depicted in Fig. 1.1. It is nearly $2m$ long and is built around a straight axis in order to create a corridor in which the atoms are slowed and captured. On one side of it resides an oven where the lithium atoms are heated up to a typical temperature of $\sim 450^0$C corresponding to a vapor density of $\sim 10^{13}$ $atoms/cm^3$. A collimated atomic beam is produced by two apertures positioned 20 cm apart with diameters of 1.5 mm and 2 mm. On the opposite side of the system a sapphire window allows the Zeeman slowing beam to enter. The laser beam's width is $\sim$ 2 cm at the window and it converges into $\sim$ 2 mm width as it reaches the closer atomic aperture. Thus it is maximizing the light's overlap with the atomic beam which ends its ballistic trajectory bashing against the window. Sapphire is preferred over a regular glass because it interacts less with lithium, thus it reduces the accumulation of particles on the window and

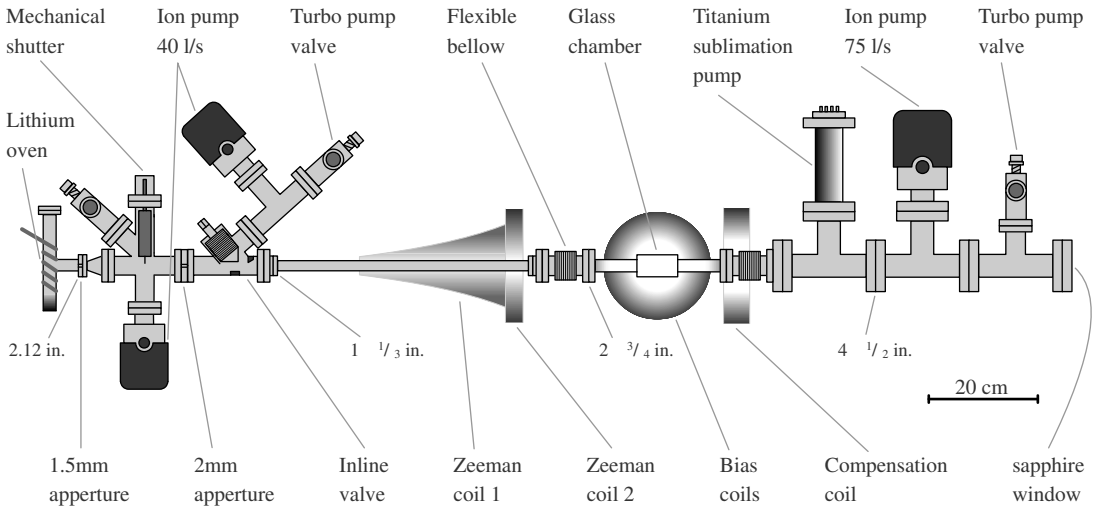

Figure 1.1: The vacuum system layout

preventing it from turning opaque. To further reduce the probability of lithium settling on the sapphire we apply moderate heating to the window.

According to vacuum condition criterion, the system can be divided roughly into three sections separated by the two atomic apertures which also serve as differential pumpers. The first section is the oven. It holds the worst vacuum due to its high temperature and the fact that it is not being directly pumped. The second section is the area in between the apertures. It serves as an intermediate zone and it is equipped with a 40 l/s ion pump which provides typical vacuum conditions during experiments of $\sim 10^{-9}$ $torr$ [1]. The last section is the largest and it contains the glass chamber in which the experiment takes place (typical vacuum conditions here are better than $\sim 10^{-11}$ $torr$). In order to provide the best vacuum in this area we chose to locate two pumps in close proximity to the glass cell: a 75 l/s ion pump and a titanium sublimation pump. Moreover, these pumps are connected to the cell via large diameter tubes to enhance their efficiency. A third ion pump is located on the other side of the Zeeman slower. This area is not being pumped efficiently by any other pump in the system due to differential pumping imposed by the

[1]Pressure values that appear in this text are taken from to the ion pump's current meter reading.

atomic aperture from one side and the long narrow Zeeman tube from the other. Adding this extra pump creates another buffer zone between the oven and the glass chamber. An inline valve, installed near the oven side, allows for repairs, such as oven replacing, to take place without contaminating other areas of the system.

1.2 Slowing and capturing the atoms

1.2.1 Lasers setup

The lasers setup which provides the Zeeman slower and the Magneto-Optical trap (MOT) with light beams to slow and capture the atoms is built in a master-slave configuration on a separate optical table, as depicted in Fig. 1.2. A master laser is frequency locked on to the Lithium's atomic resonance, thus providing the reference frequency to the setup. A set of Acousto-Optic modulators (AOMs) modify the reference beam and generate other frequencies which are then used for injection locking the high power slave lasers. More AOMs combined with mechanical shutters regulate the light power transferred to the experimental area by optical fibers.

The master laser in our setup is a "Sacher" external cavity tunable laser (Littrow configuration) which emits $\sim 20\ mW$ at 671 nm. It is coupled to a heated home-made Lithium vapor cell to produce a Doppler free saturated absorption spectroscopy. A typical absorption image can be seen in Fig. 1.3. The Doppler broadened absorption feature has a width of $\sigma = 1.3\ GHz$ implying on a temperature of $\sim 370^0 C$ inside the vapor cell which is being heated by a heating rod running a current of 1.38 A. The sub-Doppler features in Fig. 1.3 are the two ground states (upward tics) separated by 803.5 MHz and

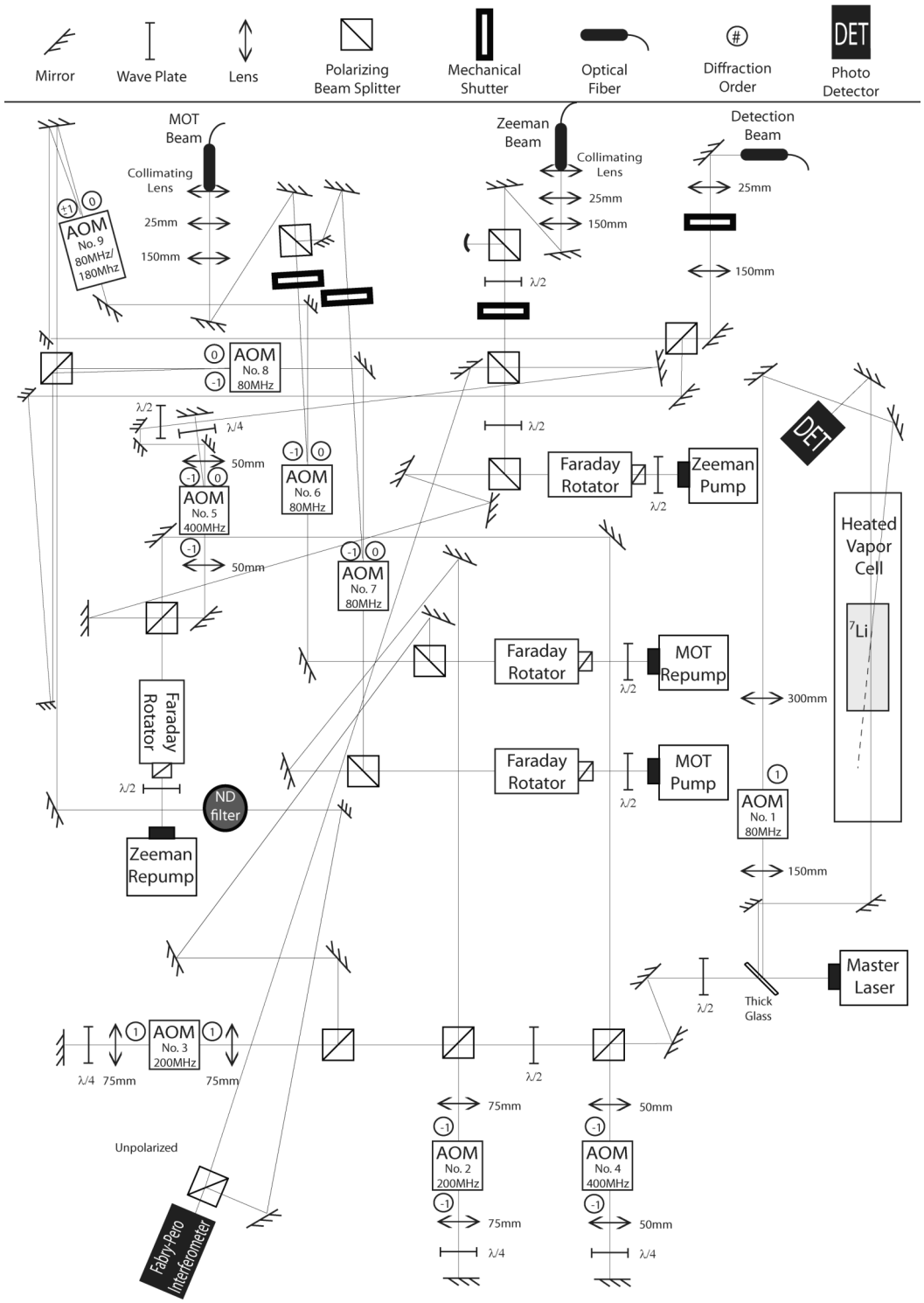

Figure 1.2: The lasers setup.

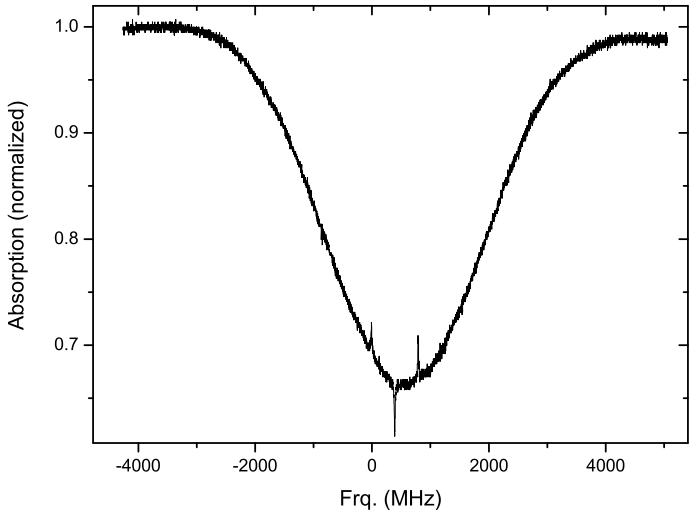

Figure 1.3: Doppler free saturated absorption spectroscopy of ^{7}Li.

the cross-over signal on which the laser is to be locked. We note that the frequency of the cross-over signal is shifted by $+40\ MHz$ from its real value due to an AOM of 80 MHz implemented in the apparatus to frequency modulate the absorption signal at a rate of 44 KHz. The modulated signal, analyzed by a lock-in-amplifier, is used for frequency locking at the absorption line center.

The Zeeman slower and the MOT need two separate frequencies each (four in total) due to the Lithium's atomic level structure which has two hyperfine splitted ground states. The frequency associated with the $|S_{1/2}, F = 2\rangle$ ($|S_{1/2}, F = 1\rangle$) ground state is denoted as Pump (Repump) and relates to an optical transition into the $|P_{3/2}, F = 3\rangle$ ($|P_{3/2}, F = 2\rangle$) excited state, as can be seen in Fig. 1.4. We employ four standard, commercially available 120 mW 661 nm diode lasers [2] as slaves. The lasers are temperature stabilized at $\sim 70^0C$ by standard "Newport" laser mounts (Model:700C) connected to "Newport" TEC controllers (Model:325B) in order to push their wavelength by $+10\ nm$ where they

[2] "Mitsubishi"; Model: ML101J27.

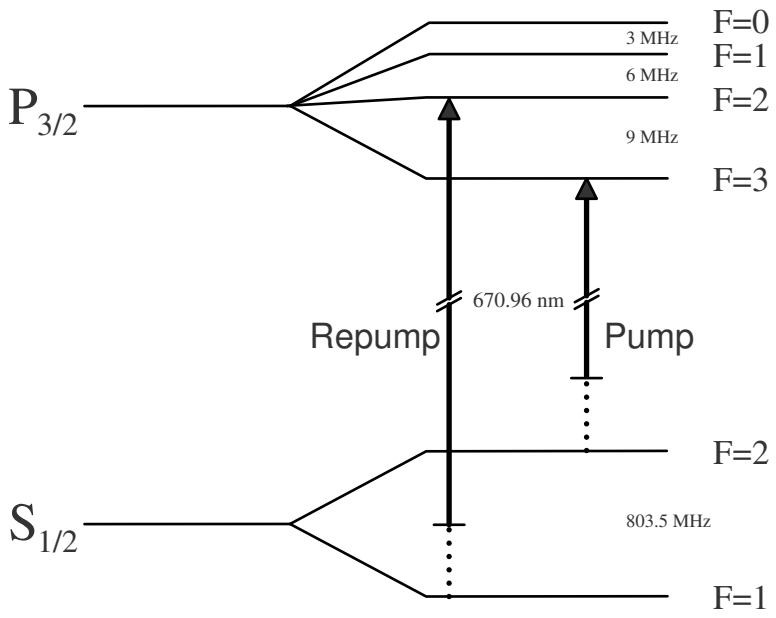

Figure 1.4: Pump and Repump laser transitions at zero magnetic field.

will be easily injection locked. The lasers frequency scheme is presented in Fig. 1.5.

While the Zeeman Pump and Repump beams don't change during the experiment besides being turned On and Off by a mechanical shutter, the MOT beams are dynamic in terms of frequency and power variations as summarized in Table 1.1. We measured the rate at which changes in frequency can be applied and found that a 30 MHz shift is accomplished in less than 0.2 ms. A power change of 0 to 100% (and vice versa) is accomplished in less than 0.1 ms.

Immediately after atoms are loaded into the optical dipole trap (see Sec. 1.3) mechanical shutters block the light of all near-resonant lasers from reaching the atoms. Black curtains made of paper or fabric surround the lasers setup optical table for the same purpose. The laser light used for atoms detection is discussed in Sec. 1.5.1.

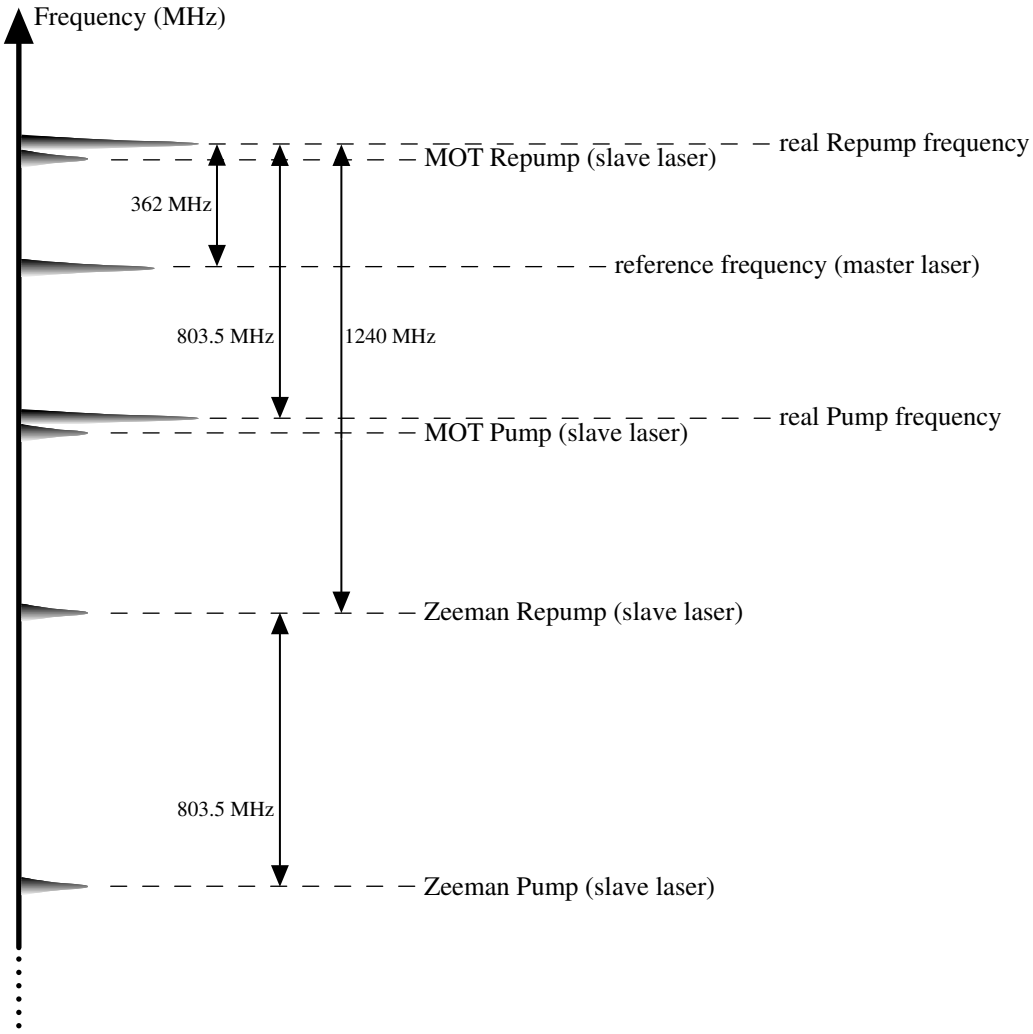

Figure 1.5: The lasers frequency scheme.

Beam	Frequency detuning	Power attenuation
MOT Pump	AOM #2 (200 MHz)	AOM #7 (80 MHz)
MOT Repump	AOM #3 (200 MHz)	AOM #6 (80 MHz)

Table 1.1: Manipulation of the MOT Pump and Repump beams by AOMs (see also Fig. 1.2 for location of each AOM in the setup). The nominal frequencies of the AOMs appear in brackets. Frequency detuning (power attenuation) is set in a double (single) pass configuration.

1.2.2 The Zeeman slower

The ballistic flight of the lithium in the collimated atomic beam is very fast ($v_{rms} \approx 1800\ m/s$) due to the high temperature inside the oven which is required for sufficient vapor pressure and the small atomic mass of the lithium. This makes the process of capturing the atoms inefficient without an intermediate slowing stage such as a Zeeman slower. In our apparatus we employ an increasing field Zeeman slower. As can be seen in Fig. 1.1, the slower is composed of two separate coils running different electric currents of 7.0 A in "Zeeman coil #1" and 58.7 A in "Zeeman coil #2" controlled by IGBT switches. Heat dissipation of 35 $Watts$ and 150 $Watts$, respectively, is extracted by passive (heat sink) and active (water cooling) methods. A detailed description of the slower can be found in Yuval Guetta's master's thesis [34].

As discussed in the previous section, the slowing laser beam is composed of two frequencies, denoted as Pump and Repump. Both frequencies are red detuned by 1240 MHz from their zero magnetic field values (see Fig. 1.5). At this detuning the beam is resonant with atoms travelling at a frontal speed of 830 m/s (due to Doppler shift) which is also the capture velocity ($\sim 6\%$ of the total atomic flux). Before the atoms enter the slower they are randomly distributed between different hyperfine states of the two ground levels. At this stage the Pump ($\sim 40\ mW$) and Repump ($\sim 0.4\ mW$), which are both σ^- polarized, pump atoms into the $|S_{1/2}, F = 2, m_F = -2\rangle$ hyperfine ground state. The slowing process will make use of a transition between this state and the $|P_{3/2}, F = 3, m_F = -3\rangle$ excited state which is a close transition, i.e. after the absorption - spontaneous emission cycle atoms end up in the initial state. The changing magnetic field along the slower makes sure that the Pump frequency is kept in resonance with this transition due to the Zeeman effect. Finally, the magnetic field reaches a maximum value of $\sim 850\ G$ at which the atoms are slowed down to a speed of $\sim 30\ m/s$.

1.2.3 The magneto-optical trap

We use a standard MOT configuration with three orthogonal pairs of counter-propagating beams and a pair of anti-Helmholtz coils. Each beam is $2-2.5\ cm$ in diameter and is composed of red detuned Pump and Repump frequencies (see Fig. 1.5) which are circularly polarized in the same direction. The Pump's intensity (per beam) is $\sim 0.6 \times I_{sat}$ [3] while the Repump is $\sim 20\%$ weaker and they are detuned by $-40\ MHz$ and $-30\ MHz$, respectively. The coils (discussed in Sec. 1.4) run a current of 60 A which yields a magnetic field gradient of $\sim 13\ G/cm$ in the primary axis.

Atoms are loaded into the MOT for $10-15$ seconds at the beginning of each experimental sequence. When this is finished they are transferred into a far-off-resonance optical dipole trap (FORT, discussed in Sec. 1.3) during a short transition period of 250 ms called the Compressed MOT (CMOT) at which the trap's parameters are changed gradually, as shown in figures 1.6 and 1.7, in order to optimize the loading process. In essence, these changes decrease the size of the trap and increase its density (typically to $\sim 10^{12}\ atoms/cm^3$) which in turn increases its spatial overlap with the FORT. Moreover, the temperature of the atomic cloud is lowered during the CMOT phase to 0.3 mK from an initial value of 1.3 mK which is significantly smaller than the FORT potential depth ($\sim 2\ mK$) and gives a better starting point for later cooling. Sub-Doppler cooling does not work with this specie and although the theoretically predicted Doppler temperature for Li is $T_D = 140\mu K$, for yet unknown reason it is not attainable with ^{7}Li. We note that our MOT performs similarly to those obtained previously by other groups [35]. Trap parameters values of the MOT and at the end of the CMOT phase are summarized in Table 1.2.

At the end of the CMOT phase we apply a short pulse (1 ms long) of the Pump beam. Its intensity and detuning are $0.3\times I_{sat}$ and $-5.1\times\Gamma$, respectively, where $\Gamma = 2\pi\times 5.9\ MHz$ (the excited level line-width). The pulse pumps atoms into the $|F=1\rangle$ ground state which

[3] Lithium's saturation intensity is $I_{sat} = 2.56\ mW/cm^2$.

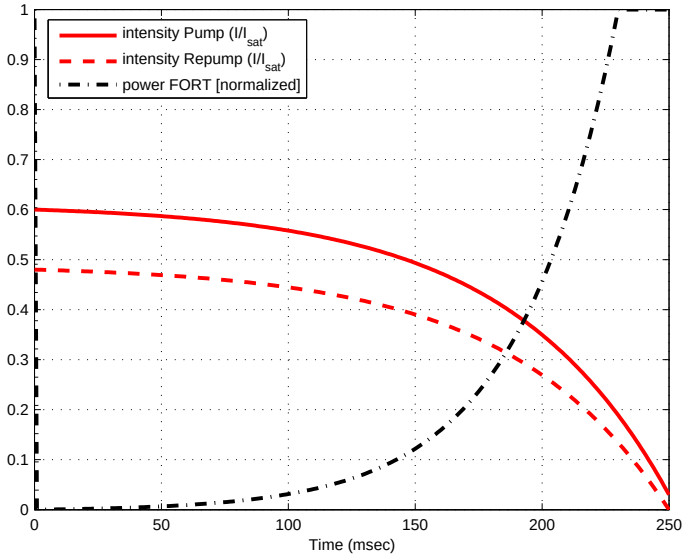

Figure 1.6: Changes in laser intensities during the CMOT phase. The change rates used by *the exponential ramp function* (see Appendix A) are -4 and -6 for the MOT beams intensities and the FORT power, respectively.

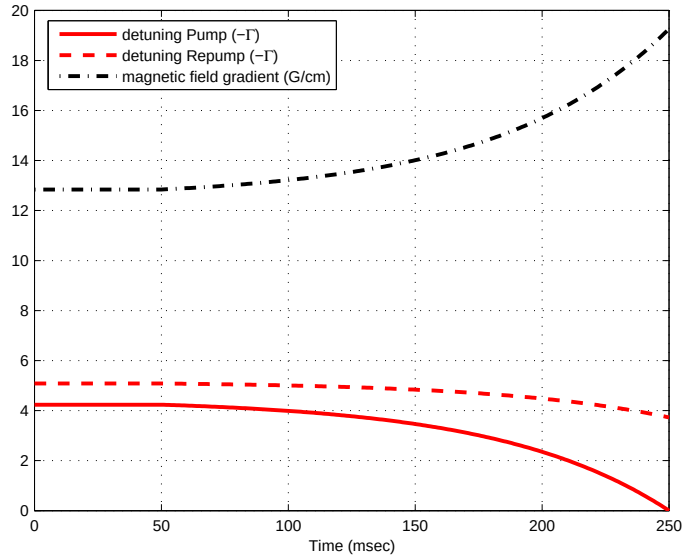

Figure 1.7: Changes in laser frequency detuning and magnetic field gradient during the CMOT phase. Note that the changes begin only after the first 50 μs. Detuning is expressed in units of $\Gamma = 2\pi \times 5.9\ MHz$ (the excited level line-width). The change rates used by *the exponential ramp function* (see Appendix A) are all -3.

Parameter	MOT	(end of) CMOT
Pump detuning	$-4.2 \times \Gamma$	0
Repump detuning	$-5.1 \times \Gamma$	$-3.7 \times \Gamma$
Pump Intensity	$0.60 \times I_{sat}$	$0.03 \times I_{sat}$
Repump Intensity	$0.48 \times I_{sat}$	0
Magnetic field current	60 A	90 A
Magnetic field gradient	12.8 G/cm	19.3 G/cm
Temperature	1.3 mK	0.3 mK
Cloud diameter (2σ)	3 mm	0.6 mm

Table 1.2: Trap parameters values of the MOT and at the end of the CMOT.

possesses Feshbach resonances that can be used to tune interatomic interactions.

Residual magnetic field from the Zeeman slower, which is 23 cm away from the center of the trap, reaches the MOT and relocates its center. In order to prevent this problem a compensation coil was added at the other side of the trap, 14 cm away from it (see Fig. 1.1). This coil operates simultaneously with the slower and eliminates the residual field.

1.3 The optical dipole trap

1.3.1 Trap setup

Our main atomic trap, in which evaporative cooling and then experiments are conducted, is a far-off resonance optical dipole trap that relies on the electric dipole interaction of atoms with far detuned light [36]. The trap exploits the fact that the dipole potential scales as I/δ, where I is the laser intensity and δ is the detuning of the light field from

the closest atomic resonance (for alkalis represented by the D1 and D2 lines), whereas the scattering rate scales as I/δ^2. Optical dipole traps therefore perform optimally with large detunings and high intensities that keep the scattering rate as low as possible for a given potential depth.

We use a 100 W "IPG" Ytterbium fiber laser ($\lambda = 1.08\mu m$) to generate the optical trap. With the help of acousto-optic modulators (AOMs) and a set of lenses the light beam is divided into two separate beams which intersect at the center of the MOT thus creating a crossed-beam trap. Fig. 1.8 depicts the trap's setup. The laser beam is first collimated by a lens (mounted at the fiber's end) which focuses it 1 m away to a waist of $\sim 300\ \mu m$. At this location a "NEOS" [4] AOM is positioned. The beam's 1^{st} diffraction order passes through two lenses that generate a $\sim 30\mu m$ waist at the center of the glass chamber. It embodies the trap's "main beam". The lens closer to the chamber is mounted on an XYZ translation stage allowing fine alignment of the beam's waist with the MOT's center. The 0^{th} order of the AOM propagates 1.1 m before it encounters a second identical AOM. This time, the -1^{st} diffraction order beam is being used. A 200 mm lens focuses this beam into a $\sim 40\mu m$ waist inside the chamber where it embodies the trap's "secondary beam". The lens is mounted on an elevating translation stage that allows fine tuning of the secondary beam's vertical height in order to properly intersect with the main beam.

The atomic life-time in the trap is determined by the vacuum quality and by scatterings due to interaction with the trapping light (in the weak interatomic interaction limit). Fig. 1.9 shows a life time measurement taken immediately after the trap is loaded from the MOT in its maximum power of $\sim 65\ W$ and in the main beam only. As can be seen, in the first 5 seconds the trap experiences excessive losses which can probably be explained by truncation of the thermal distribution due to a finite trap depth ($U/k_B \approx 2\ mK$) compared to the atomic temperature ($0.3\ mK$). After the first 5 seconds the atom number exhibits an exponential decay attributed to single body related losses. In the current trap condition a maximum light scattering rate of $\sim 2.5\ s^{-1}$, and therefore a heating rate of

[4] Model number: 35060-30-3-1.06-I-HGM-W

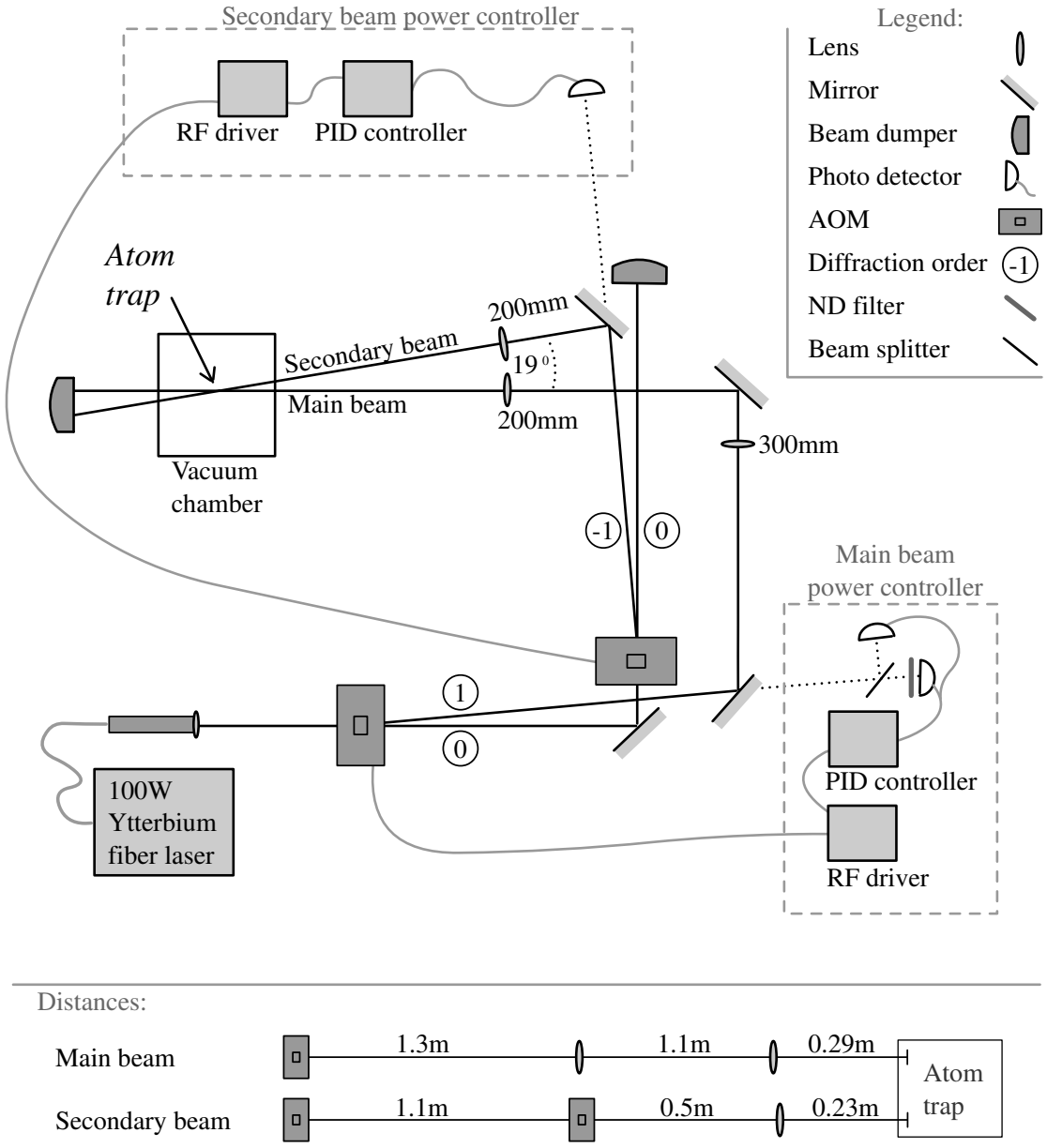

Figure 1.8: Optical dipole trap setup.

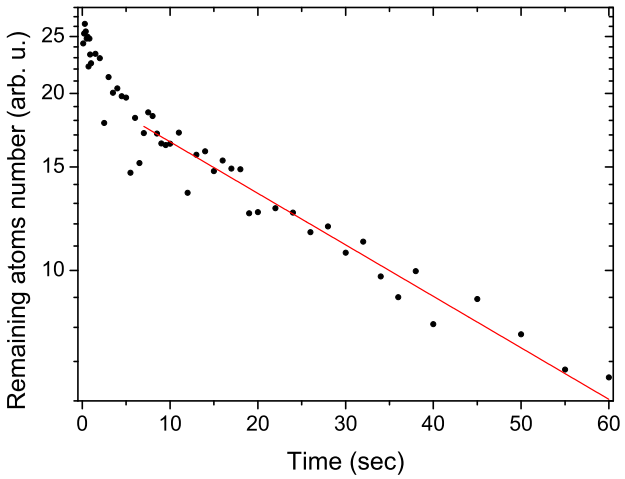

Figure 1.9: Atoms life time in the single-beam trap. The solid line represents an exponential decay fit on the long tail which yields a life time due to single-body processes of 50 s.

$\sim 2.5\ \mu K/s$ [36], is expected. A trap life time of 50 seconds measured here is probably the result of a combination between the vacuum condition and the loss mechanism due to the light scattering effect. However, the latter can be neglected at later stages of evaporation where the laser's intensity is attenuated significantly.

Interferences between the two intersecting beams may affect the life-time of the atoms in the trap. In order to diminish this problem, the beams are set orthogonal in polarization by means of mirrors manipulation. Moreover, employing a different diffraction order for each beam creates a 120 MHz frequency shift between them.

In our scheme, a precise control over the main and secondary beam intensities is crucial. It is determined by the amount of radio-frequency (rf) power injected into the first and second AOMs, respectively. Although commercially available rf-power AOM drivers can be controlled directly, they show strong temperature dependent power drifts which makes direct control unreliable. We therefore install a homemade PID feedback loop to actively stabilize the laser power. Moreover, by introducing active stabilization

we decrees the intensity noise which may cause heating of atoms in the trap [37]. During an experiment, the PID controller constantly compares the desired power for each beam with its instantaneous real value, as measured by a photo detectors (PD), and accordingly commands the AOM's rf driver to enhance or attenuate its power. During the evaporation process (discussed in Sec. 1.6) the main beam is attenuated by more than two orders of magnitude, from an initial power of $\sim 60\ W$ to less than $0.5\ W$. A single PD's dynamic range is not suffice for an accurate monitoring in the low power regime. We thus follow a scheme similar to that in Ref. [25] and add a second PD to monitor the main beam. This PD is more sensitive to weak signals and is dominant at low powers. It saturates at $\sim 3\ W$ from which it serves only as a bias to the other PD which handles the medium and high power regimes. The dual PD schematic is depicted in Fig. B.1 of Appendix B. The secondary beam, however, is controlled by a single PD as it enters at a later stage of evaporation and only ~ 1.5 orders of magnitude in its power needs to be controlled.

1.3.2 Characterizing the trap

A good estimation of the atom density inside the trap is crucial in many experiments. The Gaussian laser beam which generates the trap creates, close to its center, a $3D$ harmonic trapping potential $U(r) = \frac{1}{2}m(\omega_x^2 x^2 + \omega_y^2 y^2 + \omega_z^2 z^2)$, where m is the atomic mass and ω_i is the trap oscillation frequency in axis i. The resulting atomic distribution inside the trap is Gaussian in all directions: $n(r) = n_0 \exp(-\frac{x^2}{2\sigma_x^2}) \exp(-\frac{y^2}{2\sigma_y^2}) \exp(-\frac{z^2}{2\sigma_z^2})$, where n_0 is the peak density and $\sigma_i = \omega_i^{-1}\sqrt{k_B T/m}$ is the atomic cloud's size in axis i. Due to a resolution limitation of the imaging system the density is calculated indirectly with the help of other parameters, namely: atom number, temperature and trap oscillation frequencies. Atom number is extracted from images taken during the experiment and temperature is derived from a time-of-flight measurement (see Sec. 1.5.2). The various procedures we employ to measure the trap oscillation frequencies are discussed next.

The optical trap in our experiment has two distinct stages: it starts as a single-beam trap immediately after the CMOT loading procedure (Sec. 1.2.3) and during evaporation

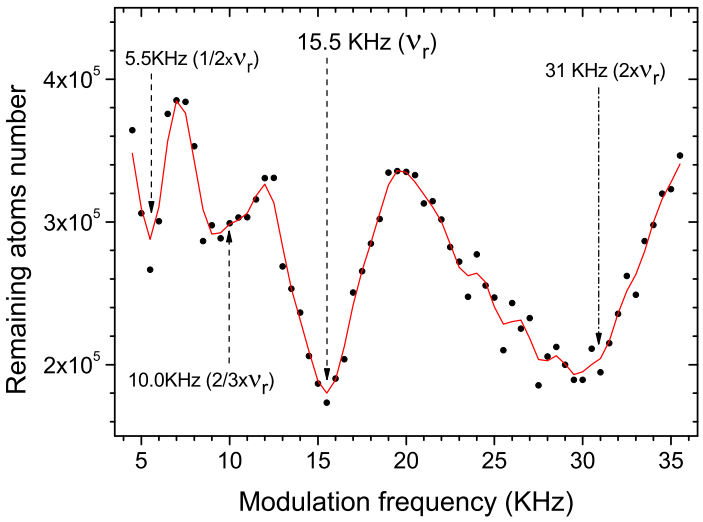

Figure 1.10: Trap radial oscillation frequency measurement via parametric resonance induced loss. The laser power is being modulated at different frequencies after which the remaining atom number is detected. The solid line is a smoothed representation of the data points.

(Sec. 1.6) it turns into a crossed-beam trap. Due to its cigar shape it also has very different radial and longitudinal oscillation frequencies which deserve different measurement methods. The radial oscillation frequency of the trap is measured via parametric resonance induced loss [36]. The laser power is being modulated at an amplitude of a few percent for ~ 1 second at different frequencies after which the remaining atom number is detected. A typical result is depicted in Fig. 1.10. The largest atom loss is observed at twice the radial eigenfrequency $\nu_r = 15.5\ KHz$. Taking into account the measured laser power ($64\ W$) we extract the waist of the Gaussian beam to be 31 μm which is very close to our prediction based on Gaussian beam propagation calculations and a measurement of the deflected beam. The asymmetry of the loss features in Fig. 1.10 can be attributed to atom loss associated with higher energy levels in the trap where deviations from the harmonic potential become important. Other losses appear at values of $2\nu_r/n$ with n integer.

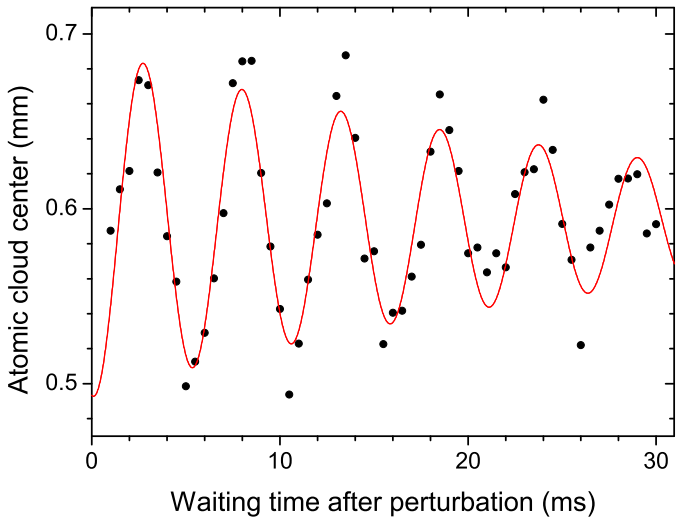

Figure 1.11: Single-beam trap longitudinal oscillation frequency measurement via cloud displacement after perturbation. A fit with a decaying oscillation solution (solid line) yields in this example a longitudinal trap frequency of 190 Hz.

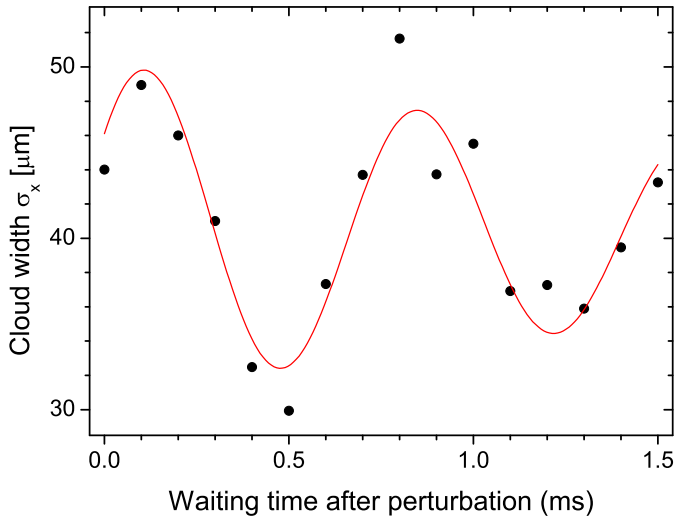

Figure 1.12: Crossed-beam trap longitudinal oscillation frequency measurement via cloud breathing after perturbation. A fit with a decaying oscillation solution (solid line) yields in this example a longitudinal trap frequency of 670 Hz.

The longitudinal oscillation frequency is measured by monitoring the atomic cloud response to elementary excitations. In the single-beam case, the power of the laser beam is increased significantly for 1 ms and then decreased back to its initial value. Due to a shift in the waist's position as a function of power the cloud is suddenly displaced from the potential center which excites a center of mass oscillation mode and when the power regains its original value the cloud starts oscillating at the longitudinal frequency ν_l around the initial waist location as can be seen in Fig. 1.11. In the crossed-beam case, the power of both beams is doubled for a period of time which is roughly $4/\nu_l$ and then decreased back to its initial value. This time the cloud's breathing oscillation mode $(2 \times \nu_l)$ is excited and measured, as depicted in Fig. 1.12.

1.4 High magnetic-field coils

1.4.1 Coils configuration

Two pairs of Helmholtz coils, different only in diameter, are situated outside the glass chamber and can generate a bias magnetic field of up to 1300 G at their mutual center which coincides with the atoms trap location. Each of the 4 coils is composed of 11 turns of a 3/16" copper tubes with inner diameter of ~ 3 mm threaded inside plastic sleeves. During operation water is running through the tubes at a rate of ~ 1 l/m to take away heat generated by the high electrical currents (up to 1.5 KW per coil). We denote the larger (smaller) pair as the external (internal) coils, as can be seen in Fig. 1.13(a) where their schematic is depicted. When the separation between two Helmholtz coils is larger than their radius, as in the case of the internal coils, a local magnetic field minimum

is created between them. For ^{7}Li atoms in the $|F = 1\rangle$ ground state at high magnetic fields this translates into an anti-trapping potential (strong-field seekers). In contrast, in the case of the external coils where the separation is smaller than the radius, a trapping potential is created. Independent control over the electric current running in each pair allows us to determine not only the magnetic field's value but also its trapping potential properties. The external coils are being used also in an anti-Helmholtz configuration to create the MOT's magnetic field.

In the setup, the bias magnetic field is generated by two 6 KW power suppliers [5], one for each pair of coils, which can run up to 400 A. As shown in Fig. 1.13(b,c) where the coils wiring diagram is depicted, IGBT switches are implemented inside the electrical circuits. Their assignment is twofold: they allow for a fast shut-off of the magnetic field and they provide a safety precaution by blocking electrical currents when water is not running (detected by a flow-meter). The two switches in the external coils scheme (Fig. 1.13(b)) have another duty. They allow the coils to operate in both Helmholtz and anti-Helmholtz configurations with two different power suppliers [6]. Although these switches are never closed simultaneously, ground (earth) loops distort the power suppliers program controls. We overcome this problem by inserting an isolation amplifier module [7] between the bias field power supplier and the computer command box.

1.4.2 Magnetic field calibration

In chapters 4, 5 and 6 we describe the mapping of three Feshbach resonances, two of which had never been observed before experimentally. Working in this uncharted territory is not feasible without an excellent knowledge of the generated magnetic field value. We used three methods to calibrate the magnetic field summarized in Fig. 1.14 and discussed here.

[5] "Delta Elektronika"; Model: SM 15-400.
[6] The MOT power supplier is a "Delta Elektronika"; Model: SM 15-100.
[7] "Delta Elektronika" Iso Amp Module.

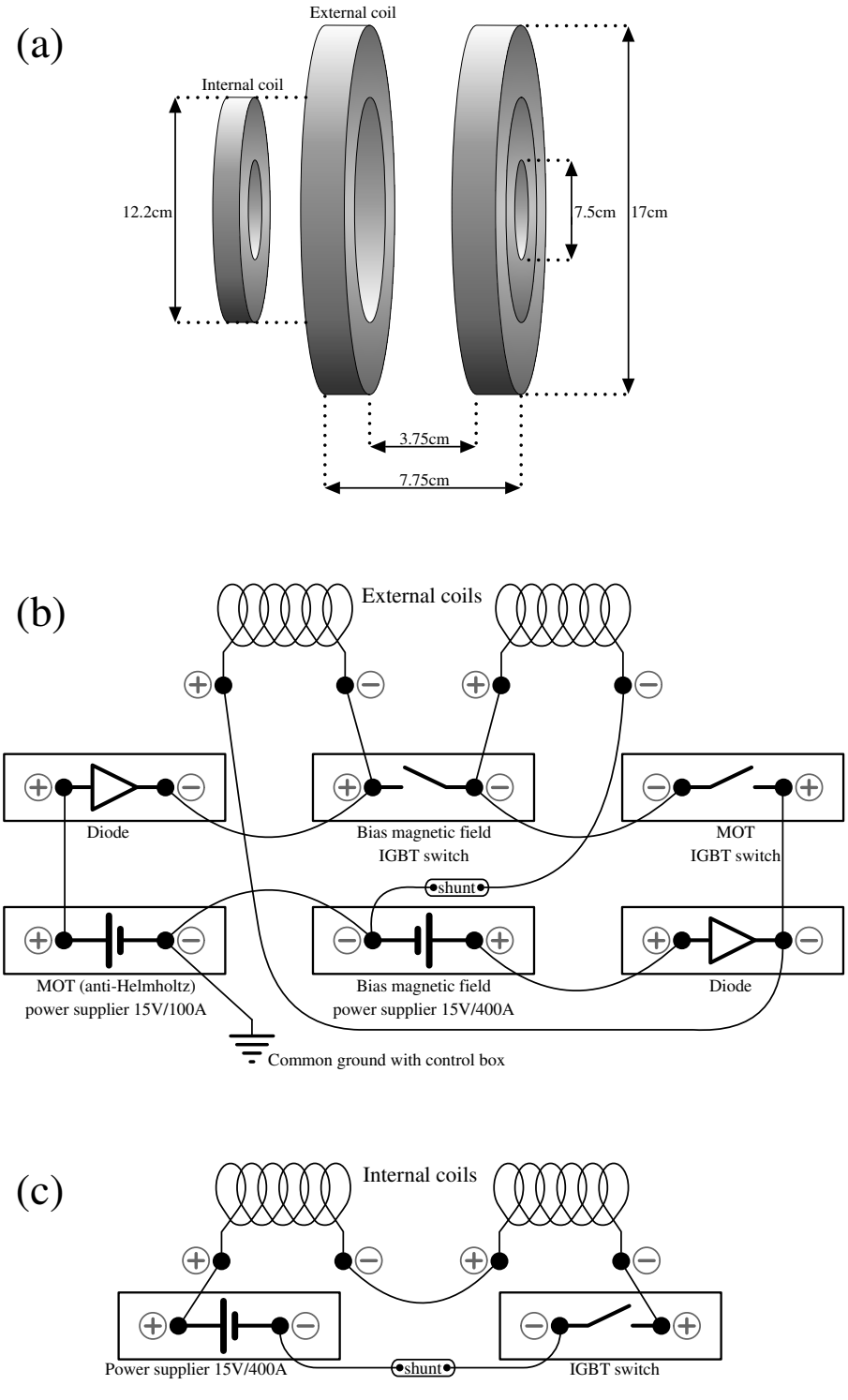

Figure 1.13: Magnetic coils configuration. (a) Coils schematic; (b) External coils wiring diagram; (c) Internal coils wiring diagram.

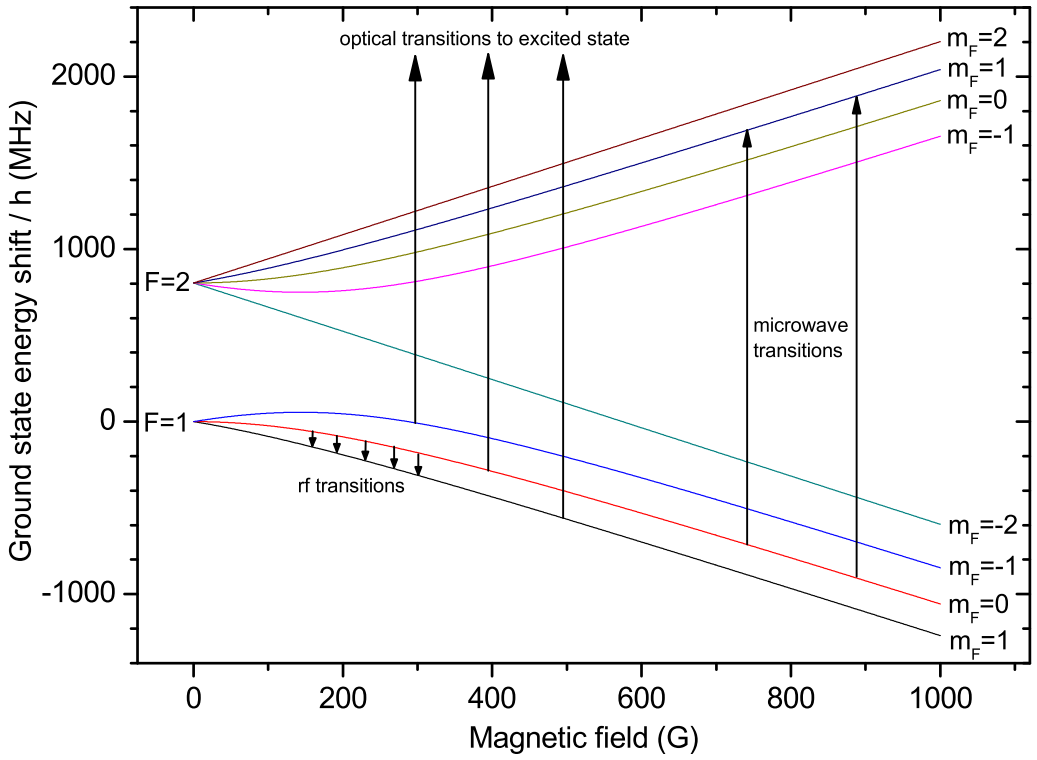

Figure 1.14: The energetic transitions used by us for magnetic field calibration depicted over the ^{7}Li ground states hyperfine splitting diagram.

Calibration via optical excitations: We find three magnetic field values at which the Pump beam is resonant with a transition between the $|S_{1/2}, F = 1\rangle$ ground state sublevels (solid lines in Fig. 1.15) and the $|P_{3/2}, m_J = -3/2\rangle$ sublevels of the excited state (dashed lines in Fig. 1.15 and red shifted by the Pump beam's frequency). Selection rules constraint for this transition is $\Delta m_I = 0$. We prepare atoms in the desired ground state and calibrate the internal and external coils independently by exposing the atoms to a Pump beam pulse at different currents and searching for the maximal atom loss. The results are shown in Fig. 1.16 for both the internal (triangles) and external (circles) coils. Fitting each set of measurements with a straight line returns the calibration ratio, which

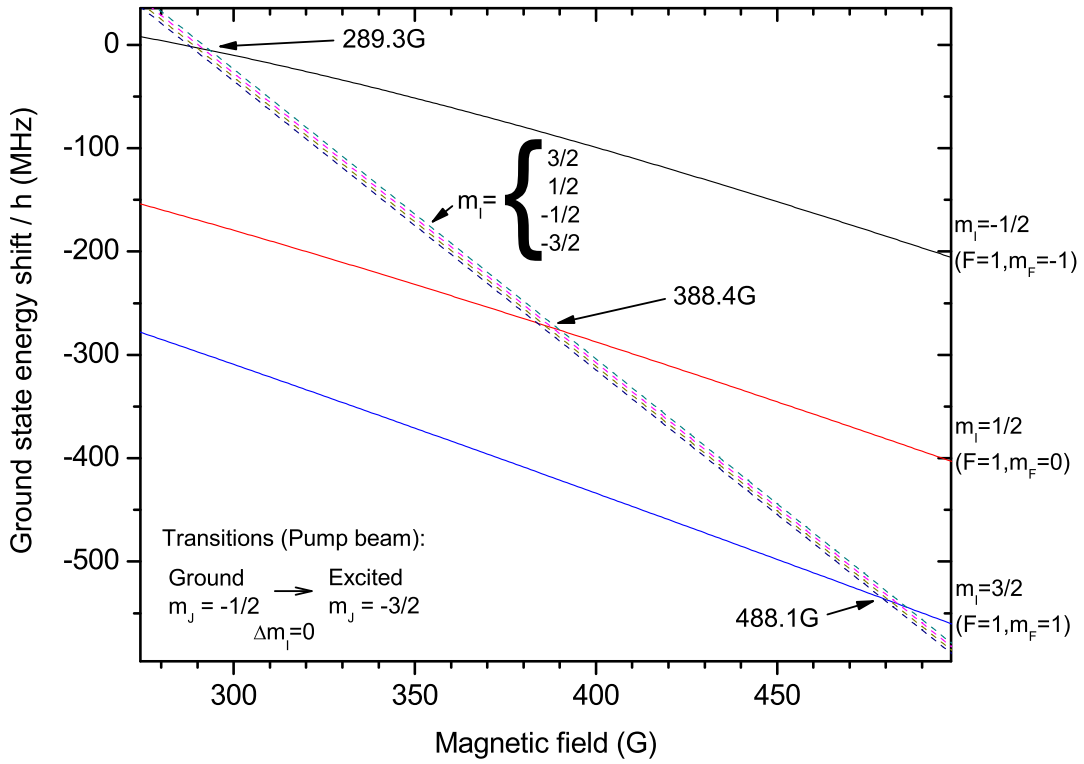

Figure 1.15: Energetic detuning of the $|S_{1/2}, F = 1\rangle$ ground state sublevels (solid lines) and the $|P_{3/2}, m_J = -3/2\rangle$ sublevels of the excited state (dashed lines) as a function of magnetic field. The excited state is shifted to the red by the Pump beam's frequency.

is 1.825(6) G/A and 1.594(22) G/A for the internal and external coils, respectively. The large horizontal error-bars which represent the loss signal width, determined by the width of the optical transition and the quality of the laser locking, suggest that this method's precision is rather poor.

Calibration via rf adiabatic following: Here we search for transitions between two ground state sublevels, from $|F = 1, m_F = 0\rangle$ to $|F = 1, m_F = 1\rangle$, by rf induced adiabatic following (see Fig. 1.14). We choose an rf frequency that corresponds to a given magnetic field and apply a frequency sweep of 200 KHz while scanning the coils currents inde-

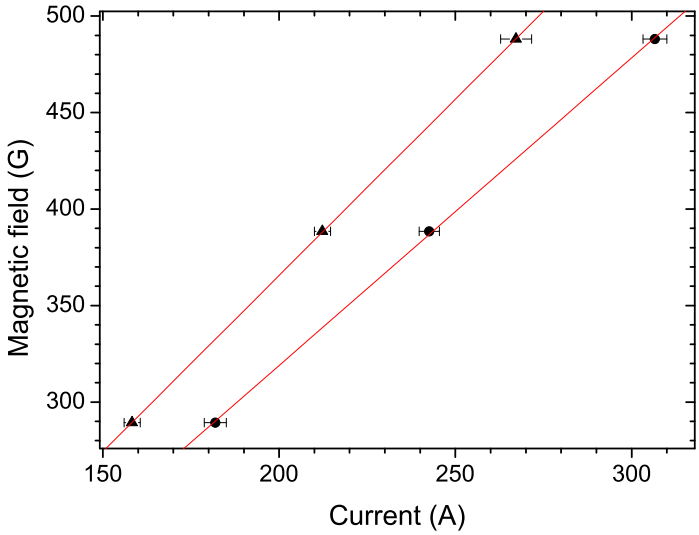

Figure 1.16: Magnetic field calibration via optical excitations for both the internal (triangles) and external (circles) coils. Each point represents the maximum atom loss and the error-bars represent the loss feature width. The straight lines are linear fits that return the G *per* A calibration ratio.

pendently to find the value which gives the most efficient transition and then repeat this procedure for different frequencies. The rf is generated by a small loop antenna (1 *inch* diameter) with 3 turns situated about an inch away from the trap perpendicular to the magnetic field axis. The results are shown in Fig. 1.17 for the internal (triangles) and external (circles) coils. Linear fitting returns the calibration ratio which is 1.8332(9) G/A and 1.5997(7) G/A for the internal and external coils, respectively. This method is much more accurate than the optical transition calibration, however, its short coming is that it is not efficient at high magnetic fields where the higher order Zeeman-shift makes this transition insensitive to changes in magnetic field. Moreover, the nuclear spin is decoupled from the electron spin at high magnetic fields and significantly stronger rf-power is required to rotate it.

Calibration via microwave adiabatic following: The transition used in this calibration

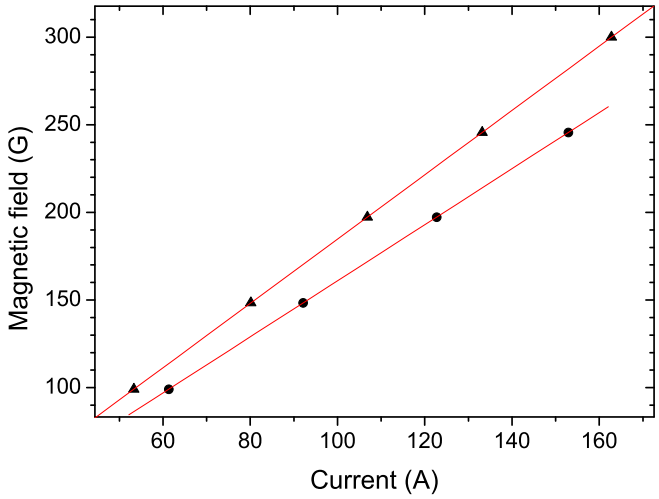

Figure 1.17: Magnetic field calibration via rf adiabatic following for both the internal (triangles) and external (circles) coils. Each point represents the most efficient adiabatic following transition at a given current. The straight lines are linear fits that return the G *per* A calibration ratio.

process is $|F = 1, m_F = 0\rangle$ to $|F = 2, m_F = 1\rangle$ which lies in the microwave frequency regime (see Fig. 1.14). Power is generated by an antenna similar to the one used in the rf calibration (with only 1 turn though) driven by a powerful 16 W amplifier. Here it was more convenient for us, due to technical reasons, to induce an adiabatic following by sweeping the magnetic field (along 200 mG) rather than the frequency. Another difference from former calibrations is that this time we were able to operate in close proximity to the magnetic fields at which the Feshbach resonances reside. However, due to the high magnetic field values a single pair could not produce it alone and the coils had to be calibrated simultaneously. We overcome this limitation by employing different weights to the internal and external coils currents. One measurement was performed at a transition frequency of 2371.2 MHz which takes place at 730 G with a current weight ratio of $I_{ext}/I_{int} = 1.40$ which is unique in that it corresponds to a flat magnetic field potential which is neither trapping nor anti-trapping. A second measurement was performed at a

Calibration method	Internal coils ratio	External coils ratio
Geometrical prediction	1.82 G/A	1.54 G/A
Optical excitation	1.825(6) G/A	1.594(22) G/A
Rf adiabatic following	1.8332(9) G/A	1.5997(7) G/A
Microwave adiabatic following	1.8398(7) G/A	1.5977(6) G/A

Table 1.3: Magnetic field calibration results by method.

transition frequency of 2772.4 MHz (880 G) and a current weight ratio of $I_{ext}/I_{int} = 0.258$ which creates an anti-trapping potential for the atoms (oscillation frequency of $i \times 15$ Hz). Each measurement was accurate to within ± 200 mG and the combination of both yielded the following calibration ratios: 1.8398(7) G/A and 1.5977(6) G/A for the internal and external coils, respectively. Thus far this is the most accurate calibration method in terms of its measuring error. Moreover, it is also the most reliable because it relates directly to magnetic fields where the experiments are performed.

Table 1.3 summarizes the results of the three calibration methods and in the first row one can also find a geometrically calculated prediction which assumes an equal distribution of current density inside the overall coil volume. Based on this geometrical model, with minor modifications to resemble the actual results, we estimate the magnetic trapping potential oscillation frequency that each pair creates and find it to be $\nu_{int} = i \times 0.84\sqrt{I_{int}}$ and $\nu_{ext} = 0.71\sqrt{I_{ext}}$. Combined with the results of the microwave calibration we produce the following formulas:

$$I_{int} = 0.24533 \times B - 0.77755 \times \nu^2 \tag{1.1}$$

and

$$I_{ext} = 0.34339 \times B + 0.89538 \times \nu^2 \tag{1.2}$$

which give us the proper currents needed in order to produce a desired magnetic field B with a magnetic trapping potential oscillation frequency ν. Note that this oscillation frequency do not include the superimposed optical trapping and it serves only for the determination of different current ratios between the two pairs of Helmholtz coils.

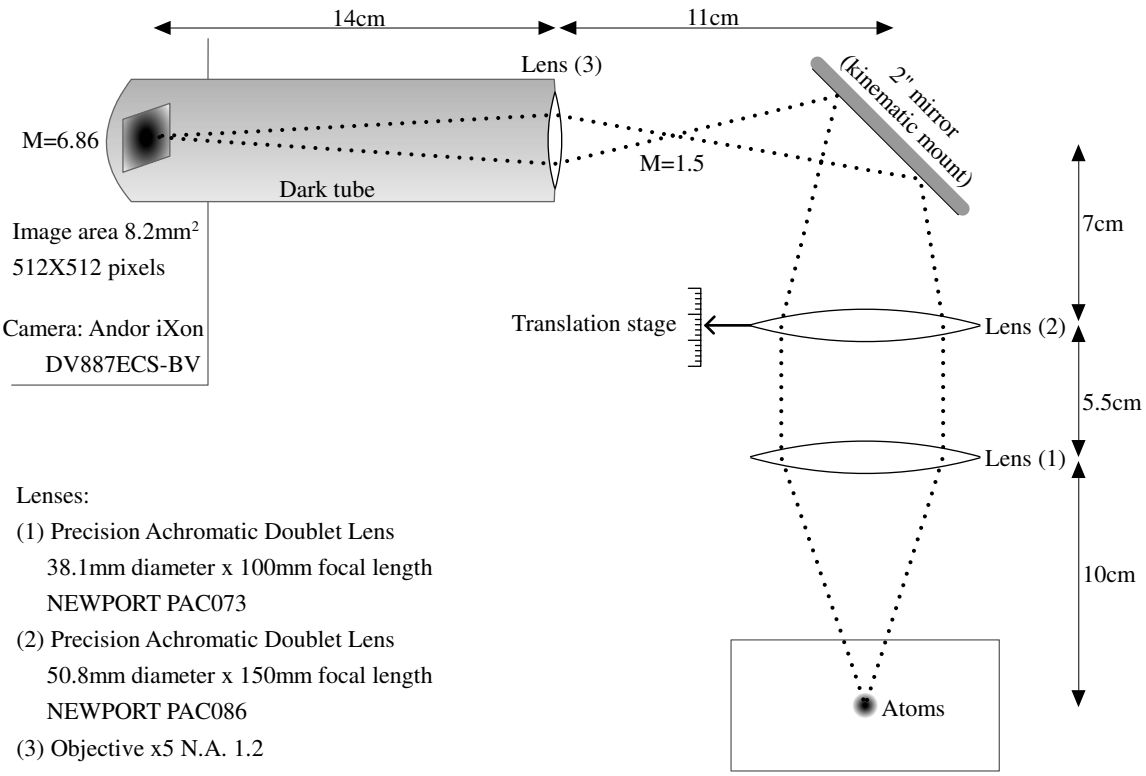

Figure 1.18: The imaging setup schematic.

1.5 Imaging and analysis

1.5.1 Absorption imaging setup

We use absorption imaging technique for atoms detection. A resonant laser beam sent through the atoms is absorbed and scattered by them. The light intensity attenuation due to scattering depends on the number of atoms it encounters. Since the beam's diameter is larger than the atomic cloud an inverse (shadow) picture of the atoms is created which is imaged onto a camera sensor. From this picture's analysis (discussed in the next section) information such as atoms number and distribution can be extracted. This method is destructive because the resonant light scatters the atoms from the trap, therefore the imaging is the last act in an experimental sequence.

Our imaging apparatus is depicted in Fig. 1.18. We use three lenses: two achromatic

doublets and one objective. The magnification after the first two lenses, according to geometrical optics considerations, is calculated to be $\times 1.50$. The objective magnification was measured outside the apparatus, when positioned at the end of the dark tube connected to the camera, to be $\times 4.57$ which brings the total magnification to $\times 6.86$. The atomic cloud image is captured by a back illuminated "iXon" DV887 camera with $> 90\%$ quantum efficiency sensor. Focus correction is enabled by adjusting the vertical position of the second lens with a translation stage. A kinematic mirror mount enables fine tuning of the imaging area.

We created several state-selective absorption imaging schemes to address diverse experimental needs. In Table 1.4, each scheme is described by the state it detects, its excited state, the laser frequency that is being used and the magnetic field at which it is resonant (B_{res}). Schemes #1 and #2 rely on the same excitations as the MOT (see Fig. 1.4) and they are good for zero magnetic field detection. The optical excitations of schemes #3 to #5 are discussed in Sec. 1.4.2 where they are used for magnetic field calibration (see Fig. 1.15). Schemes #6 and #7 employ optical transitions into the $|P_{3/2}, m_J = -1/2\rangle$ excited state, as can be seen in Fig. 1.19, where for convenience the excited state is shifted to the red by the optical transition frequency. The extra detuning of 160 MHz and 260 MHz (schemes #7 and #6, respectively) over the Repump frequency is achieved by manipulating AOM #9 (see lasers setup diagram in Fig. 1.2): in scheme #7 the 80 MHz AOM of scheme #1 is used, only this time with the $+1$ instead of the -1 diffraction order, and in scheme #6 it is replaced by a 180 MHz AOM.

By examining Fig. 1.19 one can notice the small angle at which the ground and excited states intersect each other. This fact makes these transitions unsuitable for magnetic field calibration purposes but it makes schemes #6 and #7 very good candidates for *in-situ* imaging because small changes in the beam's frequency are translated into large changes in B_{res}. In fact, the Repump laser beam can be easily detuned to the red by up to 80 MHz with AOM #3 (see Fig. 1.2 and Table 1.1 in Sec. 1.2.1) which allows for continuous *in-situ* imaging range that spreads over $\sim 170\ G$. We chose the frequency shifts of 160 MHz and

#	State detected	B_{res}	Beam used	Excited state	see Fig.
1	$\|F=1\rangle$	0	Repump	$\|P_{3/2}, F=2\rangle$	1.4
2	$\|F=2\rangle$	0	Pump	$\|P_{3/2}, F=3\rangle$	1.4
3	$\|F=1, m_F=-1\rangle$	289 G	Pump	$\|P_{3/2}, m_J=-3/2\rangle$	1.15
4	$\|F=1, m_F=0\rangle$	388 G	Pump	$\|P_{3/2}, m_J=-3/2\rangle$	1.15
5	$\|F=1, m_F=1\rangle$	488 G	Pump	$\|P_{3/2}, m_J=-3/2\rangle$	1.15
6	$\|F=1, m_F=1\rangle$	822 G	Repump+260 MHz	$\|P_{3/2}, m_J=-1/2\rangle$	1.19
7	$\|F=1, m_F=0\rangle$	983 G	Repump+160 MHz	$\|P_{3/2}, m_J=-1/2\rangle$	1.19

Table 1.4: State-selective imaging schemes.

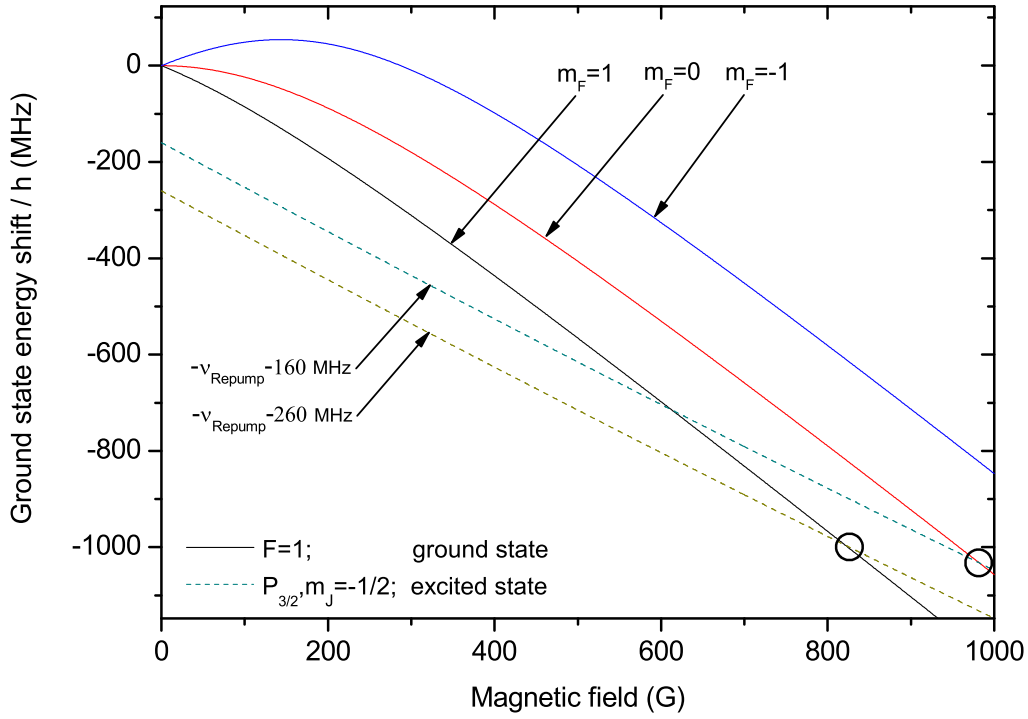

Figure 1.19: Energetic detuning of the $|S_{1/2}, F=1\rangle$ ground state sublevels (solid lines) and the $|P_{3/2}, m_J=-1/2\rangle$ sublevels branch of the excited state (dashed lines) as a function of magnetic field. The excited state appears twice for two different frequency shifts: $-(\nu_{Repump}+160\ MHz)$ and $-(\nu_{Repump}+260\ MHz)$ which are the frequencies used in detection schemes #7 and #6, respectively. Optical transitions are resonant in the crossing of excited and ground levels (circles).

260 MHz in schemes #7 and #6 so that B_{res} will be tunable across the magnetic fields of interest in our experiments. The mapping of a magnetic field value with a Repump detuning that will keep it in resonance is easy due to the fact that they change almost linearly in this regime. In practice, we find experimentally B_{res} for zero detuning and assign it as a reference magnetic field (B_{ref}). Then we measure the gradient at which the frequency changes as a function of magnetic field (∇^{ν}_{B}) and come up with the following formula:

$$\Delta\nu_{Repump} = \nabla^{\nu}_{B}(B_{ref} - B_{exp}), \tag{1.3}$$

where B_{exp} is the magnetic field at which the measurement is performed and $\Delta\nu_{Repump}$ is the Repump detuning required to make $B_{exp} = B_{res}$. The parameters for schemes #6 and #7 are summarized in Table 1.5. Note that B_{res} in Table 1.4 is actually the theoretical prediction of B_{ref}, however, they are slightly different by an amount equivalent to $\sim 5\ MHz$ which is of the order of the natural line-width of the excited state and therefore may be attributed to a small mistake in determining ν_{Repump} at zero magnetic field.

#	State detected	Magnetic field range of interest	AOM #9 configuration	B_{ref}	∇^{ν}_{B}
6	$\|F=1, m_F=1\rangle$	$700-780\ G$	$+180\ MHz$	$833\ G$	$0.485\ MHz/G$
7	$\|F=1, m_F=0\rangle$	$820-1000\ G$	$+80\ MHz$	$995\ G$	$0.476\ MHz/G$

Table 1.5: The parameters of Eq. (1.3) that are used for *in-situ* detection in schemes #6 and #7 of Table 1.4.

1.5.2 Image analysis

The detection light, propagating in z direction, is attenuated as it passes through the cloud of atoms due to its optical density (OD):

$$I_{x,y} = I^{0} \times e^{-OD_{x,y}}. \tag{1.4}$$

where I^0 is the beam's initial intensity. The OD relates to the 2D atomic density $n_{x,y}$ as follows:

$$OD_{x,y} = \sigma n_{x,y}, \tag{1.5}$$

with $\sigma = 3^*\lambda^2/(2\pi)$ being the in-resonance light scattering cross-section where λ is the light's wave length and 3^* is the angular average of the dipole operator which we use at a numerical value of $3^* = 1.5$.

Once $I_{x,y}/I^0$ is known, one can find $n_{x,y}$ and thus the atomic 2D distribution of which integration should give the number of atoms. However, due to interferences I^0 is not uniform across the detected area. Moreover, residual light which does not originate from the detection beam is captured by the camera's sensor and may bias this calculation. In order to address these concerns we derive $I_{x,y}/I^0_{x,y}$ out of three images. First we image the atoms with a light pulse which is typically 20 μs long. After a waiting time of 50 ms [8] at which the trap was turned off and the atoms have already left the detected area, a second image is taken with a light pulse similar to the one in the first image. 50 ms later a third image is captured in which the detection light remains off and exposure is made only to background light. Finally, $n_{x,y}$ is calculated in the following way:

$$n_{x,y} = \frac{1}{\sigma}\ln\frac{I_{x,y}}{I^0_{x,y}} = \frac{1}{\sigma}\ln\frac{Image^{\#1}_{x,y} - Image^{\#3}_{x,y}}{Image^{\#2}_{x,y} - Image^{\#3}_{x,y}}. \tag{1.6}$$

where x, y denotes a specific pixel in the images.

Each data unit x, y (pixel) thus represents an area A, in the large image, whose size is the pixel's length divided by the imaging magnification squared. In our setup $A = (16\mu m/6.86)^2 = 5.44\mu m^2$ and the number of atoms detected by each pixel is then $N_{x,y} = n_{x,y} \times A$. A naive calculation of the total number of atoms would be to integrate $N_{x,y}$ over all x, y units. However, since despite our efforts the first and second pulses of detection light are never identical, $N_{x,y}$ may be biased. To overcome this limitation we exploit the fact that the spacial distribution of atoms in a harmonic trap is Gaussian

[8] minimal time is 30 ms which is the iXon camera reading time.

and that the cigar-shaped trap is elongated along the x axis of the image. We integrate $N_{x,y}$ over x and y axes independently to receive two 1D arrays N_y and N_x, respectively, which are then fitted each with a Gaussian function. The atom number N is thus the area underneath the Gaussian and the background's bias is inherently set to zero. The calculation of N should give the same result for N_y and N_x, however we find the first to be usually more accurate. We also use the width of the Gaussian distribution of N_y for temperature calculations in time-of-flight measurements.

1.6 Evaporative cooling

1.6.1 Evaporative cooling near Feshbach resonances

Immediately after the atoms are loaded onto the optical dipole trap during the CMOT phase, they are optically pumped to the $|F = 1\rangle$ ground state (as discussed in Sec. 1.2.3) and are randomly distributed within its hyperfine sublevels. When the magnetic field is ramped up to high values we observe $\sim 50\%$ reduction in the atom number. Our state selective measurement shows that the remaining atoms are all on $|F = 1, m_F = 0\rangle$ state. We attribute this loss to spin-flip collisions between atoms on $|F = 1, m_F = -1\rangle$ and $|F = 1, m_F = 1\rangle$ states. The energy level splitting diagram of the $|F = 1\rangle$ state is shown in Fig. 1.20. A spin-flip collision that takes place at high magnetic fields flips the colliding atoms to $|F = 1, m_F = 0\rangle$ state and leaves them with an excess kinetic energy equals to $k_B \times 1.4\ mK$, which is comparable to the trap depth. Most of the atoms escape but we observe some increase in $|m_F = 0\rangle$ population. The opposite spin-flip process (two atoms at $|m_F = 0\rangle$ state collide and spin flip to $|m_F = 1\rangle$ and $|m_F = -1\rangle$ states) is forbidden

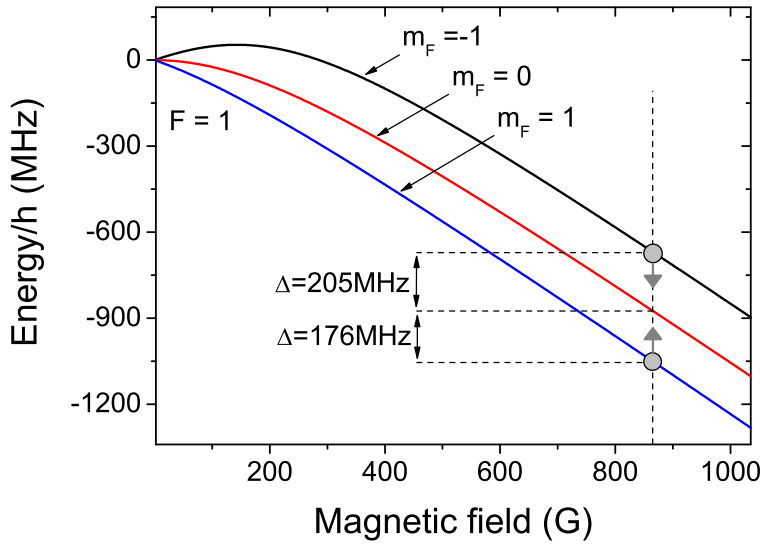

Figure 1.20: Energy level splitting of the $|F = 1\rangle$ hyper-fine state of ^{7}Li. With the presence of high magnetic fields, spin-flip collisions between $|m_F = -1\rangle$ and $|m_F = 1\rangle$ states result in their transfer into $|m_F = 0\rangle$ with an excess of kinetic energy equal to $h \times 29\ MHz$ ($\sim k_B \times 1.4\ mK$).

due to energy conservation reason. It requires an additional energy of $k_B \times 1.4\ mK$ which is absent when atoms are cooled down to $\sim 300\ \mu K$, thus $|m_F = 0\rangle$ state becomes stable against spin-exchange collisions at high magnetic fields. We therefore choose to perform the evaporative cooling process on this state.

The guiding principles for efficient evaporative cooling are: (1) aspire for high elastic-collisional-rate to accelerate rethermalization of the atoms, and (2) pursue the lowest inelastic-collisional-rates since they limit the evaporation duration time. Both types of collisional-rates enhance near Feshbach resonances since they depend on the atomic scattering length a which diverges there, as can be seen in Fig. 1.21 for $|m_F = 0\rangle$ which has two Feshbach resonances[9], one narrow and one broad, at 845 G and 894 G, respectively. With no prior knowledge about the exact inelastic losses expected in this regime

[9] A comprehensive investigation of these resonances can be found in Chapter 6.

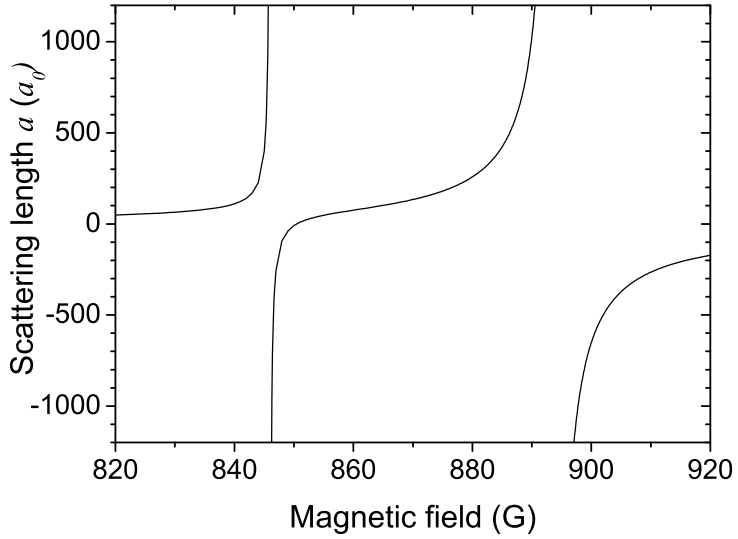

Figure 1.21: The two Feshbach resonances of the $|F = 1, m_F = 0\rangle$ state. a_0 is Bohr radius.

we determine the optimal magnetic field at which evaporation should be performed empirically. First, we conduct an experiment where the atoms are evaporatively cooled to a temperature of $\sim 70\ \mu K$ by ramping down the single-beam trap depth at two different paces: slow and fast. Measuring the remaining atoms number at the end of evaporation as a function of magnetic field gives an indication to the rate of inelastic collisions but also to the rate of elastic collisions since if rethermalization is not fast enough the hot atoms may escape the shallow trap, leading to truncation of the thermal distribution. The experiment is performed at evaporation duration times of 1.4 *sec* and 6 *sec* and the results are presented in Figures 1.22(a) and 1.22(b), respectively, where the two Feshbach resonances can be easily identified by the excessive losses in their vicinity. At a fast evaporation pace (Fig. 1.22(a)), the highest remaining atoms number is received for magnetic field values of $860 - 870\ G$ which may hint on high elastic collisions rates in between the resonances. However, at a slow evaporation pace (Fig. 1.22(b)), this area

shows poor results and the highest remaining atoms number is received for magnetic field values of $820 - 830\ G$. These results indicate that the inelastic losses rates are higher in between the resonances despite the comparable values of a. We further acknowledge this observation by another experiment that measures the remaining atoms number after a hold-time of 5 *sec* at different magnetic fields. The results here should be influenced solely by inelastic induced losses. As can be seen in Fig. 1.23(b) the magnetic field values to the left of the narrow resonance (lower values) indeed exhibit prolonged atomic lifetimes. We verify that the starting point of this measurement (initial atoms number) is uniform by a second experiment which uses a very short hold-time of 0.1 *sec* (Fig. 1.23(a)).

We thus empirically find that the magnetic field at which evaporation performs optimally is $\sim 830\ G$. Although Fig. 1.22 may suggest that similar results can be attained in between the resonances for short evaporation time durations, for lower temperatures we always get more atoms at the end of evaporation at $\sim 830\ G$.

1.6.2 The evaporation process

Evaporative cooling in an optical trap is accomplished by gradually attenuating the laser power, i.e. the trap's depth, in a rate that will allow the remaining atoms to rethermalize. Unfortunately, power attenuation also means reduction in the trap's oscillation frequencies and thus also in the atomic density which slows down the interatomic collisions rate. This inherent problem can be addressed by a trap-tilt based evaporation [38] or by employing a telescopic trap [23] whose waist narrows along with the reduction in power. The decreasing trap volume increases the atomic density which enhances the collisions rate and keeps rethermalization effective. We employ a different solution. In order to decrease the trap's volume we add a second beam at an advanced stage of the evaporation process and turn the single-beam-trap into a crossed-beam (setup details in Sec. 1.3).

We start with a single-beam trap at 100% of its laser power ($\sim 60\ W$) that holds $\sim 10^6$ atoms at a temperature of 300 μK when loaded from the MOT (see Sec. 1.2.3). Table 1.6 specifies the parameters of the different evaporative cooling stages from the initial loading

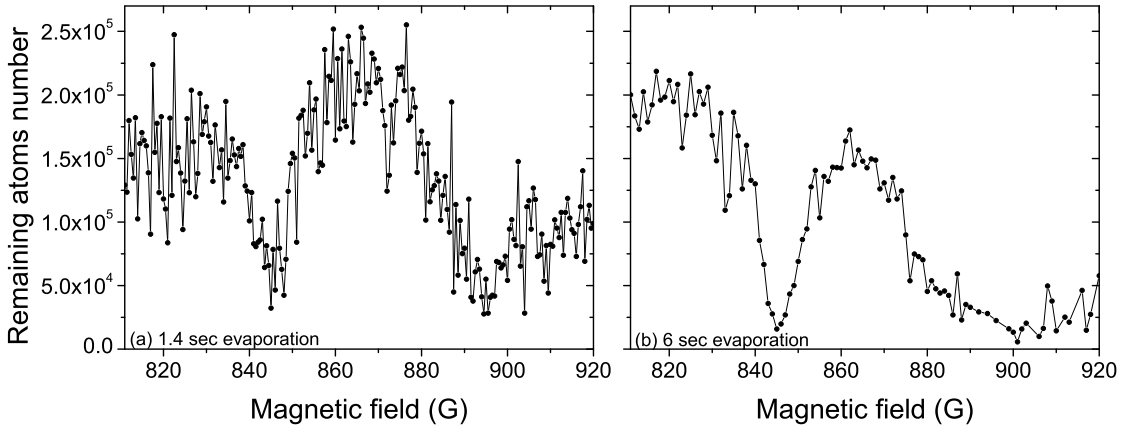

Figure 1.22: Evaporation performed on the $|F = 1, m_F = 0\rangle$ state at different duration times of 1.4 *sec* (a) and 6 *sec* (b). The two Feshbach resonances can be easily identified by the excessive losses in their vicinity.

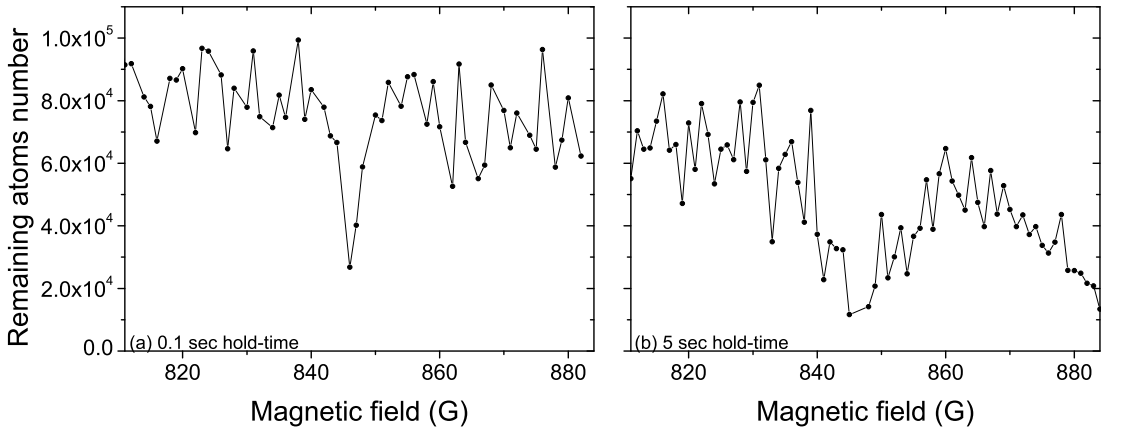

Figure 1.23: Remaining atoms number after a hold-time of 0.1 *sec* (a) and 5 *sec* (b) at different magnetic fields on the $|F = 1, m_F = 0\rangle$ state.

(step #0) up to atomic degeneracy threshold. After ramping the bias magnetic field B to 824 G the first step of evaporation begins at which the laser is attenuated to 45% of its power during 3 seconds (step #1). The change in laser power is made according to *the exponential ramp function* (see Appendix A) which receives an initial power value P_i, a final power value P_f, a time duration Δt and a change rate α. Here, each step's P_f is P_i of the step that follows it and power is expressed as percentages from the maximum power ($\sim 60\ W$ for both beams). Also shown in Table 1.6 are the atoms number N and density n, the temperature T and the phase-space density ρ at the end of each evaporation step. Step #2 is a transition stage between a single-beam to a crossed-beam trap. At the end of step #3 the trap oscillation frequencies are approximately 1.5 KHz and 200 Hz for the radial and longitudinal axes, respectively. By extending step #3 to even lower values of laser beam powers we were able to reach a Bose-Einstein condensation of $\sim$ 20000 atoms.

Step	B	Main-beam		Secondary-beam		Δt	N	n	T	ρ
	(G)	P_f	α	P_f	α			(cm^{-3})	(μK)	
#0	0	100%	$-$	0	$-$	$-$	10^6	10^{12}	300	6×10^{-5}
#1	824	45%	+6	0	$-$	3 s	5×10^5	10^{12}	80	4×10^{-4}
#2	824	22%	+8	60%	-8	3 s	5×10^5	4×10^{12}	80	2×10^{-3}
#3	832	0.85%	+2	5%	+2	8 s	10^5	4×10^{12}	1.5	0.6

Table 1.6: The different stages of evaporation from initial loading of the trap up to the atomic degeneracy threshold. B - magnetic field; P_f - final power value; α - change rate; Δt - time duration; N - atoms number; n - atomic density; T - temperature; ρ - phase-space density.

Chapter 2

Article: All optical production of ^{7}Li Bose-Einstein Condensation using Feshbach resonances

Noam Gross and Lev Khaykovich

Physical Review A

Volume 77, page 023604, February 2008

All-optical production of ^{7}Li Bose-Einstein condensation using Feshbach resonances

Noam Gross and Lev Khaykovich
Department of Physics, Bar-Ilan University, Ramat-Gan, 52900 Israel
(Received 5 December 2007; published 4 February 2008)

We show an all-optical method of making ^{7}Li condensates using the tunability of the scattering length in the proximity of a Feshbach resonance. We report the observation of two Feshbach resonances on the $|F=1,m_F=0\rangle$ state. A narrow (broad) resonance of 7 G (34 G) width is detected at 831 ± 4 G (884^{+4}_{-13} G). The position of the scattering length zero crossing between the resonances is found at 836 ± 4 G. The broad resonance is shown to be favorable for runaway evaporation which we perform in a crossed-beam optical-dipole trap. Starting directly from the phase-space density of a magneto-optical trap we observe a Bose-Einstein condensation threshold in less than 3 s of forced evaporation.

DOI: 10.1103/PhysRevA.77.023604 PACS number(s): 67.85.Hj, 34.50.Cx, 37.10.De

I. INTRODUCTION

Achieving quantum degeneracy in ultracold atomic gases by all-optical means has become a well-accepted experimental technique because of several inherent advantages [1–7]. Optical traps allow strong confinement, resulting in high collision rates and rapid evaporative cooling. Confinement of arbitrary spin states and spin state mixtures is readily obtained. The possibility to tune interactions via Feshbach resonances usually requires optical trapping as they frequently occur in states that cannot be trapped magnetically [8,9]. Finally, large current coils needed for magnetic-field trapping that restrict optical access are avoided.

The first successful demonstration of an all-optically achieved ^{87}Rb Bose-Einstein condensation (BEC) allowed a significant increase in the rate of BEC production and the resulting condensates were $F=1$ spinors [1]. However, the main driving force behind the search for all-optical techniques was the need to condense specific atoms where "conventional" evaporation in the magnetic trap was not possible. Two prominent examples are spinless, and thus magnetically untrappable, BECs of Yb atoms achieved in a doubled YAG crossed dipole trap [2] and a BEC of ^{133}Cs atoms [3] for which the strongly enhanced two-body losses from the magnetically trappable states prevent condensate formation in the "standard" way [10].

Although ^{7}Li atoms can be evaporatively cooled in a magnetic trap [11], the task remains challenging due to several reasons. First, ^{7}Li atoms posses a relatively small scattering length ($a=-27a_0$, where a_0 is the Bohr radius) and a high two-body loss rate [12]. Second, the initial phase-space density is unfavorably limited by the absence of a polarization-gradient cooling mechanism. Third, since the scattering length drops with increased temperature and crosses zero at $T=8$ mK [13], the use of adiabatic compression to increase the elastic collisional rate is ineffective. Therefore, the strong magnetic confinement needed to keep the evaporation time comparable with heavier alkali metals, such as Rb and Na, requires the design of a miniaturized trap. This is done by either a small-volume vacuum chamber and high currents [14] or a vacuum-compatible minitrap [15] which both increase the experimental complexity. Finally, even if the strong confinement is achieved, the scattering length is still negative which prevents the formation of a stable BEC.

In this paper we show an all-optical way to condense ^{7}Li atoms using tunable interatomic interactions. We use a 100-W ytterbium fiber laser to produce a ~2-mK potential well which traps $\sim10^6$ atoms from a magneto-optical trap (MOT). We explore two Feshbach resonances on the $|F=1,m_F=0\rangle$ state and find that one of them is favorable for efficient forced evaporation starting directly from a phase-space density achieved in the MOT. We obtain a BEC on the $|F=1,m_F=0\rangle$ internal state in less than 3 s of evaporation time.

II. EXPERIMENTAL DETAILS

The ^{7}Li atoms' route to quantum degeneracy starts in an oven where they are heated up to 450 °C to increase their vapor pressure. An atomic beam is collimated by two distant apertures and slowed down in an increased magnetic field Zeeman-slower. The capture velocity of the slower is set to ~800 m/s.

Our MOT design and parameters are similar to that described in Ref. [16]. After a loading time of 3 s, the trap contains $\sim10^9$ atoms at a temperature of 1.2 mK. Trap lifetime, limited by a vacuum, is measured to be 10 s. The MOT parameters, such as pump and repump detunings and magnetic field gradient, are optimized to maximize the number of atoms. To improve the initial phase-space density we implement a so-called compressed MOT (CMOT) stage [16,17]. For 50 ms the laser intensities are attenuated, detunings are decreased, and the magnetic field gradient is increased. As a result the temperature is reduced to 300 μK and nearly half of the atoms are lost. By the end of this phase $\sim5\times10^8$ atoms are left in the trap with a density of $n=4\times10^{11}$ atoms/cm^3 and a phase-space density of $\rho=2\times10^{-5}$.

The realization of the optical-dipole trap is shown in Fig. 1. A cw ytterbium fiber laser (IPG Fibertech) generates 100 W of linearly polarized light at 1.07 μm with a bandwidth of 2.83 nm. The first-order diffraction beam of an acousto-optic modulator (AOM), with 80% diffraction efficiency, is focused at the center of the MOT to a waist of 31 μm. The zeroth-order diffraction beam is only weakly focused to

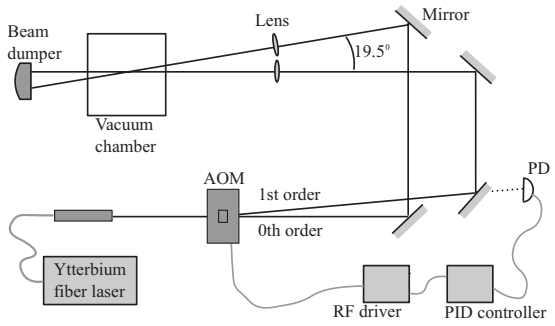

FIG. 1. A schematic representation of the optical-dipole trap experimental setup. The first-order diffraction beam is focused to a waist of 31 μm and aligned to the MOT center. The zeroth-order beam is weakly focused to 300 μm. It crosses the first-order beam at an angle of 19.5° and it only becomes important at the final stages of evaporation. AOM: acousto-optic modulator. PD: photodetector.

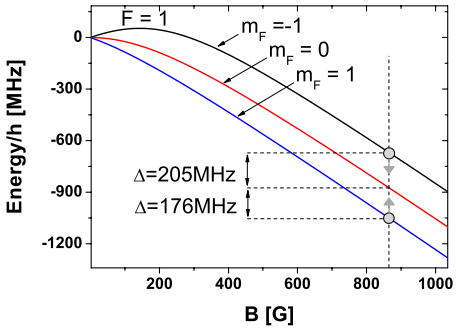

FIG. 2. (Color online) Energy-level splitting of the $|F=1\rangle$ hyperfine state of ^{7}Li atoms. With the presence of high magnetic fields, spin-flip collisions between $|m_F=-1\rangle$ and $|m_F=1\rangle$ states result in their transfer into $|m_F=0\rangle$ with an excess of kinetic energy equal to $h\times 29$ MHz ($\sim K_B\times 1.4$ mK).

300 μm, and it crosses the first-order beam at an angle of 19.5°. When maximum rf power is applied to the AOM this beam is very weak and it has no effect on the atoms. At full laser power (65 W in the trap region) the trap depth, produced by the first-order diffraction beam, is estimated to be ~ 2 mK. Oscillation frequencies in the trap are predicted to be $\omega_r=2\pi\times 16$ kHz and $\omega_z=2\pi\times 120$ Hz for the radial and longitudinal directions, respectively. The radial oscillation frequency was measured by the parametric driving technique and found to be in excellent agreement with the predicted one. We keep the first-order diffraction beam at its full power throughout the MOT loading time, and atoms are loaded into the dipole trap mainly during the CMOT phase. Mechanical shutters are then used to block all resonant light from reaching the trapped atoms. The MOT pump beam, associated with the $|F=2\rangle$ ground state, is blocked only a few milliseconds later to allow a 1-ms optical pumping pulse, effectively transferring all atoms into the $|F=1\rangle$ ground state. Eventually, we are left with $\sim 10^6$ trapped atoms. Phase-space density conditions are similar to those resulted from the CMOT phase.

We note that the loading efficiency of the optical trap from the CMOT is rather poor due to the small spatial overlap between the two traps. Even for 100 W laser power the high initial temperature of the ^{7}Li atoms oblige a tight focusing of the beam in order to create a deep enough potential. This makes the use of a compressible crossed dipole trap to improve the loading conditions impractical [5].

III. DETECTION OF FESHBACH RESONANCES ON THE $|F=1,m_F=0\rangle$ STATE

The scattering length of ^{7}Li atoms on all sublevels and sublevel mixtures of the $|F=1\rangle$ ground state at zero magnetic field is positive but very small ($\sim 10a_0$), impeding efficient evaporation cooling. However, each sublevel and their mixtures possess at least one Feshbach resonance [18]. The resonance on the absolute ground state $|F=1,m_F=1\rangle$ has been previously used for the final stage of forced evaporation in an optical trap after precooling in a magnetic trap [19,20]. The resonances on other sublevels or their mixtures were neither reported nor used before.

The search for Feshbach resonances requires high offset magnetic fields. We use two pairs of Helmholtz coils that allow variable-bias fields of up to 1200 G. When the magnetic field is ramped up to high values we observe a $\sim$50% reduction in atom number. Our state-selective measurement shows that the remaining atoms are all on the $|F=1,m_F=0\rangle$ state. We attribute this loss to spin-flip collisions between atoms on $|F=1,m_F=-1\rangle$ and $|F=1,m_F=1\rangle$ states. The energy-level splitting diagram of the $|F=1\rangle$ state is shown in Fig. 2. A spin-flip collision that takes place at high magnetic fields flips the colliding atoms to the $|F=1,m_F=0\rangle$ state and leaves them with an excess of kinetic energy equal to $K_B\times 1.4$ mK, which is comparable to the trap depth. Most of the atoms escape, but we observe some increase in the $|m_F=0\rangle$ population. Detection of losses and spontaneous spin polarization are the first manifestations of the increase in collisional cross section. As the $|m_F=0\rangle$ state is stable against spin-exchange collisions at high magnetic fields, we search for signatures of Feshbach resonances on this state.

Figure 3(a) shows a theoretical prediction of the scattering length as a function of bias magnetic field. Two Feshbach resonances between 800 G and 900 G are indicated by the divergence of the scattering length. Experimentally, the resonances are usually observed by the detection of atom loss as in their proximity the inelastic collisional rate is strongly enhanced [21,22]. For this measurement we ramp up the magnetic field to different values in 40 ms and wait 0.5 s before decreasing it to 386 G in 40 ms where *in situ* state-selective absorption imaging is performed. In Fig. 3(b) the atom number as a function of bias magnetic field is shown. The atoms are initially prepared at a temperature of 300 μK. Strong losses are observed around 830 G and 880 G featuring a narrow and a broad structure. By fitting them with simple Gaussian functions, a coarse estimation of the resonances locations and widths can be determined. According to the fit, the narrow resonance is 7 G wide ($1/e^2$ radius) and it is located at 831 ± 4 G. The uncertainty in its position is due to an uncertainty in the magnetic field calibration which is obtained by the detection of optical resonances and thus lim-

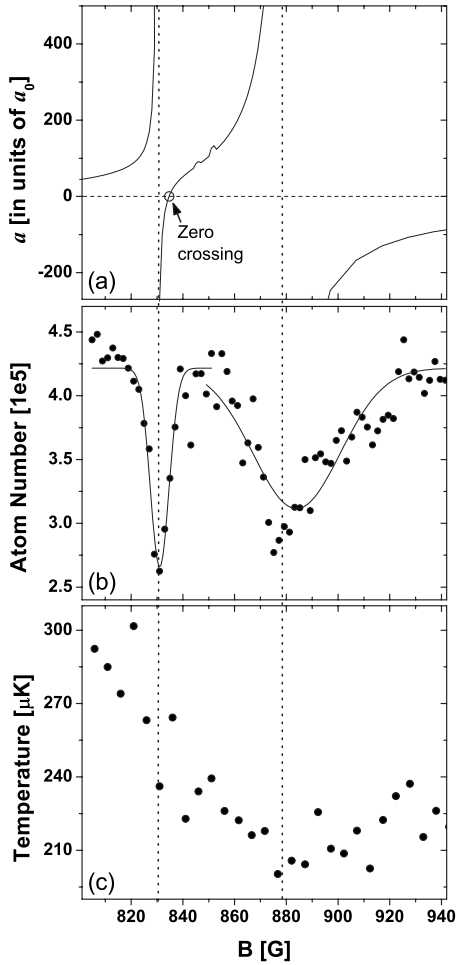

FIG. 3. (a) Theoretical predictions for the scattering length as a function of bias magnetic field in the $|F=1,m_F=0\rangle$ state [18]. Divergence of the scattering length signify the presence of two Feshbach resonances. (b) The resonances are detected by measuring atom loss due to inelastic collisions. The solid lines are Gaussian fits to define the resonance positions. Note that the maximal loss does not coincide with the minimum of the Gaussian fit for the broad resonance. (c) Temperature of the atomic cloud in the optical trap as a function of bias magnetic field. Decrease in temperature indicates cooling by free evaporation.

ited by the linewidth of the excited states and the laser locking quality. The broad resonance located at 884^{+4}_{-13} G is 34 G wide and features a notable asymmetric profile which tends to shift the center of a simple Gaussian fit to a higher magnetic field value as compared to the maximal loss position (detected at 875 G). Such an asymmetry in losses in the vicinity of broad Feshbach resonances has been recently reported for ^{39}K atoms [23] and was attributed to a larger three-body loss coefficient from the negative-scattering-length side of the resonance and mean-field effects. The study followed of molecule association showed that the position of a broad Feshbach resonance is indeed shifted to a lower value [23]. Comparison between the experimental measurements [Fig. 3(b)] and the theoretical calculations [Fig. 3(a)] shows that the maximal loss position suits better the predicted distance between the two resonances. We therefore believe that the actual location of the broad resonance is at a somewhat lower value than that given by the Gaussian fit and this systematic error increases the error bars of the experimentally detected resonance position.

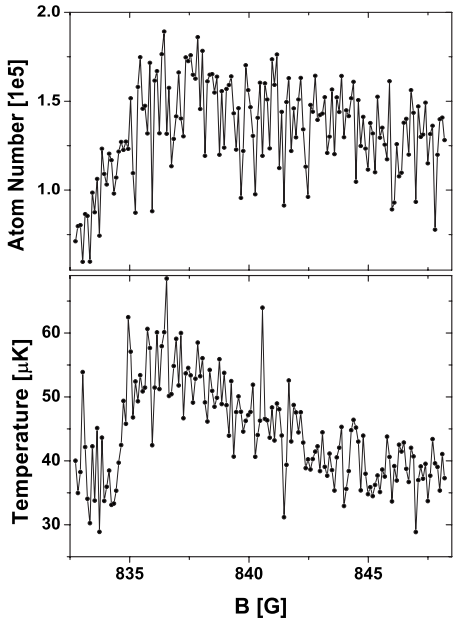

FIG. 4. The gain in atom number and increase in temperature, which indicate the lack of free evaporation cooling, reveal the zero crossing of the scattering length at 836 ± 4 G.

Most excitingly, we observe an onset of free evaporation cooling together with the enhanced inelastic losses [Fig. 3(b)]. In Fig. 3(c) we show the temperature change as a function of the bias magnetic field. A decrease in the temperature indicates cooling which we attribute to the establishment of free evaporation when the collision rate becomes high enough. The observed cooling allows us to decrease the temperature by forced evaporation and then scan for Feshbach resonances, again to improve sensitivity.

We execute a short forced evaporation of 1.5 s, reducing the trap depth to 0.3 mK, 15% of its initial value. Evaporation is performed with a bias field of 850 G which is chosen to optimize the number-to-temperature ratio based on our scans for Feshbach resonances at high temperature [Figs. 3(b) and 3(c)]. By the end of this evaporation the atoms are cooled down to a temperature of ~ 50 μK. Our scan for inelastic losses in proximity to Feshbach resonances reveals the same positions of the resonances observed before including asymmetry in the profile of the broad resonance. However, an additional feature has been identified which we were unable to detect at high temperature. In Fig. 4, zero crossing of the scattering length manifests itself in terms of an increased temperature and number of atoms [24]. The hold time at high bias field for this experiment is 0.5 s. During this time efficient free evaporation reduces the temperature to 40 μK if the collisional cross section is high enough. At zero crossing the scattering length vanishes and so does the cross section, impeding efficient free evaporation. The asymmetry in this measurement is caused by the proximity of the zero-crossing point to the narrow resonance at 831 G. The

zero-crossing point is detected at 836 ± 4 G where the maximum temperature is observed.

IV. EVAPORATION COOLING TO THE BEC THRESHOLD

Forced evaporation cooling of the optically trapped atoms down to the BEC threshold is performed by attenuating the laser power, thus reducing the trap depth which scales linearly with the power reduction factor α. A photodiode detector, located behind one of the mirrors, collects a fraction of the trap beam's power (see Fig. 1). It generates a voltage readout that is compared to a set-point signal by a PID controller. An error signal is fed back to the rf-power supplier of the AOM. With this scheme we are able to control trap depth reduction up to a factor of $\alpha = 3 \times 10^{-3}$. As is well known, trap oscillation frequencies also decrease with the attenuation of laser power ($\propto \sqrt{\alpha}$), affecting the rethermalization efficiency throughout the evaporation process. In addition to that, the strong bias magnetic field, employed during evaporation, creates a weak antitrapping potential in the longitudinal direction. This decreases further the optical confinement toward the end of the evaporation. Indeed, in a single-beam trap we were unable to cool atoms below a temperature of 10 μK. The addition of a zeroth-order diffraction beam solves this problem. At the beginning of the evaporation it has no effect on the atoms as its potential depth is negligible. However, with the reduction of the first-order diffraction intensity, it strengthens to create a confinement potential to the atoms in the longitudinal direction of the trap. The longitudinal oscillation frequency, determined by the confining beam, is $2\pi \times 60$ Hz. The zeroth-order beam can be effectively considered as a two-dimensional confining potential because it produces a very weak (0.14 Hz) oscillation frequency in its propagation direction which is easily overcome by the magnetic antitrapping potential. We note also that the crossed trap is slightly shifted from the location of the zeroth-order beam waist which reduces somewhat the potential at the end of the evaporation.

Forced evaporation is found to work most effectively when the bias field is set to 866 G. Based on the theoretical curve [Fig. 3(a)] we estimate the scattering length to be $(300 \pm 100)a_0$. The large uncertainty in the scattering length is due to the uncertainty in the position of the broad resonance. The trap depth is reduced exponentially in 3 s with a time constant of 330 ms to less than 0.5% of its initial value. In Fig. 5, *in situ* absorption imaging of the trapped atoms at 866 G reveals the onset of a BEC threshold by a familiar bimodal density distribution. The trace represents the atom longitudinal density after integrating the radial direction of the picture above it. Optical resolution is 4 μm, less than the size of the BEC. The thermal atomic cloud is fitted with a Bose-Einstein distribution function which reveals a temperature of $T = 380 \pm 40$ nK. The total number of atoms is 6×10^3 which sets the critical temperature to $T_c = 350$ nK. The fitting of the BEC with an inverted parabola reveals

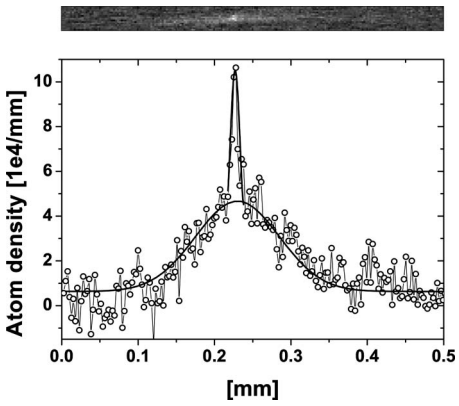

FIG. 5. Onset of BEC. *In situ* absorption imaging of atoms at the BEC threshold. The thermal atomic cloud is fitted with a Bose-Einstein distribution function which yields a temperature of 380 ± 40 nK. The number of atoms in the BEC is ~700.

~700 atoms in the condensate with a Thomas-Fermi radius of 11 μm.

V. CONCLUSIONS

To conclude, we developed a method to all-optically condense ^{7}Li atoms. This way facilitates the BEC production which is extremely demanding in magnetic traps. We observed a BEC with repulsive interactions on the $|F=1, m_F=0\rangle$ state in less than 3 s of forced evaporation in a crossed-beam optical-dipole trap. We use the tunability of the interatomic interactions in the proximity of Feshbach resonances which we observed and characterized for this internal state.

We note that the condensate lifetime was very short (a few tenths of ms), presumably because of the extremely large scattering length. Moreover, our weak optical trap at the end of the evaporation was not stable enough due to the use of a single linear photodiode detector. A number of improvements can be implemented to optimize the performance of the described method. Better laser beam stability, which can be achieved by using either two detectors [7] or a logarithmic detector, and a decrease of the scattering length toward the end of evaporation will improve the condensate lifetime. An improved vacuum would allow an increase in the number of atoms in the condensate.

ACKNOWLEDGMENTS

We thank S. Kokkelmans for providing us with theoretical calculations of Feshbach resonances on all sublevels of the ^{7}Li lower hyperfine state. This work was supported, in part, by the Israel Science Foundation, through Grant No. 1125/04.

[1] M. D. Barrett, J. A. Sauer, and M. S. Chapman, Phys. Rev. Lett. **87**, 010404 (2001).
[2] Y. Takasu, K. Maki, K. Komori, T. Takano, K. Honda, M. Kumakura, T. Yabuzaki, and Y. Takahashi, Phys. Rev. Lett. **91**, 040404 (2003).
[3] T. Weber, J. Herbig, M. Mark, H.-C. Nägerl, and R. Grimm, Science **299**, 232 (2003).
[4] S. R. Granade, M. E. Gehm, K. M. O'Hara, and J. E. Thomas, Phys. Rev. Lett. **88**, 120405 (2002).
[5] T. Kinoshita, T. Wenger and D. S. Weiss, Phys. Rev. A **71**, 011602(R) (2005).
[6] R. Dumke, M. Johanning, E. Gomez, J. D. Weinstein, K. M. Jones, and P. D. Lett, New J. Phys. **8**, 64 (2006).
[7] J. Fuchs, G. J. Duffy, G. Veeravalli, P. Dyke, M. Bartenstein, C. J. Vale, P. Hannaford, and W. J. Rowlands, J. Phys. B **40**, 4109 (2007).
[8] E. Timmermans, P. Tommasini, M. Hussein, and A. Kerman, Phys. Rep. **315**, 199 (1999).
[9] R. A. Duine and H. T. C. Stoof, Phys. Rep. **396**, 115 (2004).
[10] J. Söding, D. Guéry-Odelin, P. Desbiolles, G. Ferrari, and J. Dalibard, Phys. Rev. Lett. **80**, 1869 (1998).
[11] C. C. Bradley, C. A. Sackett, J. J. Tollett, and R. G. Hulet, Phys. Rev. Lett. **75**, 1687 (1995).
[12] E. R. I. Abraham, W. I. McAlexander, J. M. Gerton, R. G. Hulet, R. Côté, and A. Dalgarno, Phys. Rev. A **55**, R3299 (1997).
[13] J. Dalibard, in *Bose-Einstein Condensation in Atomic Gases*, Proceedings of the International School of Physics "Enrico Fermi," Course CXL, edited by M. Inguscio, S. Stringari, and C. Wieman (IOS Press, Amsterdam, 1999).
[14] F. Schreck, G. Ferrari, K. L. Corwin, J. Cubizolles, L. Khaykovich, M.-O. Mewes, and C. Salomon, Phys. Rev. A **64**, 011402(R) (2001).
[15] R. Wang, M. Liu, F. Minardi, and M. Kasevich, Phys. Rev. A **75**, 013610 (2007).
[16] U. Schünemann, H. Engler, M. Zielonkowski, M. Weidemüller, and R. Grimm, Opt. Commun. **158**, 263 (1998).
[17] M.-O. Mewes, G. Ferrari, F. Schreck, A. Sinatra, C. Salomon, Phys. Rev. A **61**, 011403(R) (1999).
[18] S. J. J. M. F. Kokkelmans (private communication).
[19] L. Khaykovich, F. Schreck, G. Ferrari, T. Bourdel, J. Cubizolles, L. D. Carr, Y. Castin, and C. Salomon, Science **296**, 1290 (2002).
[20] K. E. Strecker, G. B. Partridge, A. G. Truscott, and R. G. Hulet, Nature (London) **417**, 150 (2002).
[21] P. O. Fedichev, M. W. Reynolds, and G. V. Shlyapnikov, Phys. Rev. Lett. **77**, 2921 (1996).
[22] S. Inouye, K. B. Davis, M. R. Andrews, J. Stenger, H.-J. Miesner, D. M. Stamper-Kurn, and W. Ketterle, Nature (London) **392**, 151 (1998).
[23] C. D'Errico, M. Zaccanti, M. Fattori, G. Roati, M. Inguscio, G. Modugno, and A. Simoni, New J. Phys. **9**, 223 (2007).
[24] K. M. O'Hara, S. L. Hemmer, S. R. Granade, M. E. Gehm, J. E. Thomas, V. Venturi, E. Tiesinga, and C. J. Williams, Phys. Rev. A **66**, 041401(R) (2002).

Chapter 3

Theoretical background to Efimov physics

3.1 Low-energy two-body physics

The interatomic potential V_r between two neutral atoms in their ground states is usually referred to, for reasons of convenience, as a short-range potential. However, for real atoms it also consists of a long-range tail provided by the van der Waals interaction [1]:

$$V_r \to \frac{C_6}{r^6}, \qquad as\ r \to \infty, \tag{3.1}$$

where r is the relative coordinate. For identical atoms with mass m, the coefficient C_6 determines a length scale called the van der Waals length:

$$l_{vdW} = (mC_6/\hbar^2)^{1/4} \tag{3.2}$$

also known as the natural low-energy length scale for atoms since at sufficiently low energy, where the de Broglie wavelength λ_{dB} is much larger than l_{vdW}, the interactions between atoms are dominated by the van der Waals interaction. The binding energy of the shallowest 2-body bound state is expected to be of order $E_{vdW} = \hbar^2/2ml_{vdW}^2$ or larger.

Now let us consider a different bound state, one that has an energy E_c and is a molecular bound state of a different potential curve V_c (see Fig. 3.1). When the relative magnetic moment between the bound state and the free atoms $\delta\mu$ is non-zero, E_c can be controlled by an external magnetic field B (via Zeeman shift) as follows:

$$E_c = \delta\mu(B - B_c), \tag{3.3}$$

with $B = B_c$ being the magnetic field at which the molecular bound state reaches the free-atoms continuum (dashed line in Fig. 3.1). The story gets interesting when E_c is smaller than E_{vdW}. Then, two cold atoms scattered by the open channel potential V_r resonantly couple to the closed channel V_c which leads to strong mixing between the two channels, a phenomenon known as Feshbach resonance [2]. The bound state is then dominated by the open channel and its characteristic size is the s-wave scattering length a [17], which is given by [39]:

$$a(B) = a_{bg}(1 - \frac{\Delta}{B - B_0}), \tag{3.4}$$

where a_{bg} is the background scattering length and Δ and B_0 are the Feshbach resonance's width and position[1], respectively. In this Feshbach coupling regime the binding energy of the "dressed" molecular state takes the form

$$E_b = \hbar^2/ma^2. \tag{3.5}$$

[1]Note that B_0 is offset relative to B_c [40]

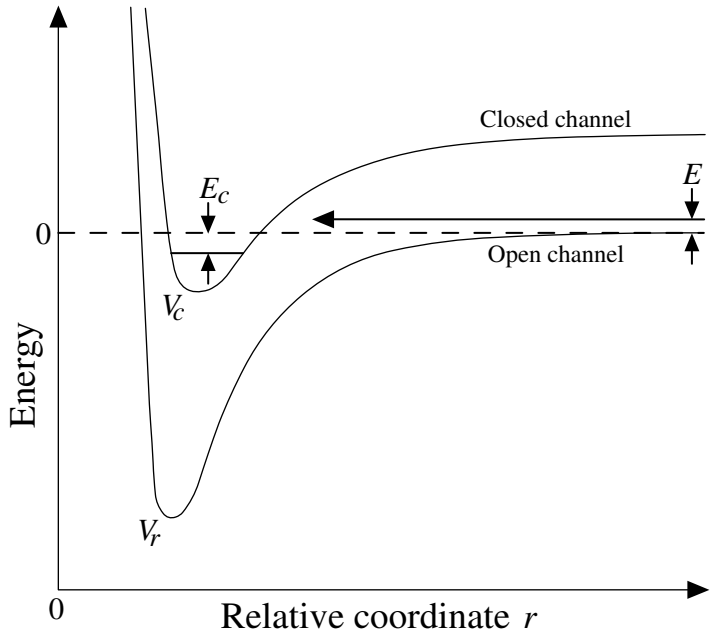

Figure 3.1: Basic two-channel model for a Feshbach resonance. V_r - the background open channel potential; V_c - the closed channel potential; E - the free atoms kinetic energy; E_c - the molecular state binding energy;

3.2 Universality of Feshbach molecules

Universality in the two-body domain is the ability to fully describe a quantum system by a single parameter, namely the two-body scattering length a. When a is large enough, atoms have universal low-energy properties that do not depend on the details of their structure or their short-range interactions. With this definition, we can determine that the Feshbach molecules whose binding energy E_b is given by Eq. (3.5) are clearly universal. The regime outside the Feshbach interaction is non-universal since the molecular binding energy, given by Eq. (3.3), cannot be derived from mere knowledge of a.

Fig. 3.2(a) shows the scattering length a as a function of magnetic field near the Feshbach resonance of the absolute ground state $|F = 1, m_F = 1\rangle$ of ^{7}Li. Below it in

Fig. 3.2(b), the binding energy of the associated molecular state is depicted under a mutual horizontal axis. A vertical dashed line represents the resonance's position ($\sim 738\ G$). One can see that close to the resonance the binding energy takes the parabolic universal form of Eq. (3.5) whereas at lower values of magnetic field it asymptotically converges into the linear change rate of Eq. (3.3) where it is no longer universal.

Very close to a Feshbach resonance the molecular binding energy has the following form [2]:

$$E_b = \frac{\hbar^2}{m(a - \bar{a} + R^*)^2}, \tag{3.6}$$

where m is the atomic mass and $\bar{a}$ and R^* accounts for a finite range and a resonance strength corrections to the universal $1/a^2$ law, respectively. $\bar{a}$ is the mean scattering length which is an alternative van der Waals length scale [41], and $R^* = \hbar^2/(m a_{bg} \Delta(\delta\mu))$ [42]. From Eq. (3.6) a condition for universality can be retrieved: it is valid only when $a \gg \bar{a}$ and R^* [2]. Finite temperature imposes an upper-bound limit to universality since a Feshbach molecule cannot extend beyond the size of λ_{dB}. The condition for universality of two-body interactions can thus be expanded to:

$$\lambda_{dB} \gg a \gg \bar{a}\ and\ R^*. \tag{3.7}$$

[2]We note that for narrow resonances R^* can be uncharacteristically large which makes them closed channel dominated with a universal regime limited only for a very narrow region in the vicinity of the Feshbach resonance.

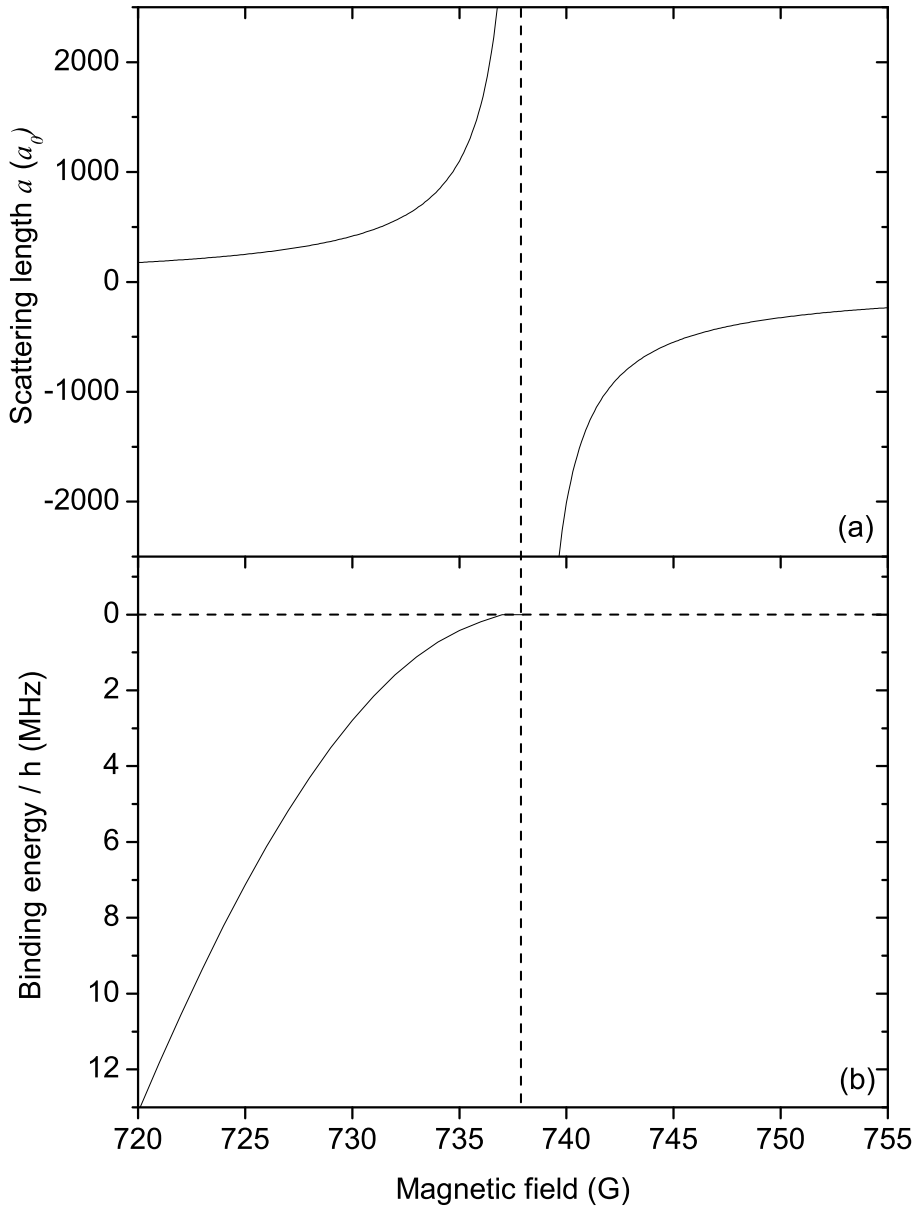

Figure 3.2: (a) The scattering length a as a function of magnetic field around the Feshbach resonance of the absolute ground state $|F = 1, m_F = 1\rangle$ of ^{7}Li (a_0 is Bohr radius); (b) The binding energy of the associated molecular state. A vertical dashed line represents the resonance's position ($\sim 738\ G$).

3.3 Efimov trimers

Universality in the three-body domain means the emergence of weakly bound three-body states known as Efimov trimers when $a \gg l_{vdW}$ [1]. The Schrödinger equation for the stationary wave function $\Psi(r1, r2, r3)$ of three atoms with mass m interacting through a potential V is:

$$\left(-\frac{\hbar^2}{2m}\sum_{i=1}^{3}\nabla_i^2 + V(r1, r2, r3)\right)\Psi = E\Psi. \tag{3.8}$$

Using the adiabatic hyperspherical approximation [43], this equation can be reduced to a 1D equation:

$$\left[\frac{\hbar^2}{2m}\left(-\frac{\partial^2}{\partial R^2} + \frac{15}{4R^2}\right) + V_n(R)\right] f_n(R) = E f_n(R) \tag{3.9}$$

where R is the *hyperradius* which is the root-mean-square separation of the atom pairs:

$$R^2 = \frac{1}{3}\left(r_{12}^2 + r_{23}^2 + r_{31}^2\right), \tag{3.10}$$

$V_n(R)$ is the n^{th} hyperspherical potential and $f_n(R)$ is the hyperradial wavefunction that is associated with it. A rigorous calculation performed by V. Efimov shows that the deepest hyperspherical potential $V_0(R)$ has a form of an attractive $1/R^2$ potential for $|a| \gg R \gg l_{vdW}$, given by [1]:

$$V_0(R) = -(4 + s_0)\frac{\hbar^2}{2mR^2}, \tag{3.11}$$

where $s_0 \approx 1.00624$. For $R > |a|$ this effective potential is no longer attractive. Other potentials $V_n(R)$ for $n \geq 1$ are repulsive $1/R^2$ potentials in the region $R \ll |a|$.

In the limit of $a \to \pm\infty$ and zero temperature the Efimov potential $V_0(R)$ can support an infinite number of three-body bound states known as Efimov states. The spatial extent A_N and binding energy E_N of the N^{th} lowest Efimov state are connected by simple scaling lows:

$$A_N = \beta^N \times \frac{1}{k_*}\sqrt{\frac{2(1 + s_0)}{3}} \tag{3.12}$$

and

$$E_N = \beta^{2N} \times \frac{\hbar^2 k_*^2}{m}; \quad (a = \pm\infty), \tag{3.13}$$

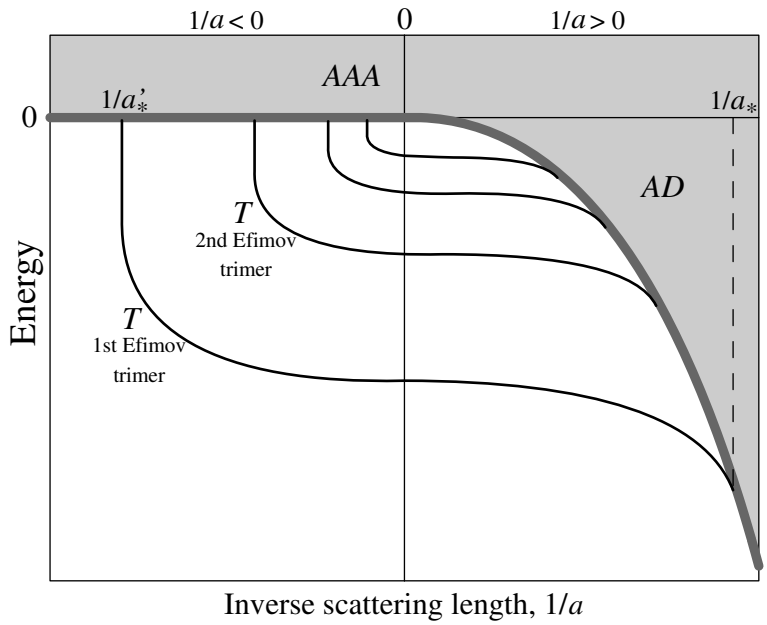

Figure 3.3: Efimov's scenario. Thick gray line indicates the scattering continuum threshold for three atoms AAA ($a < 0$) and for an atom and a dimer AD ($a > 0$). a_* (a'_*) marks the intersection of the first Efimov trimer T with the atom-dimer (three atoms) threshold.

where $\beta = e^{\pi/s_0} \approx 22.7$ is a universal constant and k_* is the Efimov parameter, also known as the three-body parameter, which depends on the three-body potential at short range thus expected to be non-universal.

The binding energies of the Efimov states are functions of a and k_*, as can be seen in Fig. 3.3 where the thick gray line indicates the scattering continuum threshold for three atoms ($a < 0$) and for an atom and a dimer ($a > 0$), and a_* (a'_*) marks the intersection of the first Efimov trimer with the atom-dimer (three atom) threshold, where $a_* = 0.0707645086901 k_*^{-1}$ [1]. The N^{th} Efimov trimer intersects with the continuum at scattering length values of $\beta^N a_*$ and $\beta^N a'_*$ which are also universally related to each other as $a'_* \approx -22.0 a_*$ [1].

Chapter 4

Article: Observation of universality in ultracold ^{7}Li three-body recombination

Noam Gross, Zav Shotan, Servaas Kokkelmans and Lev Khaykovich

Physical Review Letters

Volume 103, pages 163202, October 2009

Observation of Universality in Ultracold ^{7}Li Three-Body Recombination

Noam Gross,[1] Zav Shotan,[1] Servaas Kokkelmans,[2] and Lev Khaykovich[1]
[1]Department of Physics, Bar-Ilan University, Ramat-Gan, 52900 Israel
[2]Eindhoven University of Technology, Post Office Box 513, 5600 MB Eindhoven, The Netherlands
(Received 25 June 2009; published 13 October 2009)

We report on experimental evidence of universality in ultracold ^{7}Li atoms' three-body recombination loss in the vicinity of a Feshbach resonance. We observe a recombination minimum and an Efimov resonance in regions of positive and negative scattering lengths, respectively, which are connected through the pole of the Feshbach resonance. Both observed features lie deeply within the range of validity of the universal theory, and we find that the relations between their properties, i.e., widths and locations, are in excellent agreement with the theoretical predictions.

DOI: 10.1103/PhysRevLett.103.163202 PACS numbers: 34.50.−s, 21.45.−v, 67.85.−d

Few-body physics is universal when interparticle interactions are insensitive to the microscopic details of the short-range interaction potentials and can be characterized by only one or few universal parameters [1]. In the limit of zero collision energy, the two-body interactions are determined by a single parameter, the s-wave scattering length a. Universality requires a to greatly exceed the two-body potential range. This can be achieved by a resonant enhancement of a, yielding the appearance of the peculiar quantum states known as quantum halos whose wave function acquires long-range properties and gives rise to loosely bound states of size $\sim a$ [2]. In the case of three interacting bosons, universality means that the three-body observables show log-periodic behavior that depends only on the scattering length a and on a three-body parameter which serve as boundary conditions for the short-range physics. Such a behavior is associated with so called Efimov physics. In a series of theoretical papers, Efimov predicted and characterized an infinite set of weakly bound triatomic states (Efimov trimers) whose binding energies (in the limit of $a \to \pm\infty$) are related in powers of a universal scaling factor $\exp(-2\pi/s_0) \approx 1/515$ where $s_0 = 1.00624$ [1,3]. Efimov trimers resisted experimental observation for nearly 35 years remaining an elusive and a long-term goal in a number of physical systems [2]. Only recently have they been experimentally discovered in a gas of ultracold cesium atoms [4,5].

Ultracold atoms provide an excellent playground to study universality. The characteristic range of the two-body interaction potential r_0, basically equivalent to the van der Waals length $r_0 \simeq (mC_6/16\hbar^2)^{1/4}$ [6], usually does not exceed $100a_0$, where a_0 is the Bohr radius. The scattering length a can be easily and precisely tuned to much higher values by means of Feshbach resonances which are present in most of the ultracold atomic species [7]. Efimov physics is not revealed by direct observation of Efimov trimers but rather through their influence on a three-body observable—the recombination loss of atoms from a trap. For positive scattering lengths, effective field theory predicts log-periodic oscillations of the loss rate coefficient with zeros as minima (for the ideal, zero energy system) which can be interpreted as destructive interference effects between two possible decay pathways [1,8]. For negative scattering lengths, the loss rate coefficient exhibits a resonance enhancement each time an Efimov trimer state intersects with the continuum threshold. Positions of the minima and the maxima are expected to be universally related [1] when regions of $a > 0$ and $a < 0$ are connected through a resonance ($a \to \pm\infty$). Despite the dramatic success in the experimental demonstration of an Efimov state in Ref. [4], difficulties arose in matching between the two regions of universality, that of positive and negative a [4,5]. These were twofold: first, the interference minimum was observed at $a \approx 210a_0$, only a factor of 2 higher than the r_0 for cesium atoms and thus not strictly in the universal regime; second, the two regions of universality were connected through a zero crossing ($a = 0$) which is a nonuniversal regime and thus questions the validity of the universal relation between them [4,9]. In a more recent experiment on Efimov physics in ultracold ^{39}K atoms, the two regions of $a > 0$ and $a < 0$ were connected through a resonance, but still significant deviations from the universal relations have been reported [10]. These deviations were attributed to the influence of details of the short-range interatomic potential. Though signatures of Efimov physics have been recently observed in other ultracold atom systems [11–13], no system has yet been able to answer the conditions in which universal relations could be verified.

In this Letter, we report on evidence of universal three-body physics in ultracold ^{7}Li in the vicinity of a Feshbach resonance based on measurements of three-body recombination. We discuss the effective range of the resonance and show that it supports a wide region of universality extended to tens of Gauss around the resonance center. A recombination loss minimum and an Efimov resonance are revealed in the $a > 0$ and $a < 0$ regions, respectively, which are connected through the pole of the Feshbach resonance. The observed features lie deeply within the universal regime and verify the predictions of the universal theory regarding relations between their properties.

Compared to other atomic species currently available for laser cooling techniques, lithium has the smallest range of van der Waals potential, $r_0 \approx 31a_0$. In addition, a number of Feshbach resonances available for different Zeeman sublevels of the $|F = 1\rangle$ hyperfine state makes ^{7}Li an appropriate candidate for study of Efimov physics. In this experiment, we work with a spin polarized sample in the $|F = 1, m_F = 0\rangle$ state, which is the one but lowest Zeeman state [14]. In principle, two-body losses are possible from this state; however, they are not large, as could be the case for heavier atoms. For instance, ^{133}Cs experiences large dipolar losses caused by the second-order spin-orbit interaction [15]. We calculated the dipolar relaxation rate coefficients as a function of magnetic field via a coupled-channels calculation by using recent interaction potentials [16] and found them to be ~3 orders of magnitude smaller than the corresponding measured rate coefficients, if the experimental losses were treated as purely two-body related. Moreover, the field-dependent profile of the calculated rates is qualitatively very different from the observed rates. As a result, we exclude two-body losses and determine that the loss processes in the region of interest are related to three-body recombination.

The $|F = 1, m_F = 0\rangle$ state possesses two Feshbach resonances, a narrow and a wide one, which we experimentally detect by atom loss measurement at 845.8(7) G and 894.2(7) G, respectively. The position of the wide resonance is independently measured at 894.63(24) G by molecule association technique [17]. These positions are in agreement with theory within the uncertainty of the magnetic field calibration ($\pm$ 0.5%). In Fig. 1, two collision properties are shown as a function of magnetic field: the scattering length a and the effective range R_e. These quantities are extracted from the scattering phase shift $\delta(k)$ at small relative wave numbers k by using the effective range expansion $k\cot\delta(k) = -1/a + R_e k^2/2$ [18].

The region of universality strongly depends on the width of the Feshbach resonance which is inversely proportional to the effective range close to the resonance's center

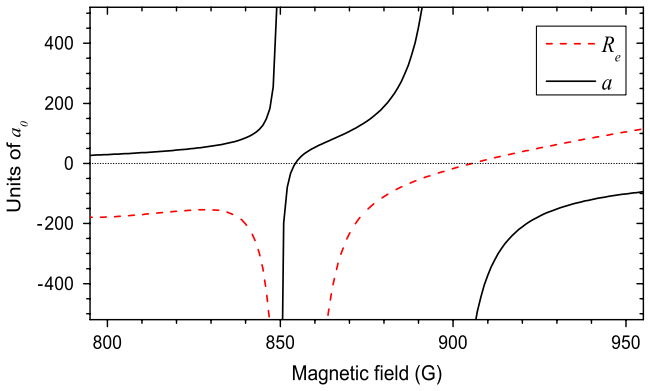

FIG. 1 (color online). The scattering length a (solid line) and the effective range R_e (dashed line) as a function of magnetic field near the two Feshbach resonances of the $|F = 1, m_F = 0\rangle$ state.

[19,20]. As a measure for the influence of the effective range, the resonance strength $s_{\rm res} = 2r_0/|R_e|$ has been introduced [7,21]. In this way, a narrow or "closed-channel dominated" resonance is characterized by $s_{\rm res} \ll 1$ and has a very narrow region of universality, for which $|a| \gg |R_e|$. In this case, R_e comes on a similar footing as and in addition to the three-body parameter to determine the short-range physics [19,22]. In contrast, a wide or "open-channel dominated" resonance is characterized by $s_{\rm res} \gg 1$. Here, the universal region spans over a broad range of magnetic field strengths for which $a \gg r_0$ and the scattering problem can be described in terms of an effective single-channel model [7].

The effective range is very large in the vicinity of the narrow resonance which signifies its "close-channel dominated" character while around the wide resonance, the effective range is small and crosses zero near the pole of the resonance (Fig. 1). This is a clear demonstration of an "open-channel dominated" resonance which expects to provide a wide region of universality extended to tens of Gauss around the resonance where $s_{\rm res}(B) \gtrsim 1$.

In the experiment, we perform measurements of three-body recombination loss as a function of magnetic field near the wide Feshbach resonance. Each loss rate coefficient is calculated from a fit of a lifetime measurement to the solution of the atom loss rate equation: $\dot{N} = -K_3\langle n^2\rangle N - \Gamma N$, where K_3 and Γ are the three- and single-body loss rates, respectively. Γ is determined independently by measuring a very long decay tail of a low density sample. This simplified model does not include effects such as saturation of K_3 to a maximal value $K_{\rm max}$ due to finite temperature (unitarity limit) [23], recombination heating and "anti-evaporation" [24]. The first and the second effects can be neglected for K_3 values which are much smaller than $K_{\rm max}$. In our case, the highest measured K_3 values are at least an order of magnitude smaller than $K_{\rm max}$, and therefore this assumption is reasonable. As for the latter, we treat the evolution of our data to no more than ~30% decrease in atom number for which "anti-evaporation" is estimated to induce a systematic error of ~23% towards higher values of K_3. This effect is evaluated not to limit the accuracy of the reported results.

Our experimental setup is described in details elsewhere [14]. In brief, we load atoms directly from a magneto-optical trap into a single-beam far-detuned optical dipole trap and perform a preliminary forced evaporation at the wing of the narrow resonance at 824 G. During a second evaporation step, we add a second beam which intersects with the first, and the atoms are loaded into a tightly confined crossed-beam dipole trap. A final evaporation step is performed at a slightly higher magnetic field of 832 G. Evaporation at this step can proceed all the way to the Bose-Einstein condensation (BEC) threshold but it is interrupted before a degeneracy is reached. A transition to the magnetic field of interest in which a lifetime measurement will be taken is performed in two main steps. The first is a rapid change in magnetic field over the position of the

Feshbach resonance to avoid strong inelastic losses. The second is an adiabatic approach to the target magnetic field. After different waiting times, the remaining atoms' number is determined by *in situ* absorption imaging.

For measurements in the positive scattering lengths, we cut the evaporation at $T \approx 2\ \mu$K and $\sim 10^5$ atoms with peak density of $\sim 5 \times 10^{12}$ cm^{-3}. We then shift rapidly to a magnetic field of 858 G in less than 1 ms while crossing the narrow resonance and wait for 500 ms to let the system relax. Then, we ramp the magnetic field in 25 ms to 880 G, roughly in the center of the region of interest, and wait there for another 100 ms before the last move to the final magnetic field (in 5 ms) where the measurements of lifetime and temperature are performed. For the negative scattering lengths, we cut the evaporation at $T \approx 1\ \mu$K, just on the verge of a BEC. A fast jump is then made to a magnetic field of 930 G, far beyond the position of the wide resonance. After a relaxation time, we slowly move to 915 G and wait there again before a last ramp to the final magnetic field is performed.

For the treatment of three-body recombination loss in the domain of universality, we adopt the language of Refs. [4,5]. The convenient form to represent the theoretically predicted loss rate coefficient is $K_3 = 3C_{\pm}(a)\hbar a^4/m$ where m is the atomic mass and where $\pm$ hints at the positive $(+)$ or negative $(-)$ region of the scattering length. In that form, an a^4 dependence [25] is separated from the additional log-periodic behavior $C_{\pm}(a) = C_{\pm}(22.7a)$ which reflects the Efimov physics of infinite series of weakly bound trimers. An effective field theory provides analytic expressions for $C_{\pm}(a)$ that we use in the form presented in Refs. [4,5] to fit our experimental results. For $a > 0$, $C_+(a)$ includes oscillations on log scale between the maximum recombination loss of $C_+(a) \sim 70$ and the minimum which in an ideal system can be vanishingly small [1]. For $a < 0$, $C_-(a)$ displays resonance behavior each time an Efimov trimer state hits the continuum threshold. The free parameters of the theory are $a_{\pm}$ which are connected to the unknown short-range part of the effective three-body potential and $\eta_{\pm}$ which describe the unknown decay rate of Efimov states. Moreover, a_- defines the resonance position in the decay rate and $\eta_{\pm}$ are assumed to be equal.

Our experimental results are shown in Fig. 2. For positive scattering lengths, we observe a pronounced minimum in the three-body recombination rate at a scattering length of $a \approx 1160a_0$ which is much larger than r_0 and in that sense occurs deep within the universal region [26]. The upper limit for universality, due to finite temperature, is estimated to be at $a \approx 2800a_0$ ($K_{\max} \approx 6 \times 10^{-21}$ cm^6/s) [23]. Adjacent minima are expected at $1160a_0/22.7 \approx 50a_0$, which is too close to the nonuniversal region, and at $1160a_0 \times 22.7 \approx 26000a_0$, well above the finite temperature limit. Our measurements are fitted remarkably well with the analytical expression of $C_+(a)$ for a large range of scattering lengths as shown by a solid line in Fig. 2. For lower scattering lengths, K_3 saturates at $\sim 130a_0$ (870 G). Interestingly, it occurs when $s_{\rm res}(B) \approx 0.4$, and it roughly corresponds to the position where the effective range $R_e(B)$ starts to diverge due to the presence of the scattering length's zero crossing (see Fig. 1), and its absolute value is about the same as that of the scattering length [$R_e(B = 870\ \text{G}) \approx -170a_0$]. From the fit, we obtain $a_+ = 243(35)a_0$, $\eta_+ = 0.232(55)$. The upper limit for the three-body recombination rate (dashed line in Fig. 2) is represented by $C_+(a) \approx 54.7$, which is smaller than the commonly known value of $C_+(a) \approx 70$ due to the relatively large value of η_+.

Measurements of three-body recombination rates for negative scattering lengths reveal a region of significant

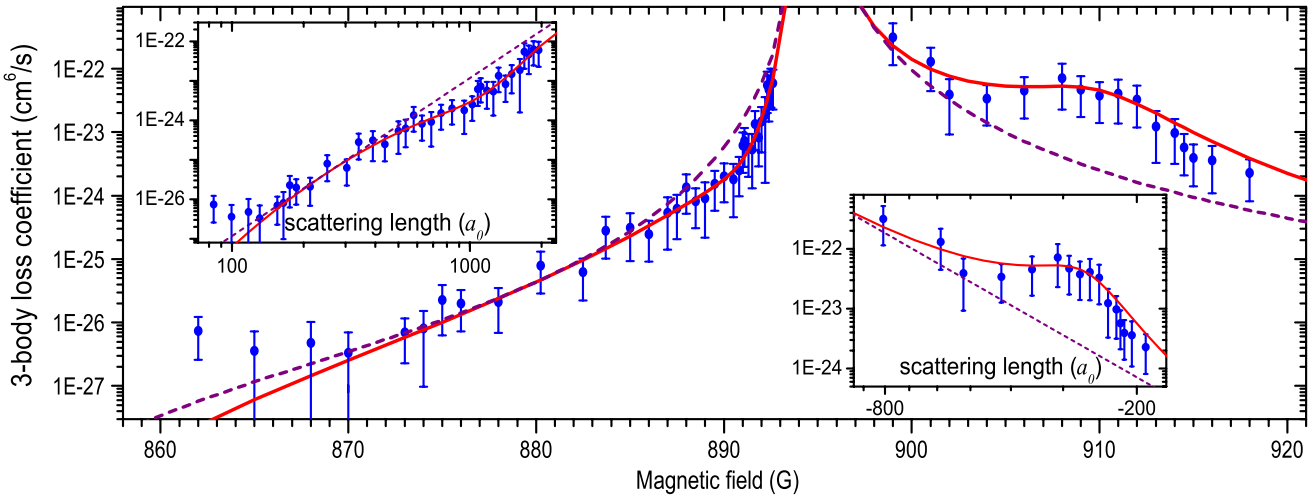

FIG. 2 (color online). Three-body loss coefficient K_3 is shown as a function of magnetic field and scattering length (insets). The solid lines represent fittings to the analytical expressions of universal theory. The dashed lines represent the upper (lower) limit of K_3 for $a > 0$ ($a < 0$). The error bars consist of two contributions: the uncertainty in temperature measurement ($\sim 20\%$) which affects the estimated atom density and the fitting error of the lifetime measurement.

enhancement of K_3 as an expected manifestation of an Efimov resonance (Fig. 2). We fit our data with the analytic expression of $C_-(a)$ (solid line) to obtain the position of the Efimov resonance at $a_- = -264(11)a_0$ and its width $\eta_- = 0.236(42)$. The resonance is observed well within the universal regime with $|a_-| \approx 8.5r_0$ and far enough from the upper limit (due to the finite temperature) which is estimated at $a \approx -1500a_0$ ($K_{\max} \approx 4 \times 10^{-21}$ cm^6/s) [23]. This limit prevents the observation of the next Efimov resonance at $a \approx -6000a_0$. The two independent fit parameters a_+ and a_- are predicted to obey the universal ratio $a_+/|a_-| = 0.96(3)$, and the experiment yields a remarkably close value of 0.92(14). This seems like an observation of the long hunted universal behavior of a three-body observable in a physical system with resonantly enhanced two-body interactions. In addition, the large width of the resonance, indicating short lifetimes of the Efimov trimer, is in excellent agreement with the theoretical assumption of $\eta_+ = \eta_-$.

For positive scattering lengths the Efimov trimer is expected to intersect with the atom-dimer threshold at $a_* \approx 1.1a_+$ [1]. Theory predicts that a_* and a_- of the same trimer state are related as $a_- \approx -22a_*$ [1]. This means that if the observed resonance at a_- indicates the lowest state, the one expected at a_* indicates the first excited state as the lowest one becomes nonuniversal.

The determination of the Feshbach resonances positions is important for the discussed fitting procedure because it defines the value of the scattering length at a given magnetic field. These positions were located by atom loss and molecule association measurements with an accuracy of <1 G. Independently, we allow the position of the wide resonance to be determined by the fitting procedure. For that purpose, we first fit the coupled-channels calculation of scattering length as a function of magnetic field (shown in Fig. 1) with a formula that includes two nearby resonances: $a = a_{\rm bg}[1 - \Delta_1/(B - B_1) - \Delta_2/(B - B_2)]$ where $a_{\rm bg}$ is a common background scattering length and Δ_1, B_1 and Δ_2, B_2 are widths and positions of the narrow and the wide resonances, respectively. We then introduce the result into the expressions of $C_\pm(a)$ while substituting B with $B - \delta B$ (δB being a fitting parameter). For $a > 0$ ($a < 0$), the fitting yields the position of the wide resonance at 894.65(11) G [893.85(37) G]. These two independent fits are in good agreement with each other as well as with the atom loss and the molecule association measurements.

It is interesting to note that the observed position of the Efimov resonance reveals the same numerical factor $|a_-|/r_0 \approx 8.5$ as in the experiments on ^{133}Cs [4] which may or may not be an accidental coincidence. It is also interesting that while our results agree with the universal theory, the results on ^{39}K show significant deviations from it [10]. This might hint at an additional parameter to describe the three-body physics of ^{39}K atoms, such as the effective range $R_e(B)$ that becomes more important for narrow Feshbach resonances.

The absolute ground state of ^{7}Li also possesses a wide Feshbach resonance across which Efimov features are expected. If so, it would provide a possibility to test universality in different channels of the same atomic system. Recently, evidence for universal four-body states related to Efimov trimers were reported [10,27]. Signatures of these states are subject for future research.

We gratefully acknowledge discussions with R. Grimm and F. Ferlaino. This work was supported, in a part, by the Israel Science Foundation and by the Netherlands Organization for Scientific Research (NWO). N. G. is supported by the Israel Academy of Sciences and Humanities.

[1] E. Braaten and H.-W. Hammer, Phys. Rep. **428**, 259 (2006).
[2] A. S. Jensen *et al.*, Rev. Mod. Phys. **76**, 215 (2004).
[3] V. Efimov, Phys. Lett. B **33**, 563 (1970); V. Efimov, Sov. J. Nucl. Phys. **12**, 589 (1971); V. Efimov, *ibid.* **29**, 546 (1979).
[4] T. Kraemer *et al.*, Nature (London) **440**, 315 (2006).
[5] S. Knoop *et al.*, Nature Phys. **5**, 227 (2009).
[6] G. F. Gribakin and V. V. Flambaum, Phys. Rev. A **48**, 546 (1993).
[7] C. Chin *et al.*, arXiv:0812.1496 [Rev. Mod. Phys. (to be published)].
[8] B. D. Esry *et al.*, Phys. Rev. Lett. **83**, 1751 (1999); E. Nielsen, and J. H. Macek, *ibid.* **83**, 1566 (1999).
[9] J. P. D'Incao *et al.*, J. Phys. B **42**, 044016 (2009).
[10] M. Zaccanti *et al.*, Nature Phys. **5**, 586 (2009).
[11] T. B. Ottenstein *et al.*, Phys. Rev. Lett. **101**, 203202 (2008).
[12] J. H. Huckans *et al.*, Phys. Rev. Lett. **102**, 165302 (2009).
[13] G. Barontini *et al.*, Phys. Rev. Lett. **103**, 043201 (2009).
[14] N. Gross and L. Khaykovich, Phys. Rev. A **77**, 023604 (2008). Note that an improved magnetic field calibration has shifted the Feshbach resonances to somewhat higher fields (see also discussion of Fig. 3 in Ref. [14]).
[15] S. J. J. M. F. Kokkelmans *et al.*, Phys. Rev. Lett. **81**, 951 (1998); F. H. Mies *et al.*, J. Res. Natl. Inst. Stand. Technol. **101**, 521 (1996).
[16] E. G. M. v. Kempen *et al.*, Phys. Rev. A **70**, 050701(R) (2004).
[17] C. A. Regal *et al.*, Nature (London) **424**, 47 (2003).
[18] J. R. Taylor, *Scattering Theory* (John Wiley and Sons, New York, 1972).
[19] D. S. Petrov, Phys. Rev. Lett. **93**, 143201 (2004).
[20] B. Marcelis *et al.*, Phys. Rev. A **70**, 012701 (2004).
[21] T. Köhler *et al.*, Rev. Mod. Phys. **78**, 1311 (2006).
[22] L. Platter *et al.*, Phys. Rev. A **79**, 022702 (2009).
[23] J. P. D'Incao *et al.*, Phys. Rev. Lett. **93**, 123201 (2004).
[24] T. Weber *et al.*, Phys. Rev. Lett. **91**, 123201 (2003).
[25] P. O. Fedichev *et al.*, Phys. Rev. Lett. **77**, 2921 (1996).
[26] J. P. D'Incao and B. D. Esry, Phys. Rev. A **72**, 032710 (2005).
[27] F. Ferlaino *et al.*, Phys. Rev. Lett. **102**, 140401 (2009).

Chapter 5

Article: Nuclear-spin-independent short-range three-body physics in ultracold atoms

Noam Gross, Zav Shotan, Servaas Kokkelmans and Lev Khaykovich

Physical Review Letters

Volume 105, page 103203, September 2010

Nuclear-Spin-Independent Short-Range Three-Body Physics in Ultracold Atoms

Noam Gross,[1] Zav Shotan,[1] Servaas Kokkelmans,[2] and Lev Khaykovich[1]

[1]*Department of Physics, Bar-Ilan University, Ramat-Gan, 52900 Israel*

[2]*Eindhoven University of Technology, Post Office Box 513, 5600 MB Eindhoven, The Netherlands*

(Received 25 March 2010; revised manuscript received 31 May 2010; published 3 September 2010)

We investigate three-body recombination loss across a Feshbach resonance in a gas of ultracold ^{7}Li atoms prepared in the absolute ground state and perform a comparison with previously reported results of a different nuclear-spin state [N. Gross *et al.*, Phys. Rev. Lett. **103**, 163202 (2009)]. We extend the previously reported universality in three-body recombination loss across a Feshbach resonance to the absolute ground state. We show that the positions and widths of recombination minima and Efimov resonances are identical for both states which indicates that the short-range physics is nuclear-spin independent.

DOI: 10.1103/PhysRevLett.105.103203 PACS numbers: 34.50.−s, 21.45.−v, 67.85.−d

A remarkable prediction of three-body theory with resonantly enhanced two-body interactions is the existence of a universal set of weakly bound triatomic states known as Efimov trimers [1]. In the limit of zero collision energy only s-wave scattering is allowed, signifying that a single parameter, the scattering length a is sufficient to describe the ultracold two-body interactions. When $|a| \rightarrow \pm\infty$ the universal long-range theory (known as ''Efimov scenario'') predicts that three-body observables exhibit log-periodic behavior which depends only on the scattering length a and on a three-body parameter which serve as boundary conditions for the short-range physics [2]. After decades of failed quests for a suitable system to study the Efimov scenario [3] a number of recent experiments with ultracold atoms have demonstrated this logarithmic periodicity and verified the ''holy grail'' of the theory, the universal scaling factor $\exp(\pi/s_0) \approx 22.7$, where $s_0 = 1.006\,24$ [4–6]. The scaling as such, however, does not provide any knowledge about the short-range part of the three-body potential which defines the absolute location and lifetime of an Efimov state. The short-range potential is given in terms of two-body potential permutations of the two-body subsystems and a true three-body potential which is of importance only when three particles are very close together. In general, it is very difficult to solve the short-range physics exactly, and therefore this region is usually treated in terms of a three-body parameter [2,7].

Among other systems of ultracold atoms which allow the study of universal three-body physics [4,8–11], bosonic lithium provides a unique opportunity to shed some light on the short-range physics. In this Letter, we exploit the possibility to study universality in two different nuclear-spin states that both possess a broad Feshbach resonance. Experimentally the three-body observable is three-body recombination loss of atoms from a trap which is always studied in the absolute ground state where higher order inelastic processes, namely, two-body inelastic collisions, are prohibited. However, recently we showed that a gas of ^{7}Li atoms, spin polarized in the one but lowest Zeeman sublevel ($|F = 1, m_F = 0\rangle$), experiences very weak two-body loss which allowed a study of the physics of three-body collisions [6]. Here we investigate three-body recombination on the absolute ground state ($|F = 1, m_F = 1\rangle$) across a Feshbach resonance at ~738 G. Comparison of the results of both states (further denoted as $|m_F = 0\rangle$ and $|m_F = 1\rangle$) reveals a remarkable identity between properties of the Efimov features. At these large magnetic fields the two states are basically similar in their electron spin, but different in their nuclear spin. As the position and width of an Efimov state are solely governed by the three-body parameter, our results suggest that at high magnetic fields the short-range physics is independent of nuclear-spin configuration and of the specific Feshbach resonance across which universality is studied.

Experimentally, three-body recombination loss is studied as a function of scattering length by means of magnetic field tuning near a Feshbach resonance [12]. For positive scattering lengths the log-periodic oscillations of the loss rate coefficient is caused by destructive interference conditions between two possible decay pathways for certain values of a [2,13]. For negative scattering lengths the loss rate coefficient exhibits a resonance enhancement each time an Efimov trimer state intersects with the continuum threshold. Recently, we found that positions of the oscillations' minimum ($a > 0$) and maximum ($a < 0$) are universally related across the Feshbach resonance on the $|m_F = 0\rangle$ state [6] in a very good agreement with theory [2,7].

Our experimental setup is described in detail elsewhere [6,14]. In brief, we perform evaporative cooling at a bias magnetic field of ~830 G near a Feshbach resonance when the gas of ^{7}Li atoms is spontaneously spin purified to the $|m_F = 0\rangle$ state [14]. The atoms are cooled down to the threshold of degeneracy and transferred into the absolute ground state $|m_F = 1\rangle$ by means of rapid adiabatic passage using a radio frequency (rf) sweep scanning 1 MHz in 20 ms at a lower bias magnetic field (35 G). The transfer efficiency is better than 90%. Finally, the bias field is

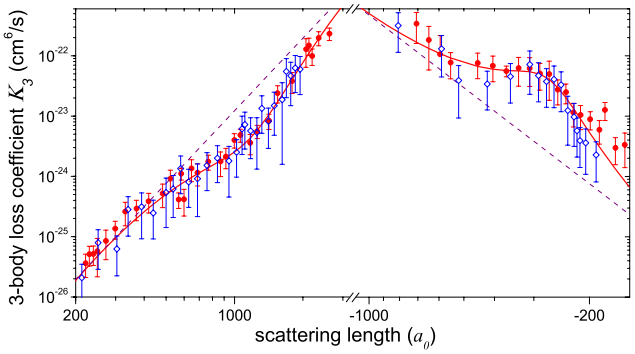

FIG. 1 (color online). Experimentally measured three-body loss coefficient K_3 as a function of scattering length (in units of Bohr radius a_0) for the $|m_F = 1\rangle$ state (red solid circles). The solid lines represent fits to the analytical expressions of universal theory. The dashed lines represent the a^4 upper (lower) limit of K_3 for $a > 0$ ($a < 0$). The error bars consist of two contributions: the uncertainty in temperature measurement which affects the estimated atom density and the fitting error of the atom-number decay measurement. K_3 values of the $|m_F = 0\rangle$ state, reported by us in Ref. [6], are represented by blue open diamonds.

ramped to the vicinity of the absolute ground state's Feshbach resonance [738.3(3) G] where we measure atom-number decay and temperature as a function of magnetic field from which we extract the three-body loss coefficient K_3. Details of the experimental procedure and the data analysis are similar to those elaborated in Ref. [6]. A typical temperature of the atoms for positive (negative) scattering lengths is 1.8 μK (1.3 μK) which matches the conditions of previously reported measurements on the $|m_F = 0\rangle$ state [6].

Experimental results of the three-body loss coefficient are summarized in Fig. 1 where K_3 is plotted as a function of the scattering length a for the $|m_F = 1\rangle$ state (red solid circles). Also plotted are the results of K_3 measurements for the wide resonance of the $|m_F = 0\rangle$ state (blue open diamonds) from Ref. [6]. The qualitative resemblance between the two measurements is striking. Further investigation is achieved by treating the three-body recombination loss as done in Ref. [6]. In short, the theoretically predicted loss rate coefficient is $K_3 = 3C_\pm(a)\hbar a^4/m$ where m is the atomic mass and where $\pm$ hints at the positive (+) or negative (−) region of the scattering length. An effective field theory provides analytic expressions for the log-periodic behavior of $C_\pm(a) = C_\pm(22.7a)$ that we use in the form presented in Ref. [8] to fit our experimental data. The free parameters are $a_\pm$ ($\eta_\pm$) which are connected to the real (imaginary) part of the three-body parameter [2,15]. Moreover, a_- defines the position of the decay rate (Efimov) resonance and the decay parameters η_+ and η_-, which describe the width of the Efimov state, are assumed to be equal. Results of this fitting procedure are summarized in Table I along with former results of the $|m_F = 0\rangle$ state [6].

TABLE I. Fitting parameters to universal theory obtained from the measured K_3 values of the $|m_F = 1\rangle$ and the previously reported $|m_F = 0\rangle$ states [6].

State	η_+	η_-	a_+/a_0	a_-/a_0	$a_+/\lvert a_-\rvert$
$\lvert m_F = 0\rangle$	0.232(55)	0.236(42)	243(35)	−264(11)	0.92(14)
$\lvert m_F = 1\rangle$	0.188(39)	0.251(60)	247(12)	−268(12)	0.92(6)

The solid line in Fig. 1 represents the fit to the measurements performed in the $|m_F = 1\rangle$ state. The theoretical assumption that the real part of the three-body parameter across a Feshbach resonance is the same for negative and positive scattering lengths regions requires a_+ and a_- to obey a universal ratio $a_+/|a_-| = 0.96(3)$ [2]. Indeed, the fit yields a remarkably close value of 0.92(6) which confirms the above assumption. Moreover, the fact that η_+ and η_- are equal within the experimental errors suggests that also the imaginary part of the three-body parameter is identical. We thus confirm the universality in three-body recombination across a Feshbach resonance which we observed earlier in the $|m_F = 0\rangle$ state [6]. Note that the recent work by the Rice group on the $|m_F = 1\rangle$ state [5] has reported different values for the fitting parameters. We shall address this apparent discrepancy later on.

Comparing the fitting parameters on different nuclear-spin states (see Table I) reveals striking similarities in corresponding numbers that agree with each other exceptionally well. We hence conclude that the three-body parameter in these states is the same within the experimental errors. We note that both Feshbach resonances are comparable yet slightly different in width (see Table II, last two rows) which has no effect on the positions of Efimov features. Moreover, in the $|m_F = 0\rangle$ state there is a narrow resonance in close proximity to the wide one (see Table II, first row) but it does not affect the positions of the Efimov features either.

The reported results crucially depend on precise knowledge of the Feshbach resonance position and the scattering length in its vicinity. We use here the same coupled-channels (CC) calculation as in Ref. [6] to predict the scattering length dependence on magnetic field, which is then fitted with a conveniently factorized expression [16]:

$$\frac{a}{a_{\mathrm{bg}}} = \prod_{i=1}^{N}\left(1 - \frac{\Delta_i}{(B - B_{0,i})}\right). \quad (1)$$

Here a_{bg} is the background scattering length, Δ_i is the i's

TABLE II. Feshbach resonance parameters for both states obtained from a fitting of the CC calculation with Eq. (1).

State	Type	B_0 (G)	Δ (G)	a_{bg}/a_0
$\lvert m_F = 0\rangle$	narrow	849.7	4.616	−18.94
$\lvert m_F = 0\rangle$	wide	898.4	−235.1	−18.94
$\lvert m_F = 1\rangle$	wide	742.2	−169.0	−20.64

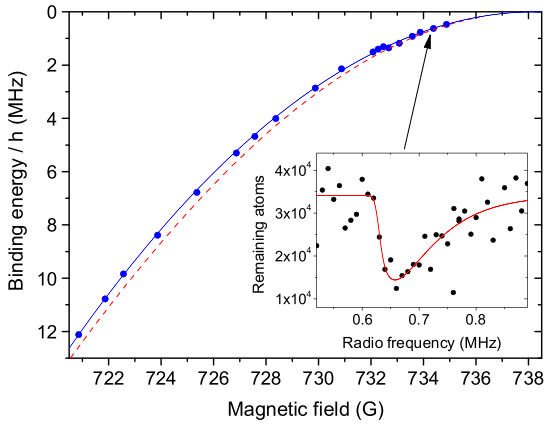

FIG. 2 (color online). rf spectroscopy of the molecular binding energy near the Feshbach resonance in the $|m_F = 1\rangle$ state. The solid line represents fitting to Eq. (2). CC calculation prediction (dashed line) is plotted as well. Inset—an example of a loss resonance at $B = 734.4$ G fitted numerically to a convolution of Maxwell-Boltzmann and a Gaussian distributions (solid line).

resonance width and $B_{0,i}$ is the i's resonance position. Table II summarizes these parameters for all Feshbach resonances in both nuclear-spin states.

To verify the $|m_F = 1\rangle$ Feshbach resonance parameters we use a powerful experimental technique that measures the binding energy of the Feshbach molecules with high precision. The method uses a weak rf field to resonantly associate weakly bound Feshbach dimers which are then rapidly lost through collisional relaxation into deeply bound states [17]. The remaining atom number is measured by absorption imaging as a function of rf frequency at a given magnetic field. In the experiment the rf modulation time is varied between 0.5 and 3 sec and the modulation amplitude ranges from 150 to 750 mG. rf-induced losses at a given magnetic field are then numerically fitted to a convolution of a Maxwell-Boltzmann and a Gaussian distributions (see inset in Fig. 2). The former accounts for broadening of the spectroscopic feature due to finite kinetic energy of atoms at a typical temperature of ~ 1.5 μK. The latter reflects broadening due to magnetic field instability and shot-to-shot atom-number fluctuations. From the fit we extract the molecular binding energy (E_b) corresponding to zero temperature. The rf spectroscopy of E_b is shown in Fig. 2.

The scattering length a in the vicinity of the Feshbach resonance can be extracted from our measurement by a numerical fit to the CC calculation. This analysis will be the subject of a future publication. Instead we plot in Fig. 2 (dashed line) the binding energies of molecules according to the prediction of the CC calculation with no fitting parameters apart from a shift of -3.9 G to the experimentally determined position of the resonance (discussed next). A notably good agreement between the measurements and theory indicates that very small corrections are needed to tune the theory to the experimental data. Here we use a simple analytical model to estimate these corrections and to pinpoint the resonance's position.

Very close to a Feshbach resonance the molecular binding energy has the following form [12]:

$$E_b = \frac{\hbar^2}{m(a - \bar{a} + R^*)^2}, \tag{2}$$

where m is the atomic mass and $\bar{a}$ and R^* accounts for a finite range and a resonance strength corrections to the universal $1/a^2$ law, respectively. $\bar{a}$ is the mean scattering length which is an alternative van der Waals length scale [18], and $R^* = \hbar^2/(m a_{\rm bg} \Delta(\delta\mu))$ [19], where $\delta\mu$ is the differential magnetic moment [12]. Equation (2) is applied in the limit of $a \gg \bar{a}$ and $a \gg 4R^*$. When Eq. (1) is substituted into Eq. (2) the latter provides us with a fitting expression that can be used to extract Δ, $a_{\rm bg}$ and B_0 from our experimental data. However, a few comments should be made.

We restrict the fit to values of $E_b/h < 4$ MHz, where $a > 300a_0$, which corresponds to $\sim 5\%$ of the Feshbach resonance width, to meet the requirement $a \gg \bar{a} = 29.88a_0$ (the fitting curve presented as a blue line in Fig. 2 is plotted to the entire range of E_b). Thus, according to Eq. (1), as $(B - B_0) \ll |\Delta|$ the fitting procedure is only sensitive to the product $\Gamma = a_{\rm bg}\Delta$. Large uncertainties are anticipated in the parameters $a_{\rm bg}$ and Δ if they are fitted simultaneously. We therefore arbitrary choose to fix the values of either $a_{\rm bg}$ or Δ to the CC calculation prediction (see Table II, last row). The values in the second row of Table III are obtained from this fitting procedure. To check the self-consistency of the use of Eq. (2) we calculate $R^* = 51.8a_0$ using the fitting data and find it to satisfy the second requirement of $a \gg 4R^*$ though less strictly. We note that Eq. (2) was verified against the CC calculation for $E_b/h < 4$ MHz and they were found to agree with each other to better than 3%.

Table III shows, along with the fitting data (second row), predictions of CC calculation (first row, same as the last row in Table II) and experimental results of the Rice group

TABLE III. The $|m_F = 1\rangle$ Feshbach resonance parameters as derived from different sources.

Source	B_0 (G)	Δ (G)	$a_{\rm bg}/a_0$	Γ (G)
CC calculation	742.2	-169.0	-20.64	3488
rf spectroscopy	738.3(3)	–	–	3600(150)
in-situ BEC size measurement [20]	736.97(7) [5]	$-192.3(3)$	$-24.5^{+3.0}_{-0.2}$	4711^{+46}_{-584}

[5,20] where a was derived from BEC *in-situ* size measurements (third row).

The parameters of the Feshbach resonance, as determined here, appear to be in poor agreement with the one reported by the Rice group. The position of the resonance B_0 is shifted to a higher value of the magnetic field beyond the experimental error [21]. As for Γ, while the current measurement only slightly modifies the CC calculation result, it differs significantly from that reported in Ref. [5]. We note that rf spectroscopy is very robust being independent of experimental parameters such as trap strength, absolute number of atoms or atomic cloud size, whereas the BEC size measurement is highly sensitive to uncertainties in these measurements [20]. The results summarized in Table I are obtained based on the CC calculation and the experimentally determined value of B_0.

The Efimov scenario was recently investigated in the $|m_F = 1\rangle$ state of ^{7}Li atoms by the Rice group in an impressive work reporting in total 11 different features on both sides of the Feshbach resonance connected to three- and four-body universal states [5]. However, a_+ and a_- parameters are in apparent discrepancy with those reported here. To address this discrepancy we compare the observed features on a magnetic field scale instead of a scattering length scale using an inverted version of Eq. (1) and the corresponding Feshbach resonances' parameters indicated in Table III. For $a > 0$, the Rice and our group's loss minima are obtained at 735.23(4) and 735.39(14) G, respectively, (we consider the second minimum in the Rice results). There is a perfect agreement between the two positions even within the fit errors only (see Table I and Ref. [5]). For $a < 0$, the Efimov resonances are located at 754.2(6) and 752.4(7) G, respectively, which also reasonably (within $\sim 2\times$ the error range) agree with each other. We therefore conclude that the only discrepancy between our groups is in the conversion of magnetic field into scattering length, caused by the use of different Feshbach resonance parameters. Stressing again the reliability and precision of the method used here for resonance characterization, we believe that a quantitative reinterpretation of the Rice group's results will most probably resolve this discrepancy.

The nuclear-spin independent short-range physics which we report here are partially due to the special conditions which apply already for two-body physics at large magnetic fields. Here we are in the Paschen-Back regime, where the electron and nuclear spins precess independently around the magnetic field. Then the hyperfine coupling can be neglected resulting in an uncoupled and (for $|m_F = 0\rangle$ and $|m_F = 1\rangle$) very similar two-body potential. This means that nonresonant parameters, such as the background scattering length, should be very similar for the two different states (see Table II). However, since the derived three-body parameters are also very similar (see Table I), it suggests that the true three-body forces [7] are either also nuclear-spin independent, or they have a relatively unimportant contribution. We note that based on similar arguments Ref. [22] predicts a negligible change in the three-body parameter for isolated Feshbach resonances in Cs atoms.

We acknowledge M. Goosen and O. Machtey for assistance. This work was supported, inpart, by the Israel Science Foundation and by the Netherlands Organization for Scientific Research (NWO). N. G. is supported by the Israel Academy of Sciences and Humanities.

[1] V. Efimov, Phys. Lett. B **33**, 563 (1970).
[2] E. Braaten and H.-W. Hammer, Phys. Rep. **428**, 259 (2006).
[3] A. S. Jensen *et al.*, Rev. Mod. Phys. **76**, 215 (2004).
[4] M. Zaccanti *et al.*, Nature Phys. **5**, 586 (2009).
[5] S. E. Pollack, D. Dries, and R. G. Hulet, Science **326**, 1683 (2009).
[6] N. Gross *et al.*, Phys. Rev. Lett. **103**, 163202 (2009).
[7] J. P. D'Incao *et al.*, J. Phys. B **42**, 044016 (2009).
[8] T. Kraemer *et al.*, Nature (London) **440**, 315 (2006); S. Knoop *et al.*, Nature Phys. **5**, 227 (2009).
[9] T. B. Ottenstein *et al.*, Phys. Rev. Lett. **101**, 203202 (2008); A. N. Wenz *et al.*, Phys. Rev. A **80**, 040702(R) (2009).
[10] J. H. Huckans *et al.*, Phys. Rev. Lett. **102**, 165302 (2009); J. R. Williams *et al.*, *ibid.* **103**, 130404 (2009).
[11] G. Barontini *et al.*, Phys. Rev. Lett. **103**, 043201 (2009).
[12] C. Chin *et al.*, Rev. Mod. Phys. **82**, 1225 (2010).
[13] B. D. Esry, C. H. Greene, and J. P. Burke, Phys. Rev. Lett. **83**, 1751 (1999); E. Nielsen and J. H. Macek, *ibid.* **83**, 1566 (1999).
[14] N. Gross and L. Khaykovich, Phys. Rev. A **77**, 023604 (2008).
[15] B. Marcelis *et al.*, Phys. Rev. A **77**, 032707 (2008).
[16] A. D. Lange *et al.*, Phys. Rev. A **79**, 013622 (2009).
[17] S. T. Thompson, E. Hodby, and C. E. Wieman, Phys. Rev. Lett. **95**, 190404 (2005).
[18] G. F. Gribakin and V. V. Flambaum, Phys. Rev. A **48**, 546 (1993).
[19] D. S. Petrov, Phys. Rev. Lett. **93**, 143201 (2004).
[20] S. E. Pollack *et al.*, Phys. Rev. Lett. **102**, 090402 (2009).
[21] We verified the position of the resonance by measuring the microwave transition between $|F = 1, m_F = 0\rangle$ and $|F = 2, m_F = 1\rangle$ states at $B = 740$ G.
[22] N. Gemelke *et al.*, *Proceedings of the XXI International Conference on Atomic Physics* (World Scientific, Singapore, 2009), p. 240.

Chapter 6

Article: Study of Efimov physics in two nuclear-spin sublevels of ^{7}Li

Noam Gross, Zav Shotan, Olga Machtey, Servaas Kokkelmans
and Lev Khaykovich

Comptes Rendus Physique
Volume 12, page 4, January 2011

C. R. Physique 12 (2011) 4–12

Contents lists available at ScienceDirect

Comptes Rendus Physique

www.sciencedirect.com

Few body problem / Problème à petit nombre de corps

Study of Efimov physics in two nuclear-spin sublevels of ^{7}Li

Étude de l'effet d'Efimov dans deux états de spin nucléaire du ^{7}Li

Noam Gross [a], Zav Shotan [a], Olga Machtey [a], Servaas Kokkelmans [b], Lev Khaykovich [a,*]

[a] *Department of Physics, Bar-Ilan University, Ramat-Gan, 52900 Israel*
[b] *Eindhoven University of Technology, P.O. Box 513, NL-5600 MB Eindhoven, The Netherlands*

ARTICLE INFO

Article history:
Available online 6 January 2011

Keywords:
Efimov effect
Feshbach resonance
Nuclear spin

Mots-clés :
Effet d'Efimov
Résonance de Feshbach
Spin nucléaire

ABSTRACT

Efimov physics in two nuclear-spin sublevels of bosonic lithium is studied and it is shown that the positions and widths of recombination minima and Efimov resonances are identical for both states within the experimental errors, which indicate that the short-range physics is nuclear-spin independent. We also find that the Efimov features are universally related across Feshbach resonances. These results crucially depend on careful mapping between the scattering length and the applied magnetic field which we achieve by characterization of the two broad Feshbach resonances in the different states by means of rf-spectroscopy of weakly bound molecules. By fitting the binding energies numerically with a coupled channels calculation we precisely determine the absolute positions of the Feshbach resonances and the values of the singlet and triplet scattering lengths.

RÉSUMÉ

On présente une étude expérimentale de l'effet d'Efimov dans deux états de spin nucléaire du lithium bosonique, et l'on montre que les positions et les largeurs des résonances d'Efimov sur le taux de recombinaison sont les mêmes pour les deux états à l'incertitude des mesures près, ce qui indique que la physique à courte portée ne dépend pas du spin nucléaire. On trouve également que les paramètres clés de la physique d'Efimov obéissent aux relations universelles attendues sur toute la résonance de Feshbach. Ces résultats dépendent crucialement de la connnaissance de la longueur de diffusion en fonction du champ magnétique, déduite d'une caractérisation des deux résonances de Feshbach larges dans les différents états par spectroscopie radio-fréquence des états moléculaires faiblement liés. En ajustant les énergies de liaison à l'aide d'un modèle numérique à voies couplées, on détermine les positions absolues des résonances de Feshbach and les valeurs des longueurs de diffusion singulet et triplet.

1. Introduction

The recent years' remarkable progress in the study of Efimov quantum states in ultracold atoms has renewed a great deal of interest in this "old-new" quantum few-body problem. Since the first prediction made by V. Efimov in the early

* Corresponding author.
E-mail address: hykovl@mail.biu.ac.il (L. Khaykovich).

1631-0705/$ – see front matter
doi:10.1016/j.crhy.2010.10.004

1970s [1], many systems were considered for an experimental study of these quantum states; however, all of them were attempted in vain. The first experimental evidence of Efimov physics was reported in 2006 in a system of ultracold ^{133}Cs atoms [2] which was later on enhanced and verified in an additional study of the same system [3]. Since then, signatures of Efimov physics have been observed in other ultracold atomic species which turn out to be the only platform up to now suitable to study this phenomenon.

It is well known that at very low collision energies the only partial wave contributing to the scattering process is the s-wave and thus the two-body interaction is completely determined by the s-wave scattering length a. When a exceeds the characteristic two-body potential range r_0, weakly bound three-body Efimov states emerge and their number scales logarithmically with a, $N_b = (s_0/\pi)\ln(|a|/r_0)$ where $s_0 = 1.00624$ [1]. When $|a| \to \pm\infty$, the number of bound states goes to infinity and their energies are related in powers of a universal scaling factor $\exp(-2\pi/s_0) \approx 1/(22.7)^2$ [1,4]. A first indirect evidence of two consecutive Efimov states was demonstrated in ultracold ^{39}K [5] and a universal scaling across a region of $|a| \to \pm\infty$ was verified in ^{7}Li [6].

Studies of Efimov physics have been rapidly extended beyond the spin polarized bosonic samples. A notable example of a three-fermion system, all in different spin states, has been shown by a number of experimental groups [7–9] one of which developed a new and promising experimental approach to probe directly the Efimov quantum states [10]. Another example of a different system is heteronuclear universal trimers observed in Ref. [11].

Recent developments extended the universal few-body physics to the domain of four-body states which was theoretically predicted [12,13] and experimentally verified [14]. Many three- and four-body features over a large dynamical range have been demonstrated in ^{7}Li in Ref. [15]. Interestingly, the universal few-body physics can be extended to N-body clusters [16] though their experimental confirmation remains obscure.

In this work we summarize our study of Efimov physics in two different energy sublevels and across two different Feshbach resonances of the same atomic system [6,17]. As both Feshbach resonances occur at high magnetic fields where nuclear and electronic spins are decoupled, the two energy sublevels are associated with two nuclear-spin states. Our main finding is that the Efimov features are identical within the experimental errors in these two states. The absolute location and lifetime of an Efimov state is defined by the unknown short-range part of the three-body potential. Most generally, the short range potential is given in terms of two-body potential permutations of the two-body subsystems and a true three-body potential which is of importance only when three particles are very close together. It is very difficult to solve the short-range physics exactly, and therefore this region is usually treated in terms of a three-body parameter [4,18]. Thus, our results should be interpreted as a proof that the three-body parameter (and thus the short range physics) is identical for the two states. We provide new and accurate characterizations of Feshbach resonances on both states and reevaluate our previously published results in accordance with this study. Though small changes in the positions of the Efimov features can be identified, the main conclusion is not affected.

This article is organized as follows. Study of Efimov physics across two different Feshbach resonances in two nuclear-spin states is reported in Section 2. We start by comparing the relevant properties of the two energy levels and their resonances. Then, after a description of the experimental procedure we report on newly fitted positions and widths of the Efimov features based on our most recent and precise characterization of the Feshbach resonances on both nuclear-spin states. The latter is based on fitting of the binding energies of weakly bound molecular states, obtained by RF spectroscopy, to a coupled channels calculation locally for each resonance and globally for both resonances. This study is crucial for an accurate mapping of the magnetic field to the scattering length and it is considered in Section 3. Finally, Section 4 concludes the paper.

2. Efimov physics across Feshbach resonances

2.1. Comparison between two nuclear-spin states

A comprehensive discussion on the experimental characterization of Feshbach resonances will be the subject of Section 3. Here we intend to draw a general comparison between the broad resonances of the $|m_F = 1\rangle$ and the $|m_F = 0\rangle$ states of ^{7}Li in the context relevant to the study of Efimov physics. In Fig. 1(a) we show the scattering length in units of Bohr radius a_0 as a function of magnetic field in the vicinity of both Feshbach resonances with their centers aligned. It can be easily recognized that the resonances are comparable in widths while the one on the $|m_F = 0\rangle$ state is slightly wider. Although there are different hyperfine states involved, these two resonances have their origin in the same molecular bound state. Another difference is that in contrast to the $|m_F = 1\rangle$ state where only one resonance exists, on the $|m_F = 0\rangle$ state there is a second resonance overlapping with the first one. It is much narrower and is positioned by atom loss measurement at ~ 845 G [6] as shown in Fig. 1(b). We note that the measurements reported here are obtained in close vicinity to the wide resonance's position, away from the narrow one by many times its width, thus it is not expected to influence the results in the region of interest.

Signature of Efimov physics is studied here by measuring three-body recombination loss of atoms as it has been investigated in all but one recent experiments. In this respect, there is an inherent difference between the two states: in the absolute ground state, two-body relaxation mechanism is fundamentally forbidden while in the $|m_F = 0\rangle$ state it is allowed. In Fig. 2 we show the dipolar relaxation rate coefficients as a function of magnetic field which were calculated via

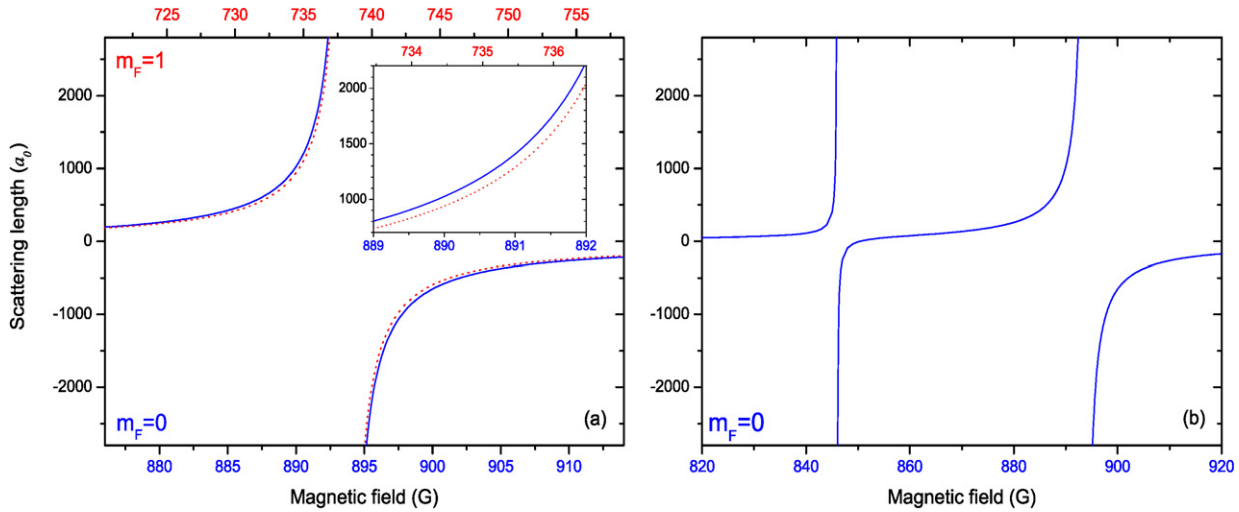

Fig. 1. (a) The broad Feshbach resonances of the $|m_F = 1\rangle$ (dashed red line) and the $|m_F = 0\rangle$ (solid blue line) states, centered at 738.2 G and 893.7 G, respectively. (b) The two Feshbach resonances of the $|m_F = 0\rangle$ state.

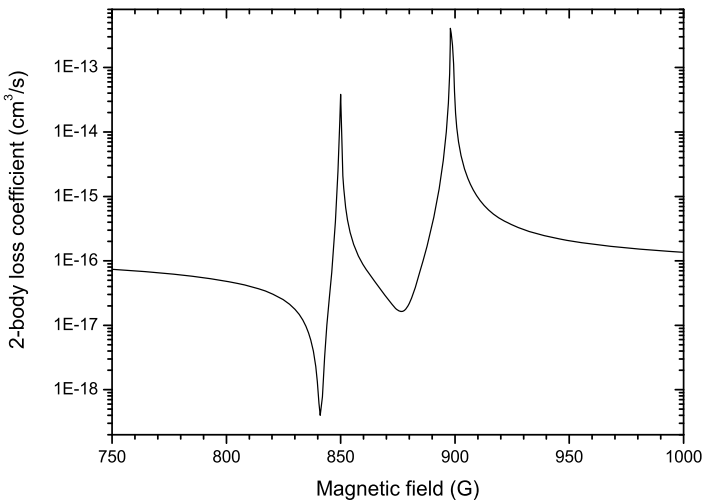

Fig. 2. A coupled-channels calculation of dipolar relaxation rate coefficients as a function of magnetic field for the $|m_F = 0\rangle$ state.

a coupled-channels calculation by using recent interaction potentials [19]. Except for two peaks which signify Feshbach resonances, the loss rate coefficients are extremely small, ~ 3 orders of magnitude smaller than the corresponding measured rate coefficients, if the experimental losses were treated as purely two-body related. For example, at 880 G the two-body loss coefficient is $\sim 5 \times 10^{-17}$ cm^3/s which yields, given that the atom density is $\sim 10^{12}$ cm^{-3}, a life time of $\sim 20\,000$ s. As a comparison, the life time in our dipole trap due to vacuum is less than 100 s. As a result, we exclude two-body losses from the analysis described below and determine that the loss processes in the region of interest are related to three-body recombination. Note that while we find this mechanism to be negligible for ^{7}Li atoms, it can be important for heavier alkali atoms. For instance, ^{133}Cs experiences large dipolar losses caused by the second-order spin–orbit interaction [20].

2.2. Experimental measurement of three-body recombination loss

According to a dimensional analysis, taking the scattering length as the only parameter describing the interaction, one finds that the three-body recombination loss rate coefficient (K_3) scales as $\hbar a^4/m$ [21]. Above this general scaling, taking into account the fact that the scattering length has to be supplemented by a three-body parameter to describe the interaction of three bosons, universal theory predicts log-periodic oscillations of K_3 due to the presence of Efimov trimer states. For positive scattering lengths the oscillations are caused by destructive interference conditions between two possible decay pathways at certain values of a [4,22]. For negative scattering lengths the loss rate coefficient exhibits a resonance enhance-

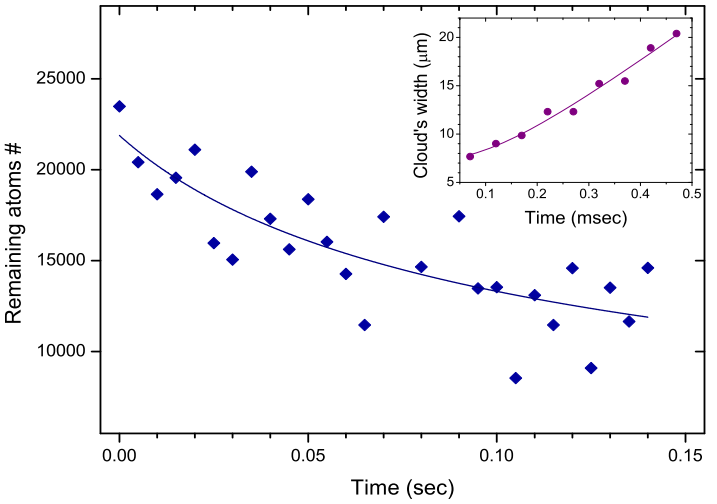

Fig. 3. A typical atom-number decay measurement on the $|m_F = 1\rangle$ state. Insert: time-of-flight measurement from which the initial temperature is deduced.

ment each time an Efimov trimer state intersects with the continuum threshold. Hence, a study of K_3 across a Feshbach resonance enables the search for an indirect evidence of Efimov trimer states.

In the experiment, we perform evaporative cooling in an optical dipole trap near a Feshbach resonance where a gas of ^{7}Li atoms is spontaneously spin purified to the $|m_F = 0\rangle$ state and is cooled down to the threshold of degeneracy [23]. For measurements in the absolute ground state ($|m_F = 1\rangle$), a rapid adiabatic passage by means of a radio-frequency (rf) sweep at a low magnetic field is used to transfer the atoms from the $|m_F = 0\rangle$ state [17]. We conduct measurements of atom-number decay and initial temperature as a function of magnetic field in the vicinity of wide Feshbach resonances on both states. An example of such set of measurements is shown in Fig. 3. We use the temperature measurement, together with a precise characterization of the trap frequencies, to estimate the initial atom density. Then, the K_3 value is extracted by fitting the atom-number decay measurement with the atom-loss rate equation solution:

$$\dot{N} = -K_3\langle n^2\rangle N - \Gamma N, \tag{1}$$

where K_3 and Γ are the three- and single-body loss rate coefficients, respectively. Γ is determined independently by measuring a very long decay tail of a low density sample. Note that this simplified model does not include several important effects, one of which is the saturation of K_3 to a maximal value K_{max} due to finite temperature (unitarity limit) and it can be represented as [24]:

$$K_{max} = c\frac{125\pi^2\hbar^5}{m^3k_B^2T^2}, \tag{2}$$

where m is the atomic mass, k_B is the Boltzmann's constant and c is a numerical constant distinguishing between the two threshold regimes of the collision energies, $c = 1$ for $a > 0$ and $c \approx 0.1$ for $a < 0$. To address this limitation, measurements for which $K_3 \gtrsim 0.1K_{max}$ are omitted from the analysis of Efimov features (see Section 2.3).

Other effects which are not included in the model are 'anti-evaporation' and recombination heating [25]. The first is an effective heating caused by a preferential loss of atoms from the densest (and thus coldest) part of the cloud. We treat the evolution of our data to no more than $\sim 30\%$ decrease in atom number, as can be seen in Fig. 3, for which 'anti-evaporation' is estimated to induce a systematic error of $\sim 23\%$ towards higher values of K_3. The error is evaluated based on an analytical solution to coupled atom-loss rate and temperature evolution equations [25,5] and it is estimated not to limit the accuracy of the reported results. Recombination heating can be neglected for $K_3 \ll K_{max}$ because in this case the trap depth (which scales with temperature) is smaller than the energy released in the recombination process leading to an immediate loss of the colliding partners. Moreover, this approach, together with the small decrease in atom number, allows time evolution of the unitarity limit ($K_{max}(t)$) to be neglected within a single atom-number decay measurement. Note, that 'anti-evaporation' and recombination heating pose strong limitations on the measurement's dynamical range in the large scattering lengths limit where more careful model than Eq. (1) has to be considered. This is demonstrated for $|m_F = 1\rangle$ state in Fig. 4 where a dramatic increase in the initial temperature of the atom-number decay measurement near the resonance corresponds to a reduction in the value of K_{max} according to Eq. (2).

2.3. Efimov features and universality

Experimental results of the three-body loss measurements are summarized in Fig. 5 where K_3 is plotted as a function of the scattering length a for the $|m_F = 1\rangle$ state (red solid circles) and the $|m_F = 0\rangle$ state (blue open diamonds). Magnetic

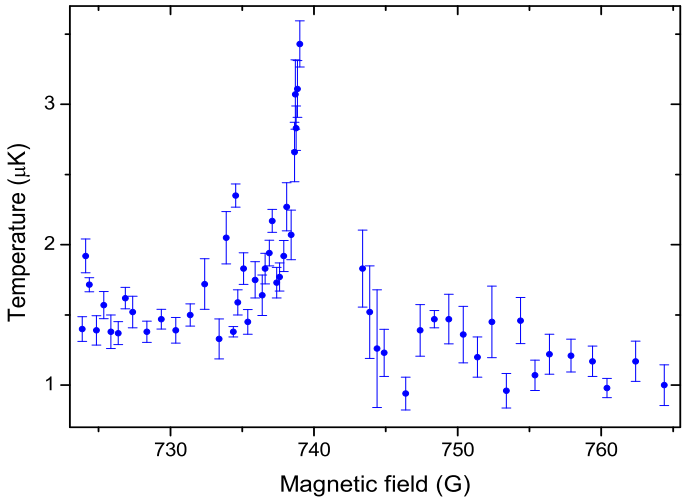

Fig. 4. Initial temperature of the atom-number decay measurement around the Feshbach resonance on the $|m_F = 1\rangle$ state from which the atom density is extracted for the calculation of K_3. Each point is deduced from a time-of-flight measurement (see insert in Fig. 3). The error bars represent the fitting errors.

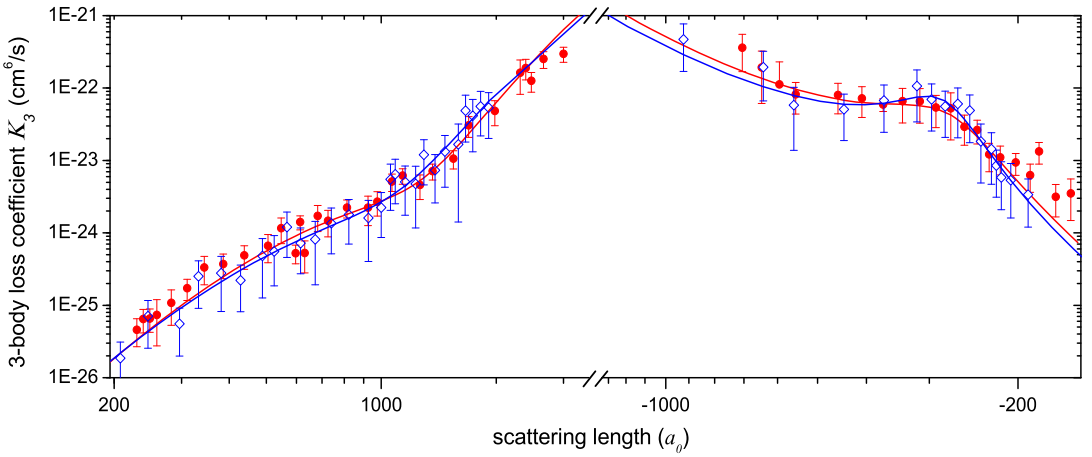

Fig. 5. Experimentally measured three-body loss coefficient K_3 as a function of scattering length (in units of Bohr radius a_0) for the $|m_F = 1\rangle$ state (red solid circles) and the $|m_F = 0\rangle$ state (blue open diamonds). The solid lines (red and blue, respectively) represent fits to the analytical expressions of universal theory.[2] The error bars consist of two contributions: the uncertainty in temperature measurement which affects the estimated atom density and the fitting error of the atom-number decay measurement.

field values are converted to scattering lengths via a careful analysis of the Feshbach resonances, that will be discussed in Section 3. A qualitative analysis indicates a striking similarity between the two sets of measurements for both positive and negative scattering lengths. We can further verify this similarity quantitatively by fitting the measured K_3 data to a prediction of universal theory. For that purpose we represent the loss rate coefficient in a convenient form [4]:

$$K_3 = 3C_{\pm}(a)\hbar a^4/m \tag{3}$$

where $\pm$ hints at the positive $(+)$ or negative $(-)$ region of the scattering length. An effective field theory provides analytic expressions for $C_{\pm}(a)$ that we use in the form represented in [2,3]:

$$C_+(a) = 67.1e^{-2\eta_+}\left(\cos^2\left[s_0\ln(a/a_+)\right] + \sinh^2\eta_+\right) + 16.8\left(1 - e^{-4\eta_+}\right) \tag{4}$$

and

$$C_-(a) = 4590\sinh(2\eta_-)/\left(\sin^2\left[s_0\ln(|a|/a_-)\right] + \sinh^2\eta_-\right), \tag{5}$$

[2] We note that the four points with the highest values of K_3 on $|m_F = 1\rangle$ $a > 0$ were omitted from the fitting procedure on the grounds of approaching the finite temperature saturation value K_{max} (unitarity limit) [24] which is $\sim 4.5 \times 10^{-21}$ cm^6/s for a temperature of 3.5 μK.

Table 1
Fitting parameters to universal theory obtained from the measured K_3 values of the $|m_F = 1\rangle$ and the $|m_F = 0\rangle$ states.

State	η_+	η_-	a_+/a_0	a_-/a_0	$a_+/\lvert a_-\rvert$
$\lvert m_F = 0\rangle$	0.213(79)	0.180(48)	238(25)	−280(12)	0.85(11)
$\lvert m_F = 1\rangle$	0.170(41)	0.253(62)	265(16)	−274(12)	0.97(8)

where the free parameters of the fits are $a_\pm$ and $\eta_\pm$ which are connected to the real and the imaginary parts of the three-body parameter, respectively [4,26]. The fitting results are represented by solid lines in corresponding colors in Fig. 5 (see footnote 2) and the fitting parameters are summarized in Table 1. Comparing corresponding parameters in different states acknowledges the notion that the Efimov features are identical within the experimental errors which signifies that the short-range physics is nuclear-spin independent. An interesting conclusion can be drawn from this observation. Recall that the short range potential is given in terms of two-body potential permutations of the two-body subsystems and a true three-body potential. As the two Feshbach resonances occur at high magnetic fields where the nuclear and electron spins are effectively decoupled, the two-body potentials are similar for both states. Therefore, if the short-range physics is spin-independent, the true three-body forces are either also nuclear-spin independent or play a relatively minor role.

Moreover, two predictions of universal theory are also verified here: first, the decay parameters η_+ and η_-, which describe the lifetime of the Efimov state, are assumed to be equal and indeed they are (within the experimental errors). This suggests that the imaginary part of the three-body parameter is identical. Second, the theoretical assumption that the real part of the three-body parameter across a Feshbach resonance is the same for negative and positive scattering length regions requires a_+ and a_- to obey a universal ratio $a_+/|a_-| = 0.96(3)$ [4]. The fits yield values of 0.85(11) and 0.97(8) for $|m_F = 0\rangle$ and $|m_F = 1\rangle$, respectively, which overlap with each other and with the predicted value within the experimental and theoretical error bars. We thus confirm that the three-body parameter is preserved across two different Feshbach resonances and between two different nuclear-spin states. Note that slight deviations of our measurements from the universally predicted values can be explained by finite effective range corrections which were recently evaluated by means of an effective field theory [27].

For positive scattering lengths, the Efimov trimer is expected to intersect with the atom-dimer threshold at $a_* \approx 1.1a_+$ [4]. Theory predicts that a_* and a_- of the same trimer state are related as $a_- \approx -22a_*$ [4]. Therefore, if the observed Efimov resonance at a_- indicates the lowest state, the one expected at a_* indicates the first excited state as the lowest one becomes nonuniversal.

3. Characterization of Feshbach resonances

3.1. Experimental measurements of binding energy of Feshbach molecules

For a correct investigation of the K_3 coefficients dependence on the two-body scattering length, it is crucial to have an accurate mapping between the scattering length and the applied magnetic field. For this purpose, the binding energies of the underlying bound states which give rise to the two broad Feshbach resonances are carefully measured using rf molecule association. This method uses a weak rf field to resonantly associate weakly bound Feshbach dimers which are then rapidly lost through collisional relaxation into deeply bound states [28]. In the experiment the rf modulation time is varied between 0.5 and 3 sec and the modulation amplitude ranges from 150 to 750 mG. The remaining atom number is measured by absorption imaging as a function of rf frequency at a given magnetic field and the rf-induced losses are then numerically fitted to a convolution of a Maxwell–Boltzmann and a Gaussian distributions. The former accounts for broadening of the spectroscopic feature due to finite kinetic energy of atoms at a typical temperature of ~ 1.5 μK [29]. The latter reflects broadening due to magnetic field instability and shot-to-shot atom number fluctuations. From the fit we extract the molecular binding energy (E_b) corresponding to zero temperature. An example of a molecule association induced loss feature is depicted in Fig. 6 where the characteristic asymmetry of the obtained profile is clearly seen [29]. Results of the binding energy rf spectroscopy for both states are shown in Fig. 7. We analyze these results by fitting them with a coupled-channels calculation which is discussed in the next section.

3.2. Analysis of two-body interactions

Very close to resonance, the binding energy is related to the scattering length as

$$E_b(a) = -\frac{\hbar^2}{ma^2}. \tag{6}$$

This expression shows that ultracold scattering physics is closely related to bound state physics just below the dissociation threshold. However, this simple relationship rapidly breaks down when going further away from resonance, and is therefore not sufficient to interpret three-body recombination in terms of the scattering length.

In order to make a correct mapping between binding energy and scattering length, we make use of a coupled-channels two-body interaction model for lithium, which has been discussed earlier [19], and we use the interaction potentials dis-

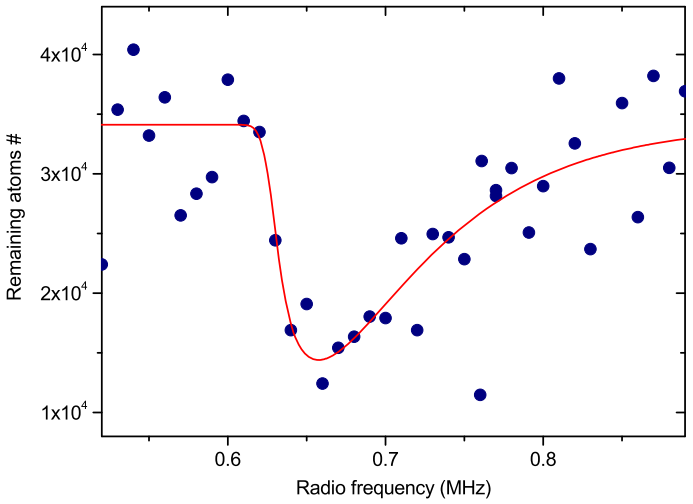

Fig. 6. rf association of molecules at $B = 734.4$ G on the $|m_F = 1\rangle$ state. The loss resonance is fitted numerically to a convolution of Maxwell–Boltzmann and a Gaussian distributions (solid line).

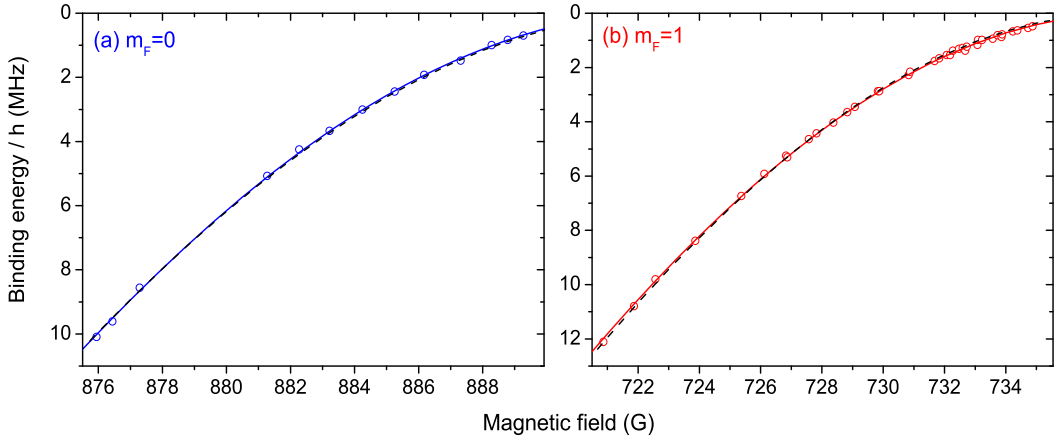

Fig. 7. rf spectroscopy of the molecular binding energy near the Feshbach resonance in the $|m_F = 0\rangle$ (a) and the $|m_F = 1\rangle$ (b) states. The solid line represents an independent fit to CC calculation while the dark dashed line is the combined fit for both states simultaneously.

cussed there as a starting point for our analysis. For large interatomic separations r the singlet ($S = 0$) and a triplet ($S = 1$) potentials are given by

$$V_S(r) = -\frac{C_6}{r^6} - \frac{C_8}{r^8} - \frac{C_{10}}{r^{10}} - (-1)^S C^{ex} r^{7/2\alpha - 1} e^{-2\alpha r}, \tag{7}$$

with van der Waals coefficients C_6, C_8, C_{10} [32], exchange parameter C^{ex} [33,34], and the ionization energy $\alpha^2/2$ [35]. For the short radial range r we use model singlet and triplet potentials which have also been used in Refs. [36,37].

The short-range and long-range potentials are smoothly connected at $r = 18a_0$. We improve the accuracies of the short range potentials considerably, by making use of the accumulated phase method [36]. Therefore a boundary condition is applied on the partial-wave radial wave functions at $r = 7a_0$ in the form of a WKB phase

$$\phi_{S,T}(E, \ell) = \phi^0_{S,T}(E, \ell) + \Delta\phi_{S,T}. \tag{8}$$

The first term on the right is calculated by radial integration of the model potential up to $7a_0$ and is sufficiently accurate to account for the energy and angular momentum dependence of the accumulated phase. The corrections $\Delta\phi_{S,T}$ to the accumulated singlet and triplet phases are independent of energy and angular momentum.

The most crucial parameters in the coupled channels model are $\Delta\phi_S$, $\Delta\phi_T$ and C_6, which we take as free parameters that we determine from our experimental binding energies. We perform a χ^2 minimization with respect to the free parameters, and this allows us to determine the positions of both Feshbach resonances, and the direct mapping of the scattering length on the magnetic field $a(B)$. In order to extract the resonance's parameters we fit $a(B)$ with a factorized expression [38]:

Table 2
Feshbach resonance parameters for both states as obtained from independent fits of the CC calculation to the molecular binding energies (solid lines in Fig. 7).

State	Type	a_{bg}/a_0	Δ (G)	B_0 (G)
$\|m_F = 0\rangle$	narrow	−18.24	+4.518	846.0
$\|m_F = 0\rangle$	wide	−18.24	−237.8	893.7(3)
$\|m_F = 1\rangle$	wide	−20.98	−171.0	738.2(2)

Table 3
Feshbach resonances' positions (B_0) as obtained from a combined fitting of the molecular binding energy measurements in both states simultaneously to the CC calculation. The experimentally determined positions are presented in the last column where the narrow resonance was determined by atom loss measurement [6] and the two wide ones where determined by independent fits of the molecular binding energies (see Table 2). The field calibration uncertainty is included in the experimental errors.

State	Type	B_0 (G)	
		Combined fit	Experimental
$\|m_F = 0\rangle$	narrow	845.54	844.9(8)
$\|m_F = 0\rangle$	wide	893.95(5)	893.7(4)
$\|m_F = 1\rangle$	wide	737.88(2)	738.2(4)

$$\frac{a}{a_{bg}} = \prod_{i=1}^{N}\left(1 - \frac{\Delta_i}{(B - B_{0,i})}\right), \tag{9}$$

where a_{bg} is the background scattering length, Δ_i is the i's resonance width and $B_{0,i}$ is the i's resonance position.

We analyze the data in two different ways. First we perform an independent fit of the model to the $|m_F = 0\rangle$ and the $|m_F = 1\rangle$ binding energies, represented by solid blue and red lines in Fig. 7(a) and (b), respectively. Then, a combined fit for both m_F states is performed (dashed black line in Fig. 7(a,b)), which allows us to check the consistency between the two different experiments, within the same interaction model. Deviations of the second case from the first one are a hint for possible different systematic shifts in magnetic field calibration for both states. This can be explained by the fact that a precise calibration of the magnetic field is performed locally by microwave transitions in the vicinity of each of the wide resonances. Note that each set of measurements is limited to a range of ± 20 G around the resonances while the distance between them is ~ 150 G. We therefore use the results of the independent fits for the K_3 analysis which was discussed previously in this paper. The resonances' parameters as obtained from the independent fits are summarized in Table 2.

Table 3 represents the resonances' positions obtained from the combined fit and compares them with our most precise to-date experimental values, i.e. an atom loss measurement for the narrow resonance of $|m_F = 0\rangle$ [6] and the two independent fits of the wide resonances (Table 2). A field calibration uncertainty of 0.3 G is added to the fitting errors of the experimental values.

We find the results in Table 3 mutually consistent. Moreover, the determined values for ϕ_S, $\Delta\phi_T$ and C_6 are all consistent with the bound of earlier performed analysis [36,30,37,19]. Since our combined analysis only weakly depends on the value of the C_6 coefficient, we present our results with a fixed value of C_6 which was found in the *ab initio* calculations [32, 31]. The determined parameters ϕ_S and $\Delta\phi_T$ correspond to the singlet and triplet scattering lengths $a_S = 34.33(2)\ a_0$ and $a_T = -26.87(8)\ a_0$.

4. Conclusions

In this work we study experimentally Efimov physics in two nuclear-spin sublevels of bosonic lithium and show that the positions and widths of recombination minima and Efimov resonances are identical for both states within the experimental errors. As the properties of Efimov features are governed by the three-body parameter, our study indicates that the short-range physics is nuclear-spin independent. We also find that the Efimov features are universally related across the Feshbach resonances. Let us note that the observed position of the Efimov resonance reveals the same numerical factor $|a_-|/r_0 \approx 8.5$ as in the experiments on ^{133}Cs [2] which may or may not be an accidental coincidence.

The reported results crucially depend on a careful mapping between the scattering length and the magnetic field. We characterize two wide Feshbach resonances in different states by fitting the binding energies of weakly bound molecules, created by rf-association, with a coupled channels analysis. This gives rise to a very precise determination of the absolute positions of the Feshbach resonances and the values of the singlet and triplet scattering length that characterize the molecular potentials of lithium.

Acknowledgements

This work was supported, in part, by the Israel Science Foundation and by the Netherlands Organization for Scientific Research (NWO). N.G. is supported by the Adams Fellowship Program of the Israel Academy of Sciences and Humanities.

References

[1] V. Efimov, Phys. Lett. B 33 (1970) 563; Sov. J. Nucl. Phys. 12 (1971) 589; Sov. J. Nucl. Phys. 29 (1979) 546.
[2] T. Kraemer, M. Mark, P. Waldburger, J.G. Danzl, C. Chin, B. Engeser, A.D. Lange, K. Pilch, A. Jaakkola, H.-C. Nägerl, R. Grimm, Nature 440 (2006) 315.
[3] S. Knoop, F. Ferlaino, M. Berninger, M. Mark, H.-C. Nägerl, R. Grimm, Nature Phys. 5 (2009) 227.
[4] E. Braaten, H.-W. Hammer, Phys. Rep. 428 (2006) 259.
[5] M. Zaccanti, B. Deissler, C. D'Errico, M. Fattori, M. Jona-Lasinio, S. Müller, G. Roati, M. Inguscio, G. Modugno, Nature Phys. 5 (2009) 586.
[6] N. Gross, Z. Shotan, S.J.J.M.F. Kokkelmans, L. Khaykovich, Phys. Rev. Lett. 103 (2009) 163202.
[7] T.B. Ottenstein, T. Lompe, M. Kohnen, A.N. Wenz, S. Jochim, Phys. Rev. Lett. 101 (2008) 203202;
A.N. Wenz, T. Lompe, T.B. Ottenstein, F. Serwane, G. Zürn, S. Jochim, Phys. Rev. A 80 (2009) 040702(R);
T. Lompe, T.B. Ottenstein, F. Serwane, K. Viering, A.N. Wenz, G. Zürn, S. Jochim, Phys. Rev. Lett. 105 (2010) 103201.
[8] J.H. Huckans, J.R. Williams, E.L. Hazlett, R.W. Stites, K.M. O'Hara, Phys. Rev. Lett. 102 (2009) 165302;
J.R. Williams, E.L. Hazlett, J.H. Huckans, R.W. Stites, Y. Zhang, K.M. O'Hara, Phys. Rev. Lett. 103 (2009) 130404.
[9] S. Nakajima, M. Horikoshi, T. Mukaiyama, P. Naidon, M. Ueda, Phys. Rev. Lett. 105 (2010) 023201.
[10] T. Lompe, T.B. Ottenstein, F. Serwane, A.N. Wenz, G. Zürn, S. Jochim, arXiv:1006.2241.
[11] G. Barontini, C. Weber, F. Rabatti, J. Catani, G. Thalhammer, M. Inguscio, F. Minardi, Phys. Rev. Lett. 103 (2009) 043201.
[12] L. Platter, H.-W. Hammer, Ulf-G. Meißner, Phys. Rev. A 70 (2004) 052101.
[13] J. von Stecher, J.P. D'Incao, C.H. Greene, Nature Phys. 5 (2009) 417.
[14] F. Ferlaino, S. Knoop, M. Berninger, W. Harm, J.P. D'Incao, H.-C. Nägerl, R. Grimm, Phys. Rev. Lett. 102 (2009) 140401.
[15] S.E. Pollack, D. Dries, R.G. Hulet, Science 326 (2009) 1683.
[16] J. von Stecher, J. Phys. B 43 (2010) 101002;
G.J. Hanna, D. Blume, Phys. Rev. A 74 (2006) 063604.
[17] N. Gross, Z. Shotan, S.J.J.M.F. Kokkelmans, L. Khaykovich, Phys. Rev. Lett. 105 (2010) 103203.
[18] J.P. D'Incao, C.H. Greene, B.D. Esry, J. Phys. B 42 (2009) 044016.
[19] E.G.M.v. Kempen, B. Marcelis, S.J.J.M.F. Kokkelmans, Phys. Rev. A 70 (2004) 050701(R).
[20] S.J.J.M.F. Kokkelmans, B.J. Verhaar, K. Gibble, Phys. Rev. Lett. 81 (1998) 951;
F.H. Mies, C.J. Williams, P.S. Julienne, M. Krauss, J. Res. Natl. Inst. Stand. Technol. 101 (1996) 521.
[21] P.O. Fedichev, M.W. Reynolds, G.V. Shlyapnikov, Phys. Rev. Lett. 77 (1996) 2921.
[22] B.D. Esry, C.H. Greene, J.P. Burke, Phys. Rev. Lett. 83 (1999) 1751;
E. Nielsen, J.H. Macek, Phys. Rev. Lett. 83 (1999) 1566.
[23] N. Gross, L. Khaykovich, Phys. Rev. A 77 (2008) 023604.
[24] J.P. D'Incao, H. Suno, B.D. Esry, Phys. Rev. Lett. 93 (2004) 123201.
[25] T. Weber, J. Herbig, M. Mark, H.-C. Nägerl, R. Grimm, Phys. Rev. Lett. 91 (2003) 123201.
[26] B. Marcelis, S.J.J.M.F. Kokkelmans, G.V. Shlyapnikov, D.S. Petrov, Phys. Rev. A 77 (2008) 032707.
[27] C. Ji, D. Phillips, L. Platter, Europhys. Lett. 92 (2010) 13003.
[28] S.T. Thompson, E. Hodby, C.E. Wieman, Phys. Rev. Lett. 95 (2005) 190404.
[29] T.M. Hanna, T. Köler, K. Burnett, Phys. Rev. A 75 (2007) 013606.
[30] E.R.I. Abraham, W.I. McAlexander, J.M. Gerton, R.G. Hulet, R. Côté, A. Dalgarno, Phys. Rev. A 55 (1997) R3299.
[31] A. Derevianko, J.F. Babb, A. Dalgarno, Phys. Rev. A 63 (2001) 052704.
[32] Z.-C. Yan, J.F. Babb, A. Dalgarno, G.W.F. Drake, Phys. Rev. A 54 (1996) 2824.
[33] W.T. Zemke, W.C. Stwalley, J. Chem. Phys. 111 (1999) 4962.
[34] M. Marinescu, A. Dalgarno, Z. Phys. D 36 (1996) 239.
[35] C.J. Lorenzen, K. Niemax, J. Phys. B 15 (1982) L139–L145.
[36] A.J. Moerdijk, B.J. Verhaar, Phys. Rev. Lett. 73 (1994) 518.
[37] F.A. van Abeelen, B.J. Verhaar, A.J. Moerdijk, Phys. Rev. A 55 (1997) 4377.
[38] A.D. Lange, K. Pilch, A. Prantner, F. Ferlaino, B. Engeser, H.-C. Nägerl, R. Grimm, C. Chin, Phys. Rev. A 79 (2009) 013622.

Chapter 7

Conclusions and outlook

This work starts with a detailed description of the design and construction of an experimental apparatus that cools bosonic lithium atoms in an all-optical method down to ultracold temperatures and quantum degeneracy. Using this tool we investigate and characterize two wide Feshbach resonances in different Zeeman sublevels of lithium's lower hyperfine state. Precise determination of the resonances' absolute positions and energy widths allow for the calculation of improved values of the singlet and triplet scattering lengths that characterize the interatomic potential. In the vicinity of Feshbach resonances, we study Efimov physics in two nuclear-spin sublevels of lithium atoms and show that the positions and widths of recombination minima and Efimov resonances are identical for both states within the experimental errors. As these properties of Efimov features are solely governed by a non-universal (three-body) parameter, our study indicates that the short-range physics is thus nuclear-spin independent. This empirical result is beyond the reach of theory at its present stage. We also confirm the basic result of universal theory that Efimov features are universally related across a Feshbach resonance.

Most recently, the Innsbruck group, led by R. Grimm, investigated universal few-body physics with ultracold gas of cesium atoms and detected five distinct Efimov resonances in the same spin channel, all resulting from different Feshbach resonances [44]. Interestingly, all the Efimov resonances occur at the same scattering length value, which points

to universality across all Feshbach resonances and rules out a significant variation of the three-body parameter as a function of the magnetic field. These results are on the same footing as our finding that the three-body parameter is nuclear-spin independent. Moreover, our observed Efimov resonance position (a_-) reveals the same numerical factor $|a_-|/l_{vdW} \approx 8.5$ as in the ^{133}Cs experiments [7] (l_{vdW} is the van der Waals length). If this is not an accidental coincidence, we can point out on a certain universality which seems to exist in the non-universal (related to the three-body parameter) part of universal theory which requires further investigation.

Experimental study of Efimov physics is still at its infancy. Many controversies and open questions are yet to be addressed. I list here some of them. While our work confirms the basic phenomenology of universal few-body physics, other experimental observations, such as that in Ref. [11], show significant quantitative deviations from it. More effort, theoretical and experimental, is needed in order to understand the predictive power of universal theories as applied to real-world systems.

The universal properties of a closed-channel dominated Feshbach resonance are expected to be different and have yet to be studied. In that context, the $|F = 1, m_F = 0\rangle$ state of ^{7}Li provides a unique opportunity to investigate universality across a broad and a narrow Feshbach resonances in the same spin channel.

Recent theoretical publications by S. Tan [45] and E. Braaten [46] have shown general connections between few-body interactions and the essential properties of many-body systems. The few-body approach can give new insights into the many-body physics of strongly interacting systems.

Finally we note that studies of Efimov physics have been rapidly extended beyond the spin polarized bosonic samples. A notable example of a three-fermion system, all in different spin states, has been shown by a number of experimental groups [9, 47, 48, 10, 49, 16] one of which developed a new and promising experimental approach to probe directly the Efimov quantum states [50]. Another example of a different system is heteronuclear universal trimers observed in Ref. [14]. The Efimov problem considered in the framework

of distinguishable particles is another avenue yet to be explored [51, 52]. Interestingly, the mass ratio changes the geometric scaling factor and for extreme ratios it can be much smaller than 22.7. Observation of these denser spectra of Efimov states can become an ultimate check of universality. Recent developments extended the universal few-body physics to the domain of four-body states which was theoretically predicted [53, 54] and experimentally verified [55]. Interestingly, the universal few-body physics can be extended to N-body clusters [56] though their experimental confirmation remains obscure.

Appendix A

The exponential ramp function

During the CMOT and the evaporation phases some system variables are optimally changed with an exponential decay/growth. Out of the four parameters that describe an exponential change, namely: the initial value V_i, the final value V_f, the time duration Δt and the change rate α, only three at a time can be set independently. With V_i usually given, we wanted to construct a function in which V_f and Δt can be set explicitly while giving us freedom to determine α. We have found a solution in the form of a biased exponential function. One can always find a bias value V_0 that will satisfy the equation:

$$(V_i - V_0)e^{-\alpha} = V_f - V_0, \tag{A.1}$$

hence giving:

$$V_0 = V_i + \frac{V_f - V_i}{1 - e^{-\alpha}}, \tag{A.2}$$

and the biased exponential function will look as follows:

$$V(t) = V_0 + (V_i - V_0)e^{-\frac{\alpha}{\Delta t}t}, \tag{A.3}$$

where

$$0 \leq t \leq \Delta t. \tag{A.4}$$

The big advantage of this function is that all parameters are predetermined. The compromise is that it is not a real exponential function and α is not the actual decay

rate but rather a relative value that we can increase or decrease by need. $\alpha = 0$ can be assigned with positive or negative values while $\alpha = 0$ results in a linear change. Note that increasing Δt merely "stretches" the function which comes in handy when searching for the optimal evaporation duration time.

Appendix B

The dual photo-detector

A schematic of the dual PD that is used to monitor and control the power of the main beam of the optical dipole trap (see Sec. 1.3) is depicted in Fig. B.1. The PD was designed and built by Eli Perel.

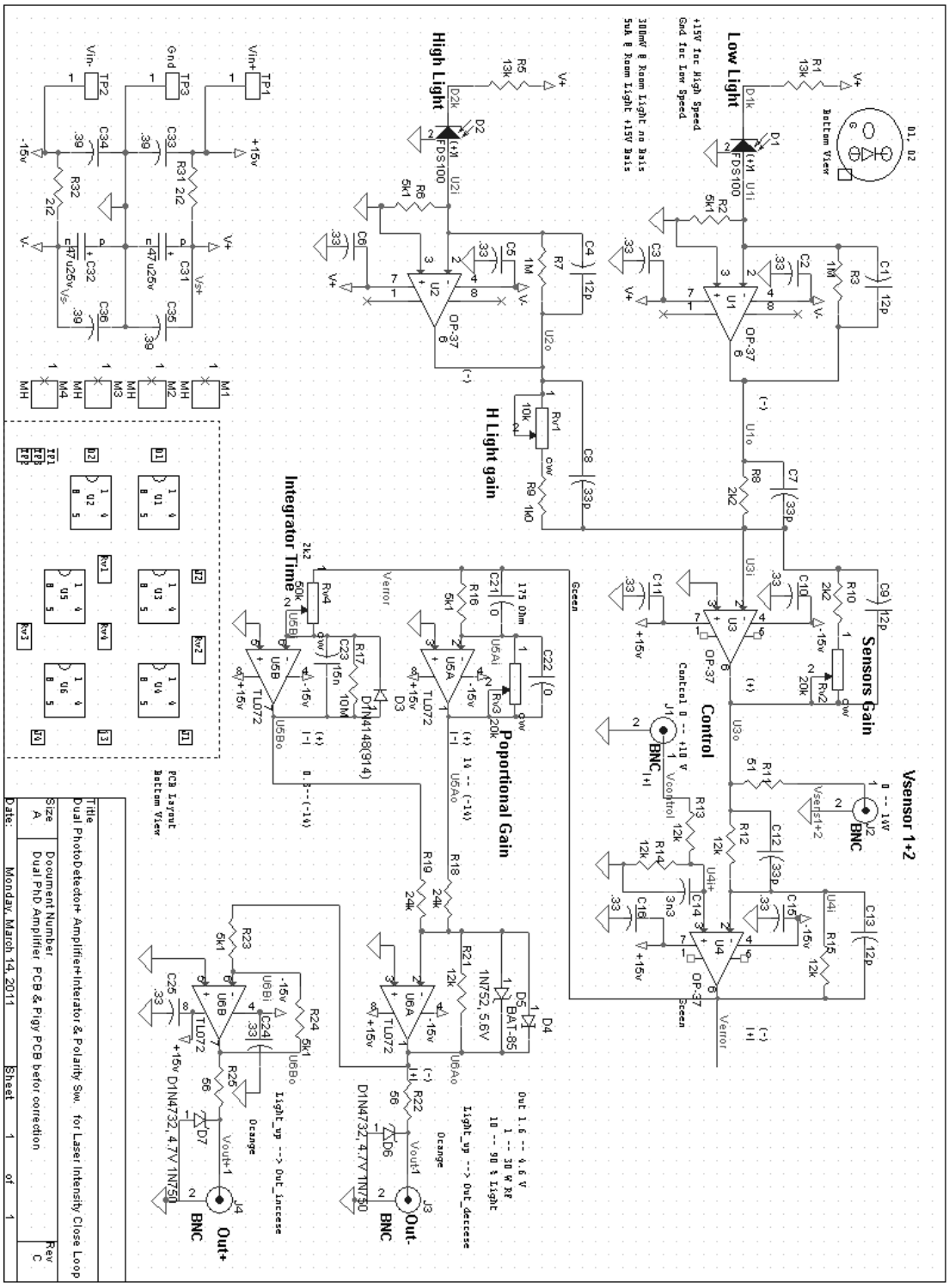

Figure B.1: The dual photo-detector schematic.

Bibliography

[1] E. Braaten and H.W. Hammer. Efimov physics in cold atoms. *Annals of Physics*, 322(1):120–163, 2007.

[2] C. Chin, R. Grimm, P. Julienne, and E. Tiesinga. Feshbach resonances in ultracold gases. *Reviews of Modern Physics*, 82(2):1225, 2010.

[3] AS Jensen, K. Riisager, D.V. Fedorov, and E. Garrido. Structure and reactions of quantum halos. *Reviews of Modern Physics*, 76(1):215, 2004.

[4] V. Efimov. Energy levels arising from resonant two-body forces in a three-body system. *Physics Letters B*, 33(8):563–564, 1970.

[5] V. Efimov. Weakly-bound states of three resonantly-interacting particles. *Sov. J. Nucl. Phys*, 12:589, 1971.

[6] V. Efimov. Low-energy properties of three resonantly interacting particles. *Sov. J. Nucl. Phys*, 29:546, 1979.

[7] T. Kraemer, M. Mark, P. Waldburger, JG Danzl, C. Chin, B. Engeser, AD Lange, K. Pilch, A. Jaakkola, H.C. Nägerl, and R. Grimm. Evidence for Efimov quantum states in an ultracold gas of caesium atoms. *Nature*, 440(7082):315–318, 2006.

[8] S. Knoop, F. Ferlaino, M. Mark, M. Berninger, H. Schäbel, H.C. Nägerl, and R. Grimm. Observation of an Efimov-like trimer resonance in ultracold atom–dimer scattering. *Nature Physics*, 5(3):227–230, 2009.

[9] TB Ottenstein, T. Lompe, M. Kohnen, AN Wenz, and S. Jochim. Collisional stability of a three-component degenerate Fermi gas. *Physical Review Letters*, 101(20):203202, 2008.

[10] JH Huckans, JR Williams, EL Hazlett, RW Stites, and KM OHara. Three-body recombination in a three-state Fermi gas with widely tunable interactions. *Physical Review Letters*, 102(16):165302, 2009.

[11] M. Zaccanti, B. Deissler, C. DErrico, M. Fattori, M. Jona-Lasinio, S. Müller, G. Roati, M. Inguscio, and G. Modugno. Observation of an Efimov spectrum in an atomic system. *Nature Physics*, 5(8):586–591, 2009.

[12] N. Gross, Z. Shotan, S. Kokkelmans, and L. Khaykovich. Observation of Universality in Ultracold ^{7}Li Three-Body Recombination. *Physical Review Letters*, 103(16):163202, 2009.

[13] S.E. Pollack, D. Dries, and R.G. Hulet. Universality in three-and four-body bound states of ultracold atoms. *Science*, 326(5960):1683, 2009.

[14] G. Barontini, C. Weber, F. Rabatti, J. Catani, G. Thalhammer, M. Inguscio, and F. Minardi. Observation of heteronuclear atomic Efimov resonances. *Physical Review Letters*, 103(4):43201, 2009.

[15] N. Gross, Z. Shotan, S. Kokkelmans, and L. Khaykovich. Nuclear-spin-independent short-range three-body physics in ultracold atoms. *Physical Review Letters*, 105(10):103203, 2010.

[16] S. Nakajima, M. Horikoshi, T. Mukaiyama, P. Naidon, and M. Ueda. Nonuniversal Efimov Atom-Dimer Resonances in a Three-Component Mixture of ^{6}Li. *Physical Review Letters*, 105(2):23201, 2010.

[17] E. Braaten and H.W. Hammer. Universality in few-body systems with large scattering length. *Physics Reports*, 428(5-6):259–390, 2006.

[18] JP D'Incao, C.H. Greene, and BD Esry. The short-range three-body phase and other issues impacting the observation of Efimov physics in ultracold quantum gases. *Journal of Physics B: Atomic, Molecular and Optical Physics*, 42:044016, 2009.

[19] MD Barrett, JA Sauer, and MS Chapman. All-optical formation of an atomic Bose-Einstein condensate. *Physical Review Letters*, 87(1):10404, 2001.

[20] Y. Takasu, K. Maki, K. Komori, T. Takano, K. Honda, M. Kumakura, T. Yabuzaki, and Y. Takahashi. Spin-singlet Bose-Einstein condensation of two-electron atoms. *Physical Review Letters*, 91(4):40404, 2003.

[21] T. Weber, J. Herbig, M. Mark, H.C. Nagerl, and R. Grimm. Bose-Einstein Condensation of Cesium. *Science*, 299(5604):232, 2003.

[22] SR Granade, ME Gehm, KM O'Hara, and JE Thomas. All-optical production of a degenerate Fermi gas. *Physical Review Letters*, 88(12):120405, 2002.

[23] T. Kinoshita, T. Wenger, and D.S. Weiss. All-optical Bose-Einstein condensation using a compressible crossed dipole trap. *Physical Review A*, 71(1):11602, 2005.

[24] R. Dumke, M. Johanning, E. Gomez, JD Weinstein, and KM Jones. All-optical generation and photoassociative probing of sodium Bose–Einstein condensates. *New Journal of Physics*, 8:64, 2006.

[25] J. Fuchs, GJ Duffy, G. Veeravalli, P. Dyke, M. Bartenstein, CJ Vale, P. Hannaford, and WJ Rowlands. Molecular Bose–Einstein condensation in a versatile low power crossed dipole trap. *Journal of Physics B: Atomic, Molecular and Optical Physics*, 40:4109, 2007.

[26] E. Timmermans, P. Tommasini, M. Hussein, and A. Kerman. Feshbach resonances in atomic Bose-Einstein condensates. *Physics Reports*, 315(1):199–230, 1999.

[27] R.A. Duine and HTC Stoof. Atom-molecule coherence in Bose gases. *Physics Reports*, 396(3):115–195, 2004.

[28] J. Söding, D. Guéry-Odelin, P. Desbiolles, G. Ferrari, and J. Dalibard. Giant spin relaxation of an ultracold cesium gas. *Physical Review Letters*, 80(9):1869–1872, 1998.

[29] CC Bradley, CA Sackett, JJ Tollett, and RG Hulet. Evidence of Bose-Einstein condensation in an atomic gas with attractive interactions. *Physical Review Letters*, 75(9):1687–1690, 1995.

[30] ERI Abraham, WI McAlexander, JM Gerton, RG Hulet, R. Côté, and A. Dalgarno. Triplet s-wave resonance in ^{6}Li collisions and scattering lengths of ^{6}Li and ^{7}Li. *Physical Review A*, 55(5):3299–3302, 1997.

[31] J. Dalibard. Bose-Einstein Condensation in Atomic Gases. *Proceedings of the International School of Physics Enrico Fermi, edited by M. Inguscio, S. Stringari, and C. Wieman (AIOS Press, Amsterdam)*, 1999.

[32] F. Schreck, G. Ferrari, KL Corwin, J. Cubizolles, L. Khaykovich, M.O. Mewes, and C. Salomon. Sympathetic cooling of bosonic and fermionic lithium gases towards quantum degeneracy. *Physical Review A*, 64(1):11402, 2001.

[33] R. Wang, M. Liu, F. Minardi, and M. Kasevich. Reaching ^{7}Li quantum degeneracy with a minitrap. *Physical Review A*, 75(1):13610, 2007.

[34] Yuval Guetta. Slowing and trapping of ^{7}Li atoms in a magneto-optical trap. Master's thesis, Bar-Ilan University, 2007.

[35] U. Schünemann, H. Engler, M. Zielonkowski, M. Weidemüller, and R. Grimm. Magneto-optic trapping of lithium using semiconductor lasers. *Optics Communications*, 158(1-6):263–272, 1998.

[36] R. Grimm, M. Weidemüller, and Y.B. Ovchinnikov. Optical dipole traps for neutral atoms. *Advances in atomic, molecular, and optical physics*, 42:95–170, 2000.

[37] TA Savard, KM Ohara, and JE Thomas. Laser-noise-induced heating in far-off resonance optical traps. *Physical Review A*, 56(2):1095–1098, 1997.

[38] C.L. Hung, X. Zhang, N. Gemelke, and C. Chin. Accelerating evaporative cooling of atoms into Bose-Einstein condensation in optical traps. *Physical Review A*, 78(1):011604, 2008.

[39] AJ Moerdijk, BJ Verhaar, and A. Axelsson. Resonances in ultracold collisions of 6Li, 7Li, and 23Na. *Physical Review A*, 51:4852–4861, 1995.

[40] N. Gemelke, C.L. Hung, X. Zhang, and C. Chin. Exploring Universality of Few-Body Physics Based on Ultracold Atoms Near Feshbach Resonances. In *21st International Conference on Atomic Physics*, page 240. World Scientific Pub Co Inc, 2009.

[41] GF Gribakin and VV Flambaum. Calculation of the scattering length in atomic collisions using the semiclassical approximation. *Physical Review A*, 48(1):546, 1993.

[42] DS Petrov. Three-boson problem near a narrow Feshbach resonance. *Physical Review Letters*, 93(14):143201, 2004.

[43] Z. Zhen and J. Macek. Loosely bound states of three particles. *Physical Review A*, 38(3):1193, 1988.

[44] M. Berninger, A. Zenesini, B. Huang, H.-C. Nägerl, F. Ferlaino, R. Grimm, P. Julienne, and J. Hutson. New results on Efimov physics and the creation of RbCs molecules. *Abstract for an Invited Paper for the DAMOP11 Meeting of The American Physical Society*, 2011.

[45] S. Tan. Energetics of a strongly correlated Fermi gas. *Annals of Physics*, 323(12):2952–2970, 2008.

[46] E. Braaten. How the tail wags the dog in ultracold atomic gases. *Physics, vol. 2, Issue, id. 9*, 2:9, 2009.

[47] AN Wenz, T. Lompe, TB Ottenstein, F. Serwane, G. Zürn, and S. Jochim. Universal trimer in a three-component Fermi gas. *Physical Review A*, 80(4):040702, 2009.

[48] T. Lompe, TB Ottenstein, F. Serwane, K. Viering, AN Wenz, G. Zürn, and S. Jochim. Atom-Dimer Scattering in a Three-Component Fermi Gas. *Physical Review Letters*, 105(10):103201, 2010.

[49] JR Williams, EL Hazlett, JH Huckans, RW Stites, Y. Zhang, and KM OHara. Evidence for an excited-state Efimov trimer in a three-component Fermi gas. *Physical Review Letters*, 103(13):130404, 2009.

[50] T. Lompe, T.B. Ottenstein, F. Serwane, A.N. Wenz, G. Zürn, and S. Jochim. Radio-Frequency Association of Efimov Trimers. *Science*, 330(6006):940, 2010.

[51] V. Efimov. Energy levels of three resonantly interacting particles. *Nuclear Physics A*, 210(1):157–188, 1973.

[52] JP DIncao and BD Esry. Mass dependence of ultracold three-body collision rates. *Physical Review A*, 73(3):030702, 2006.

[53] L. Platter, H.W. Hammer, and U.G. Meißner. Four-boson system with short-range interactions. *Physical Review A*, 70(5):052101, 2004.

[54] J. Von Stecher, JP DIncao, and C.H. Greene. Signatures of universal four-body phenomena and their relation to the Efimov effect. *Nature Physics*, 5(6):417–421, 2009.

[55] F. Ferlaino, S. Knoop, M. Berninger, W. Harm, JP Dincao, H.C. Nägerl, and R. Grimm. Evidence for universal four-body states tied to an Efimov trimer. *Physical Review Letters*, 102(14):140401, 2009.

[56] J. Stecher. Weakly bound cluster states of Efimov character. *Journal of Physics B: Atomic, Molecular and Optical Physics*, 43:101002, 2010.

מחקר של פיסיקה תלת-חלקיקית אוניברסאלית תלוי בצורה מכריעה בידיעה מדויקת של הפוטנציאל הדו-חלקיקי כיוון שעל אורך הפיזור a להיות ממופה בזהירות למשתנה הניסויי, השדה המגנטי, על מנת לאפשר השוואה ישירה עם התיאוריה האוניברסאלית. אנו מאפיינים את תהודות הפשבך בעזרת כלי ניסיוני מדויק המודד בצורה ישירה את אנרגיית הקשר של מולקולות קשורות בקרבת אזור התהודה. המדידות הללו מספקות קרקע מוצקה למחקרנו בפיסיקת אפימוב. יותר מכך, באמצעותן חישבנו ערכים מדויקים יותר עבור אורכי הפיזור הסינגלטי והטריפלטי (singlet and triplet) של הפוטנציאל הבין-חלקיקי.

תקציר

אוניברסאליות היא תכונה יסודית של מערכות מעוטות-חלקיקים (few-body systems) רבות כגון גרעיני אטומים, מולקולות פשוטות ואטומים קרים. היא מקושרת לתופעה ייחודית מתחום מכאניקת-הקוונטים שנתגלתה ע״י תיאורטיקן רוסי בשם ויטאלי אפימוב בראשית שנות ה-70. פועל יוצא של עבודת אפימוב היה קיומם של אינסוף רמות אנרגיה לשלושה חלקיקים קשורים, גם במקרה שפוטנציאל הטווח-הקצר של שני חלקיקים אינו עמוק מספיק לצורך קשירת שני חלקיקים יחדיו. תגלית זו, המנוגדת לאינטואיציה פיסיקאלית, משכה עניין רב אך חסרה הוכחה ניסיונית במשך שנים רבות. בעיות במציאת מערכת בה הפוטנציאל הבין-חלקיקי ניתן בקלות לשינוי נענו לאחרונה עם ההדגמה הניסיונית של תהודת פשבך (Feshbach) באטומים קרים.

בגבול של אנרגיית התנגשות אפסית האינטראקציות בין שני חלקיקים נקבעות ע״י פרמטר בודד, אורך הפיזור a (scattering length), המוגדר ע״י שינוי הפאזה בפיזור מסוג s-wave באנרגיות נמוכות. בקרבת תהודת פשבך פרמטר זה מתבדר ויכול להיות מכוון ללא קושי לערכים גדולים וסימנים שונים באמצעים ניסיוניים פשוטים של שינוי ערך השדה המגנטי החיצוני. התנהגות אוניברסאלית צפויה כאשר a הופך לקנה המידה הארוך ביותר במערכת. במקרה זה הנצפים התלת-חלקיקיים (three-body observables) תלויים רק ב-a ובפרמטר התלת-חלקיקי (three-body parameter) המשמש כתנאי סף לפיסיקת הטווח-הקצר.

העדות הניסיונית הראשונה לקיומם של מצבי אפימוב קוונטים דווחה ב-2006 במערכת של אטומי ^{133}Cs קרים ע״י קבוצה מאינסברוק. הם חקרו איבודים של אטומים ממלכודת אופטית רדודה שנגרמו כתוצאה מהתאחדות תלת-חלקיקית (three-body recombination) והראו הגברה של האיבודים בערכים מסוימים של a. אלה יוחסו כביטוי עקיף לקיומו של מצב אפימוב. עבודה זו בוצעה ברמת היסוד הנמוכה ביותר היכן שאיבודים כתוצאה מהתנגשויות דו-חלקיקיות אינם קיימים.

בעבודת דוקטורט זו אני מציג את מחקרנו העוסק בפיסיקה תלת-חלקיקית אוניברסאלית בגז דליל של אטומי ליתיום בוזוני קר. אנו מודדים קצבי התאחדות תלת-חלקיקית בשתי רמות אנרגיה המשויכות לספיני גרעין שונים ולרוחב שתי תהודות פשבך שונות של אותה מערכת אטומית. אנו מזהים הגברה ודיכוי של קצבי האיבודים אותם אנו משייכים לפיסיקת אפימוב ומגלים שתכונות אלו זהות בתחום השגיאה הניסויית בשתי הרמות. מכיוון שמאפייני תכונות אפימוב נקבעים על-פי הפרמטר התלת-חלקיקי, מחקרנו מצביע על כך שפיסיקת הטווח-הקצר אינה תלויה בספין הגרעין. אנו גם מאשרים את התוצאה הבסיסית של התיאוריה האוניברסאלית הטוענת שתכונות אפימוב מקושרות בצורה אוניברסאלית משני צידי תהודת פשבך.

ניסויינו מבוצעים ברמת האנרגיה הנמוכה ביותר והשנייה הנמוכה ביותר של ליתיום בוזוני. בעוד שברמה הנמוכה ביותר איבודים כתוצאה מהתנגשויות דו-חלקיקיות אינם קיימים, ברמה הבאה אחריה הם מותרים ברמת העיקרון. אולם אנו מראים שאיבודים אלו זניחים במקרה שלנו ולכן לא משפיעים על המחקר של איבודים מסדר גבוה יותר, האיבודים התלת-חלקיקיים.

תוכן העניינים

עבודה זו נעשתה בהדרכתו של ד״ר לב חייקוביץ מן המחלקה לפיסיקה של אוניברסיטת בר-אילן.

מחקר ניסיוני בפיסיקה תלת-חלקיקית אוניברסאלית באמצעות ליתיום בוזוני קר

חיבור לשם קבלת התואר "דוקטור לפילוסופיה"

מאת:

נועם גרוס
המחלקה לפיסיקה

הוגש לסנט של אוניברסיטת בר-אילן

רמת גן ניסן, תשע"א